# SORPTION MECHANISMS OF DIBENZO-P-DIOXIN/FURAN FROM WATER BY SMECTITE CLAYS AND THEORETICAL STUDIES ON FORMATION PATHWAYS OF CHLORODIBENZO-P-DIOXINS FROM PRECURSOR CHLOROPHENOLS ON SMECTITE CLAYS

By

**CUN LIU** 

#### A DISSERTATION

Submitted to
Michigan State University
in partial fulfillment of the requirements
for the degree of

DOCTOR OF PHILOSOPHY

Crop and Soil Sciences

2010

#### ABSTRACT

SORPTION MECHANISMS OF DIBENZO-p-DIOXIN/FURAN FROM WATER BY SMECTITE CLAYS AND THEORETICAL STUDIES ON FORMATION PATHWAYS OF CHLORODIBENZO-p-DIOXINS FROM PRECURSOR CHLOROPHENOLS ON SMECTITE CLAYS

By

#### **CUN LIU**

Clay minerals may be an important sorptive phase for dioxins in soils, and dioxins are often found in natural clay deposits. Sorption experiments demonstrated that smectites, especially Cs-saponite, effectively adsorbed dibenzo-p-dioxin /furan from water. Adsorption was promoted by exchangeable cations with low hydration energies, and negative charge in the smectite arising from the tetrahedral siloxane sheets. X-ray diffraction measurements revealed that as dibenzo-p-dioxin (DD) loading increased to  $\geq$ 8,000 mg/kg the clay basal spacing increased abruptly from 12.3 to 15.2 Å, thereby demonstrating DD intercalation. The 12.3 Å spacing provides an interlayer distance that closely matches the molecular thickness of DD. The geometrical configurations of intercalated DD in the interlayer were investigated by a combination method of ab initio calculations and Fourier transformation infrared spectroscopy. Molecular dynamics simulations of saponites saturated with different exchangeable cations ( $Na^+$ ,  $K^+$ ,  $Cs^+$  and Ca<sup>2+</sup>) with one, two and three layers of water in the interlayer regions further supported the hypothesis that O<sub>dd</sub>-interlayer cation complexation plays an important role in adsorption and the order of coordination numbers between  $O_{\mbox{\scriptsize dd}}$ -interlayer cation follows

Cs<sup>+</sup>>K<sup>+</sup>>Na<sup>+</sup>>Ca<sup>2+</sup>, in good agreement with the observed DD adsorption to the smectites from water.

Octachlorodibenzodioxin (OCDD) forms spontaneously from pentachlorophenol (PCP) on the surfaces of Fe(III)-saturated smectite clay. Here, in situ FTIR methods and quantum mechanical calculations were used to determine the mechanism by which this reaction is initiated. As the clay was dehydrated, vibrational spectra showed new peaks that grew and then reversibly disappeared as the clay rehydrated. Density functional theory (DFT) calculations of hydrated Fe-PCP clusters reproduced these transient FTIR peaks when inner-sphere complexation and concomitant electron transfer produced Fe(II) and PCP radical cations. Thus, our experimental (FTIR) and theoretical (quantum mechanical) results mutually support the hypothesis that OCDD formation on Fe-smectite surfaces is initiated by the reversible formation of metastable PCP radical cations via single electron transfer from PCP to Fe(III). The negatively charged clay surface apparently selects for this reaction mechanism by stabilizing PCP radical cations. DFT methods were further applied to the calculations of 2,4,5-trichlorophenol (2,4,5-TCP) interacting with iron(III) species to evaluate the possible reaction pathways and the associated reaction energies and activation energies. The calculations support the formation of the direct precursors of the most toxic PCDD congener, 2,3,7,8-TCDD, and of 1,2,4,7,8-pentachlorodizenzodioxin, and two additional dimers, from the reaction of 2,4,5-TCP with Fe(III)-montmorillonite clay, which imply that soil contaminated with 2,4,5-trichlorophenol may have the potential risk for 2,3,7,8-TCDD contamination.

# **DEDICATION**

To my daughter, Yuewei, wife Wu, Di, and family

#### **ACKNOWLEDGEMENTS**

I would especially like to thank my advisor, Dr. Brian Teppen, for his guidance, support, and encouragement throughout this research and also with my professional development. This dissertation could not have been completed without his help and support. I would also like to thank my co-advisors Dr. Stephen Boyd and Dr. Hui Li for all their supports. Dr. Boyd has been helpful in providing extremely valuable directions and resources during my graduate student career, and I would also like to express my deepest gratitude to him for his countless help on writings and dedication in editing and revising the manuscripts. Dr. Li has always been supportive and has provided me insightful guidance in research and advices in life. I also thank my guidance committee member Dr. Thomas Pinnavaia for his insight and helpful comments.

I am appreciative of the help from Dr. Cheng Gu and Dr. Michael Roberts who have been always of enormous assistance to me whenever I need. I also thank Dr. Wan-Ru Chen, Dr. Vaneet Aggarwal, Dr. Yao-Ying Chien, Yunjie Ding, Mark Bezdek, and all other members of soil chemistry laboratories who have encouraged and supported me over the years.

Finally, my special thanks go to my wonderful family, my wife Di Wu, our precious daughter Yuewei, my parents, my parents in law and my sister, who provided endless and priceless support, encouragement and understanding. I am and will forever thankful and grateful for every moment we share together.

## TABLE OF CONTENTS

LIST OF TABLES.	viii
LIST OF FIGURES.	ix
CHAPTER I: INTRODUCTION	1
BACKGROUND AND RATIONALE	2
DIOXIN LEVELS IN SOILS AND CLAY DEPOSITS.	
ADSORPTION MECHANISMS OF DIOXIN ON CLAY MINERALS	
SOURCE OF OCDD	8
OBJECTIVES AND APPROACH	11
LITERATURE CITED	
CHAPTER II: MECHANISMS ASSOCIATED WITH THE HIGH ADSO	RPTION
OF DIBENZO-P-DIOXIN FROM WATER BY SMECTITE CLAYS	24
ABSTRACT	25
INTRODUCTION	26
MATERIALS AND METHODS	30
RESULTS AND DISCUSSION	35
LITERATURE CITED	49
CHAPTER III: MECHANISMS ASSOCIATED WITH THE HIGH ADSO	ORPTION
OF DIBENZO-P-DIOXIN FROM WATER BY SMECTITE CLAYS	54
ABSTRACT	55
INTRODUCTION	56
MATERIALS AND METHODS	60
RESULTS AND DISCUSSION	
LITERATURE CITED	80
CHAPTER IV: PENTACHLOROPHENOL RADICAL CATIONS GEN	
ON FE(III)-MONTMORILLONITE INITIATE OCTACHLORODIB	
DIOXIN FORMATION IN CLAYS	
ABSTRACT	
INTRODUCTION	
MATERIALS AND METHODS	
RESULTS AND DISCUSSION	
LITERATURE CITED	119
CHAPTER V: CLAY MEDIATED ROUTE TO NATURAL FORMATION	
POLYCHLORODIBENZO-P-DIOXINS: A DFT STUDY	
ABSTRACT	
INTRODUCTIONMATERIALS AND METHODS	
IVIA LEKTALA AND IVIETHUDA	1 / X

RESULTS AND DISCUSSION	129
LITERATURE CITED.	140

## LIST OF TABLES

Table II-1. Characteristics of clay minerals used as adsorbents for dibenzodioxin and dibenzofuran
Table II-2. Computed binding energies (ΔE <sub>ZPE</sub> ) and geometrical parameters for Cs <sup>+</sup> dibenzodioxin complexes illustrated in Figure II-332
Table III-1. Characteristics of clay minerals used as adsorbents for dibenzodioxin61
Table III-2. Values of the first neighbor distance(r) and corresponding coordination number $(C_N)$ for dioxin oxygen $(O_{dd})$ with water hydrogen $(H_w)$ and interlayer cation $(Cs^+, K^+, Na^+ \text{ and } Ca^{2+})$
Table IV-1. Selected computed geometrical parameters of pentachlorophenol (PCP) PCP/H <sub>2</sub> O and PCP/Fe(OH)(H <sub>2</sub> O) <sub>n</sub> <sup>2+</sup> in the gas phase (units: distances (Å and angles (degree))
Table IV-2. Additional geometry parameters of PCP/Fe(OH)(H <sub>2</sub> O) <sub>n</sub> <sup>2+</sup> in gas phase. (uni distances (Å), angles (degree) and energies (kcal/mol))
Table IV-3. The calculated FTIR frequencies of all pentachlorophenol (PCP) species compared with experimental results, and the corresponding potential energy distribution analysis (PED) (percentages, in parentheses)
Table IV-4. Selected computed geometry parameters of ONIOM pentachloropheno (PCP)-smectite clay clusters (units: distances (Å) and angles (degree energies (kcal/mol))
Table V-1. Reaction ( $E_R$ ) and activation energies ( $E_A$ ) (in kcal/mol) of the predioxin formations calculated at B3LYP/6-31G*/LANL2DZ level of theory135

# LIST OF FIGURES

Figure I-1.	Source, fate and transport of PCDDs in the environment
Figure II-	1. Adsorption isotherms representing (A) dibenzodioxin (DD) or (B) dibenzofuran (DF) uptake from water by Cs-saturated smectites (saponite SapCa-2; montmorillonite, Upton and SWy-2; hectorite, SHCa) and comparison of (C) dibenzodioxin (DD) or (D) dibenzofuran (DF) adsorption by homoionic saponite saturated with different exchange cations. The amount sorbed by soil organic matter was estimated using the equation $\log K_{OM} = 0.904 \log K_{OW} - 0.779$
Figure II-2	2. X-ray diffraction patterns of Cs-saponite clay films equilibrated with increasing concentrations of aqueous dibenzodioxin (DD) solutions, Cs-saponite blank (no DD adsorbed) and crystalline DD. 2 Theta represents the diffracted angle relative to the incident X-ray beam
Figure II-3	8. Schematic views of three possible conformations of $Cs^+$ -dibenzodioxin complexes with respect to the siloxane surface of smectite clay; top (left) and side views. The atom coloring scheme for atoms is $Cs = yellow$ , $O = red$ , $H = white$ , $C = gray$ , tetrahedral siloxane of clay minerals=light gray. Geometrical parameters are listed in table II-2. (I) $C_{2v}$ symmetry; (II) $C_{s}$ symmetry
Figure II-4	Polarized ATR-FTIR spectra of dibenzodioxin (DD) sorbed to Cs-saponite ir aqueous suspension. The in-plane vibrational bands of DD at 1248, 1298 and 1492 cm <sup>-1</sup> are magnified in the insert
Figure III-	1. Adsorption isotherms of dioxin by Cs-, NH <sub>4</sub> -, K-, Fe-, Al-, Mg-, and Ca-saturated montmorillonite (SWy-2) from water
Figure III-2	2. The comparison of dioxin adsorption by different smectite clays (SapCa-2 SHCa-1, SWy-2, SWa-1 and SAZ-1) in the homoionic Ca <sup>2+</sup> and K <sup>+</sup> forms Similar trends in the ordering of clays as adsorbents for dioxin are observed for both Ca <sup>2+</sup> (left) and K <sup>+</sup> (right) saturated clays. Higher adsorption generally is related (directly) to higher tetrahedral charge and (inversely) to clay surface charge density.
Figure III-	3. A snapshot of molecular dynamics simulations for 12 Å Cs-saponite hydrates containing 3 dioxin molecules per supercell. The color scheme for dioxin molecules is: red=O; gray=C; white=H. The Cs <sup>+</sup> interlayer exchangeable cations are shown in blue. The distances shown (in Å) are the Cs <sup>+</sup> -O bond distances for complexes formed between Cs <sup>+</sup> and dibenzo- ring oxygens of dioxin. Upper panel: top surface view of Cs-saponite; lower left

	cross-sectional view; lower right: enlarge of a typical interlayer Cs-dioxin complex
Figure III-4	4 Radius distribution function for $O_{dd}$ - $H_{w}$ , $O_{dd}$ - $H_{dd}$ and $O_{dd}$ -cation for Cs, K, Na and Ca-Saponite at different water contents. (purple: $O_{dd}$ -exchangeable cation, blue: $O_{dd}$ - $H_{w}$ )
Figure IV-	1. Atom numbering scheme for pentachlorophenol (PCP)94
Figure IV-	2. FTIR spectra of homoionic Fe(III)-montmorillonite clay/pentachlorophenol self-supporting clay film exposed to vacuum as a function of time: 0 (a), 10 (b), 20 (c), 50 (d) and 120 min (e). After obtaining spectrum at t = 120 min, vacuum was closed and water was added to the cell, spectra were collected at 2 (f), 10 (g), 22 (h) and 35 (i) min after exposure to water vapor97
Figure IV	-3. Integrated intensities of selected IR bands in homoionic Fe(III)-montmorillonite clay/pentachlorophenol as a function of exposure time to vacuum ( $0 < t < 120 \text{ min}$ ) and water vapor ( $t > 120 \text{ min}$ )98
Figure IV	-4. Optimized geometries of pentachlorophenol (PCP), PCP/H <sub>2</sub> O and PCP/Fe(OH)(H <sub>2</sub> O) <sub>n</sub> <sup>2+</sup> in the gas phase. Color scheme is: dark gray=carbon; green=chlorine; red=oxygen; light gray=hydrogen
Figure IV	-5. Potential energy profile for the stable conformers of PCP/FeOH <sup>2+</sup> complexes. The configuration a is the collinear structure of the pentachlorophenol (PCP) cation radical with FeOH <sup>+</sup> , and the configuration b is the PCP phenoxy radical with FeOH <sub>2</sub> <sup>2+</sup>
Figure IV-6	6. Molecular orbital energy level diagrams (the d block) for bare FeOH $^{2+}$ (left) and PCP/FeOH $^{2+}$ (right) systems. The insets on the right panel show the 18 and 2 $\sigma$ molecular orbitals. One electron transferred from PCP molecule fills into the non-bonding 1 $\delta$ orbital, which is localized primarily on the Fe d <sub>x</sub> $^2$ -y orbital. The 2 $\sigma$ molecular orbital consists of collinear overlaps between Fe d <sub>z</sub> $^2$ and PCP oxygen pz orbitals
Figure IV-	7. DFT calculated infrared spectra of selected PCP/Fe(OH)( $H_2O$ ) <sub>n</sub> <sup>2+</sup> systems with the number of coordination water n equal to 3(a), 2(b), 1(c) and 0(d)
Figure IV-	8. Comparison of experimental infrared spectra of Fe(III)-montmorillonite clay/pentachlorophenol (PCP) system: (a) observed spectrum after exposure to water vapor, (b) observed spectrum under vacuum, and calculated spectra (c) (d) and (e) for PCP/FeOH <sup>2+</sup> (structure 0a of Figure IV-4), PCP/H <sub>2</sub> O and

PCP respectively. Lines 1, 2 indicate the peak shifts of 1420 and 1381cm <sup>-1</sup> . Lines 4 and 5 indicate new peaks due to formation of radical cation in experimental (b) and calculated (c) spectra. The scaling factor was 0.98111
Figure IV-9. Left: Calculated infrared spectra of selected PCP/Fe(OH)( $H_2O$ ) <sub>n</sub> <sup>2+</sup> systems (for structures refer to Figure IV-4) with the number of coordinated water molecules increasing from 0 to 3. Right: Correlations of intensity of the simulated infrared peak at 1360 cm <sup>-1</sup> ( $\blacksquare$ ), and the binding energies of pentachlorophenol (PCP) onto Fe(OH)( $H_2O$ ) <sub>n</sub> <sup>2+</sup> ( $\bullet$ ) versus the total coordination number of the Fe center.
Figure IV-10. ONIOM models of the pentachlorophenol (PCP) molecule (a) PCP radical cation (b) and PCP phenoxy radical adsorbed on smectite clay surface. Color scheme for PCP: red=O; green=Cl; dark gray=C; light gray=H. The 2:1 aluminosilicate clay layer is shown below the PCP structures. Color scheme for the clay layer: red=O; dark gray=Si; light gray=H; pink=Al
Figure V-1. Proposed reaction pathways for 2,4,5-TCP with Fe(III)-montmorillonite, leading to the formation of dimerization products, including predioxins (B and C)
Figure V-2. Reaction profiles for the predioxin formation pathways from 2,4,5-TCP with or without Fe(III)O <sup>+</sup> /Fe(II)(OH) <sup>+</sup> (blue lines for systems w/o iron, and red lines for systems w iron). The energies of TCP phenoxy radical/2,4,5-TCP complexes with or without Fe(III)O <sup>+</sup> /Fe(II)(OH) <sup>+</sup> were set to zero. (See notes of Table V-1 for the description of TS <sub>1</sub> * in pathway A)

# CHAPTER I INTRODUCTION

#### BACKGROUND AND RATIONALE

Polychlorinated dibenzo-p-dioxins and dibenzofurans (PCDD/Fs) are two families of chlorinated organic compounds that are among the most potent multi-site carcinogens in humans and other mammals (Mandal, 2005). Understanding the human health threat posed by potential exposures to PCDD/Fs in the environment requires accurate assessments of the environmental fate and transport of PCDD/Fs (Figure I-1). Many anthropogenic activities such as industrial chemical synthesis, pesticide manufacture, wastewater treatment and waste incineration along with more than 20 other processes have been identified as PCDD/F sources in which PCDD/Fs are produced as unintentional by-products, and these human activities are thought to contribute the major portion of PCDD/Fs released into the environment (Brzuzy and Hites, 1996; Kjeller et al., 1991). During the past 30 years, a significant reduction of PCDD/F emissions by human activities has been successfully achieved as a result of regulations and new technologies (Hays and Aylward, 2003).

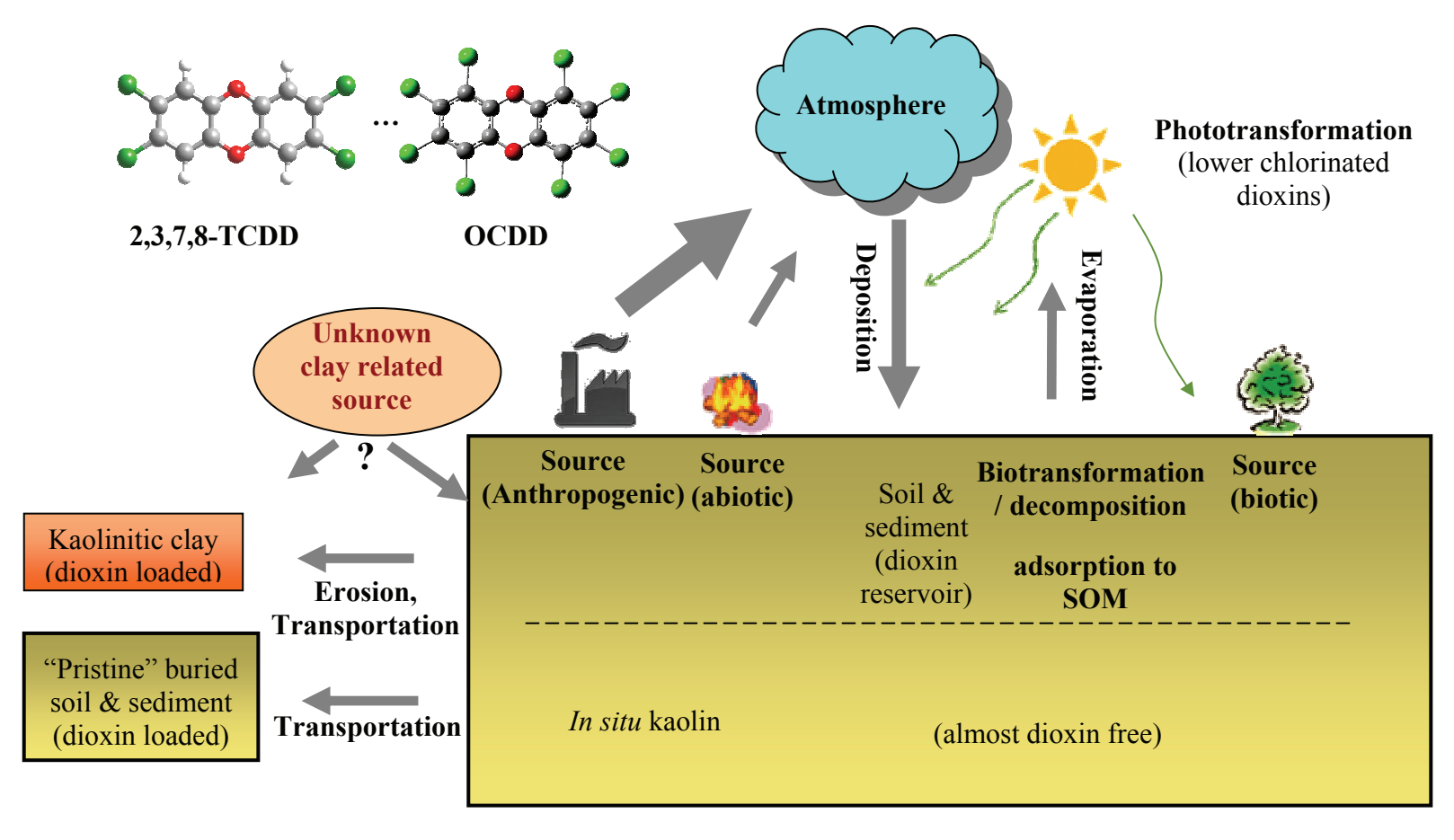


Figure I-1. Source, fate and transport of PCDDs in the environment (modified from (Schmitz et al.)).

"For interpretation of the references to color in this and all other figures, the reader is referred to the electronic version of this

However, attempting to quantify a global PCDD/F mass balance indicates that the total amount of PCDD/Fs found in various environmental sinks, especially soils, exceeds the total estimates for anthropogenic PCDD/F emissions (Baker and Hites, 2000). In a survey conducted by USEPA, both urban and (apparently uncontaminated) rural soils were found contaminated with PCDDs at levels potentially damaging to human and ecosystem health (EPA., 2007; Holt et al., 2008). Additionally, prehistoric clay deposits (e.g., ball clays) are found contaminated with high levels of PCDDs (Ferrario et al., 2000; Gadomski et al., 2004; Gaus et al., 2001; Gaus et al., 2002; Green et al., 2004; Hoekstra et al., 1999; Holmstrand et al., 2006; Horii et al., 2008; Rappe et al., 1997). In both instances a unique PCDD congener profile different from any known anthropogenic emissions is present, and is dominated by the most highly chlorinated congeners, especially octachlorodibenzodioxin (OCDD), and contains few chlorodibenzofurans (Holt et al., 2008). The high levels of PCDDs in ball clays are surprising and unexpected, since organic matter is often considered as the primary sorptive compartment in soils for hydrophobic compounds like PCDD/Fs, while sorption on clay mineral surfaces is generally considered negligible for neutral organic contaminants (Means et al., 1980). There is a lack of knowledge whether clay minerals may play an important role in adsorbing PCDD/Fs, and the adsorption mechanism responsible for the high concentration found in clay deposits and soils with very low SOM content remains unclear.

In addition, the origin of these (apparently non-anthropogenic) PCDDs in soils and clay deposits remains unsolved. Detailed accounting of PCDD emissions into the atmosphere, with subsequent deposition, cannot reconcile the levels of PCDDs in soils,

suggesting some other unknown source of PCDDs (Baker and Hites, 2000). Naturally insitu formation of PCDD/Fs by microbial activities in the presence of chloride (Hoekstra et al., 1999), and by abiotic processes such as volcanic eruptions and forest fires (Bumb et al., 1980) provide potential solutions. Holt et al. (Holt et al., 2008) hypothesized that OCDD is formed in soils from pesticide derived precursors, most notably pentachlorophenol (PCP). Gu et al. (Gu et al., 2008) first demonstrated that OCDD can be formed abiotically from PCP in presence of Fe(III) saturated montmorillonite under environmentally relevant conditions, suggesting that PCDDs, and OCDD in particular, can be synthesized in soils via clay-facilitated reactions from precursor chlorophenols, and that such synthesis in soils can help close the PCDD mass balance. However, there have been no systematic studies capable of unveiling the molecular-level reaction mechanisms, the energetic aspects of the reactions and the plausibility of hypothetical pathways.

In order to gain a better understanding of adsorption and possible *in situ* formation of PCDD/Fs on clay minerals, this research specifically aims to investigate: (1) the extent of PCDD/F adsorption on various clay minerals using dibenzo-p-dioxin and dibenzofuran (DD/DF) as the model molecules (2) the interaction mechanisms between DD/DF and clay minerals, and (3) the reaction mechanisms and pathways leading to the formation of PCDDs from precursor chlorophenols, and the energetic aspects of the reactions. These aims will be attacked by using several sets of complementary experimental and modeling techniques: 1) Batch adsorption experiments of DD/DF on different clay minerals with various exchange-cations to investigate the effects of clay properties on sorption; 2) Infrared spectroscopy and X-ray diffraction coupled with quantum mechanics/molecular

dynamics simulations to elucidate sorption mechanisms; 3) Infrared spectroscopy coupled with quantum mechanics to construct and verify the PCDD formation pathway from PCP and 2,4,5-TCP, identify major reaction intermediates and at least semi-quantitatively obtain the thermodynamic properties, such as the potential energy profiles of the reactions.

#### DIOXIN LEVELS IN SOILS AND CLAY DEPOSITS

Rural and apparently pristine soils are found to be contaminated with PCDD/Fs, especially OCDD, which cannot be traced back to any identified anthropogenic source (Ferrario and Byrne, 2002; Ferrario et al., 1999; Ferrario et al., 2000; Holmstrand et al., 2006; Horii et al., 2008). In one recent study of 34 sampling sites, the mean OCDD concentration was ~1500 pg/g with some individual samples showing concentrations above 10,000 pg/g (EPA., 2007). In another study of 2081 soil samples (Franzblau et al., 2009), 371 soil samples were taken as background controls and they contained mean OCDD concentrations of 590 and 650 pg/g for the 0-to-1-inch and 1-to-6-inch soil depths, respectively.

Prehistoric clay mineral deposits were found to contain even higher level of PCDDs. In a study of 27 samples from different ball clay cores, the concentrations of OCDD were as high as ~450,000 pg/g (Gadomski et al., 2004). Comparable levels of PCDDs with similar distribution patterns of PCDD congeners were found in ball clay and kaolin samples from different parts of world including the U.S., Germany, and Spain

(Jobst and Aldag, 2000; Rappe, 2001). In another study of clay mineral samples including six montmorillonites/bentonites (Ferrario et al., 2000), the concentrations of OCDD were found in a range from 70 to 37,519 pg/g in these smectites.

All of these pristine soils, sediments, and clays feature similar distribution patterns of PCDD/F congeners, in which PCDF concentrations were 3 to 4 orders of magnitude lower than those of PCDDs; OCDD was the most abundant congener with concentrations up to 450 ppb (in ball clay); and the homologue distribution of PCDDs followed the order: OCDD > HeptaCDD > HexaCDD > PentaCDD > TetraCDD. It is interesting that the pattern also holds for montmorillonites/bentonites (smectites) (Ferrario et al., 2000), which are major constituents of soils. One interpretation of these data is that smectites (the swelling clay minerals) may be selectively sequestering the more highly chlorinated dioxins, and may be selecting for PCDDs over PCDFs (Ferrario et al., 2000).

#### ADSORPTION MECHANISMS OF DIOXIN ON CLAY MINERALS

An earlier work by Nolan et al. (Nolan et al., 1989) examined sorption of dioxins by aluminum-pillared smectite clay using radioisotope analysis methods. They measured adsorption coefficients (K) to be  $67,000 \pm 6,000$  L/kg for 2,3,7,8-TCDD and 94,000  $\pm$  10,000 L/kg for OCDD. In mass terms, they saw 450  $\mu$ g OCDD (g clay)<sup>-1</sup> adsorbed from 0.005 ppb OCDD in water/THF solution and about 20  $\mu$ g 2,3,7,8-TCDD (g clay)<sup>-1</sup> adsorbed from 0.3 ppb aqueous solution. These results indicate substantial sorption of dioxins, and fit well with the notion that smectites could be a key environmental sink for

dioxins. It's noticeable that these sorption coefficients for Al-pillared smectites ( $10^4$  to  $10^5$ ) are about 1/3 the K<sub>d</sub> values one would predict (Chiou, 2002) for sorption by pure soil organic matter. The potential predominant contribution of clays to dioxin sorption is easily recognized considering the much higher clay contents of soils, subsoil, and aquifer materials (up to 50%) compared to organic matter contents (often <1%). Despite this potential role of soil clays as a major sink for environmental dioxins, no other work has been reported since then that explicitly studied dioxin sorption to clays.

Based on the above observations that rural soils and natural clay deposits are enriched in specific types of dioxins, along with one study (Nolan et al., 1989) showing strong dioxin adsorption to clays, it is hypothesized in this research that there are favorable clay-dioxin interactions that have not been considered in relation to dioxin environmental fate. If so, then modern anthropogenic dioxins, too, might be expected to accumulate in clay minerals, possibly with inherent selectivity for certain congeners. Such sequestration of dioxins in clay minerals would have important implications for bioavailability of dioxins to bacteria and higher organisms.

#### SOURCE OF OCDD

Several studies have attempted global PCDD budgets. In almost every instance, the concentrations or total mass of PCDDs in soils cannot be accounted for by the known sources of PCDDs. From some estimates, apparent air-borne PCDD "deposition" (actually, accumulation of measured PCDD concentrations in soils) was 10-20 times

higher than annual emissions (Rappe et al., 1997). A more recent detailed mass balance study of combustion as the major source of PCDDs in the environment, including rural soils, concluded that such "deposition" of PCDDs exceeded emissions by a factor of at least 2 (Baker and Hites, 2000). This is especially important for rural soils, where the only logical known source of PCDD would be deposition. Clearly, these studies and others (Holmstrand et al., 2006) suggest the possibility of *in situ* synthesis of PCDDs in the soil environment. Chlorophenol volatilization with subsequent photochemical formation of PCDDs in the atmosphere, followed by deposition with rainfall, has been hypothesized, a priori, to be the most significant source of soil PCDDs (Baker and Hites, 2000). However, this scenario clearly cannot account for the presence of high levels of PCDDs, with unique OCDD-dominated congener profiles, in prehistoric clay deposits, as due to their extraordinarily low water solubilities, it is impossible to reconcile PCDDs in deep buried clay deposits by attributing them to leaching. A more plausible route for the widespread occurrence of OCDD at depth is the in situ formation of PCDDs in soils and clay deposits from precursor chlorophenols, especially PCP. This general idea has been suggested in several recent studies (Holmstrand et al., 2006; Holt et al., 2008; Horii et al., 2008), though no known mechanisms exist or have even been suggested to account for formation of PCDDs, nor for the preferential formation of OCDD.

When considering the imbalance between PCDD emissions and subsequent deposition, OCDD presents the most glaring misbalance among the PCDD congeners; estimates by Baker and Hites (Baker and Hites, 2000) conclude that OCDD has about 40 times more "apparent deposition" than emission. The logical precursor molecule is PCP. Pentachlorophenol was used worldwide as biocide during the 1940s to 1990s (for

example in treated lumber); in 1985 PCP production was 10<sup>8</sup> kg/yr (Wild et al., 1992). The vapor pressure of PCP is around 0.1 Pa (Mackay et al., 1992). Large production and propensity for volatilization could lead to global atmospheric transportation of PCP. In fact, significant levels of PCP have been detected in air samples worldwide. In Canada, PCP concentration in air samples were ~ 1 to 1200 ng/m<sup>3</sup> (Waite et al., 1998). Pentachlorophenol has also been detected in rain water at concentrations of 10 to 100 ng/L (Fingler et al., 1994; Leuenberger et al., 1985; Wild et al., 1992). Using an assumed average PCP concentration in water of 20 ng/L, and multiplying this by average rainfall, PCP wet deposition to the surface of the Earth would be about 10<sup>7</sup> kg/yr. If only a small portion of this PCP (i.e. 0.05%) was subsequently converted to OCDD, it would produce enough OCDD to close the PCDD mass balance. Recall that the imbalance is due primarily to higher OCDD levels in soils than expected based on OCDD emissions (Baker and Hites, 2000). It is unknown whether the PCDD levels in soils are increasing, but it seems plausible that they are. Interestingly, the PCDD congener profiles in ball clays are also dominated by OCDD, and Holmstrand et al. (Holmstrand et al., 2006) proposed that some type of in situ OCDD formation by clay-mineral facilitated reactions must occur (obviously photochemical reactions in these buried clay deposits is not plausible). Under neutral or near neutral conditions in soils PCP (pKa = 4.7) exists as phenolate (>99% at pH 7), i.e. is anionic, leading to high water solubility and mobility in soils (Huang et al., 2000; Hyun et al., 2003; Lee et al., 1990). Hence, subsurface clay deposits that were buried long before the advent of synthetic organochlorine pesticides

such as PCP could have become contaminated by relatively recent PCP leaching followed by clay-catalyzed dimerization to OCDD.

#### **OBJECTIVES AND APPROACH**

1. Objective 1: To determine the extent to which dioxin and dibenzofuran are adsorbed on clay minerals and the factors affecting the extent of adsorption.

In this research non-chlorinated dioxin (DD) and dibenzofuran (DF) are used as the model compounds to evaluate the extent of their sorption by smectite clays possessing a wide range of surface areas, surface charge densities, and distribution of layer charge (i.e. octahedral vs. tetrahedral isomorphic substitution). The smectite clays of different structures will be saturated by exchangeable cations with different hydration energies (e.g. K<sup>+</sup>, Mg<sup>2+</sup>, Ca<sup>2+</sup> and Al<sup>3+</sup>, as well as Cs<sup>+</sup>). Sorption isotherms in aqueous solution will be obtained using a batch equilibration method, and DD/DF will be analyzed by high-performance liquid chromatography (HPLC) equipped with a UV-visible detector.

Smectite clays with lower CEC values are expected to provide more neutral siloxane surface domains for the adsorption of DD/DF. To test this hypothesis, the sorption isotherms will be measured for SWy-2, Upton montmorillonite, SHCa-1 and SAz-1, which feature CEC values in the range 78 to 130 cmolc/kg. The source of negative charges (tetrahedral vs. octahedral isomorphic substitution) is hypothesized to influence

the adsorption with a greater sorption expected for clays with tetrahedral substitution. This hypothesis will be examined by comparing sorption on clays with similar CEC values but with a different source of layer charge, e.g., Upton montmorillonite vs. SapCa-2 and SBId-1 vs. SAz-1.

In this research it is hypothesized that the retention of DD/DF on smectite is strongly influenced by the nature of exchangeable interlayer cations, i.e., the hydration energy. Lower hydration energy and the resultant smaller hydrated radius of certain exchangeable cations, e.g.,  $K^+$ ,  $Cs^+$ , would plausibly provide more unobscured hydrophobic planar clay siloxane surface, and also be more likely to allow direct interactions/complexations between exchangeable cations and electron donating groups (e.g., oxygen or aromatic  $\pi$  systems) of DD/DF molecules. A compound with similar molecular dimensions but a stronger aromatic  $\pi$  system and without hetero atoms, anthracene, will be compared with DD/DF to elucidate the interlayer cation influence.

Additional sorption isotherms on organic matter (a peat soil) will also be conducted for DD/DF to quantify the different sorption mechanisms and compare with the clays.

2. Objective 2: To determine the molecular mechanisms for the sorption of DD/DF by clay minerals in aqueous systems.

Previous work has characterized both the extent and mechanisms of chemical interactions of many polar and semi-polar organic solutes with clays using a combination of molecular simulations, spectroscopic methods adapted to aqueous systems, X-ray diffraction techniques, and detailed macroscopic measurements of bulk behavior

(Aggarwal et al., 2006; Boyd et al., 2001; Chappell et al., 2005; Gadomski et al., 2004; Hyun et al., 2003; Johnston et al., 2002; Li et al., 2007). FTIR spectroscopy coupled with quantum mechanics calculations can provide information about the clay-organic interaction, the local chemical environment, the orientation of the organic molecules on the clay surfaces, as well as the influence of clay type and concentration (Boyd et al., 2001).

Molecular dynamics has proven to be a successful technique to investigate molecular-scale interactions occurring in large complex systems such as clay minerals (Chang et al., 1995; Teppen et al., 1997), and will be used here to gain insight into the mechanisms and forces involved in dioxin adsorption by smectite clay. The adsorption of dibenzo-p-dioxin, by a systematic set of clay minerals which differed in the amount and source of clay layer charge, and several exchangeable cations, which differed in the hydration propensities will be simulated in order to explore the molecular-scale interactions of dibenzo-p-dioxin on hydrated clay surfaces. The modeling can integrate the interactions between interlayer water-water, clay surface-water, interlayer cationwater, and interlayer cation-clay surface, and allow a detailed description of the mechanisms and forces operative in the adsorption of dioxin in smectite clay interlayers.

Potential sorption mechanisms of DD/DF at mineral surfaces

a. Hydrophobic effect.

Since the DD/DF, are non polar, nonionic organic solutes, it has been thought that their sorption to mineral surfaces is primarily controlled by "hydrophobic effects," a combination of relatively small van der Waals bonding forces and a substantial entropic

gradient that drives the organic molecules out of aqueous solution (Israelachvili, 1992; Tanford, 1980; Voice and Weber, 1983). Previous studies observed that the association of organic solutes with an inorganic surface increased with decreasing aqueous solubility of the compounds (Boyd et al., 2001; Curtiss et al., 1986; Lee et al., 1990; Mader et al., 1997; Schwarzenbach and Westall, 1981; Van Bladel and Moreale, 1974).

Expandable clay minerals are known to be strongly hydrophilic on a macroscopic scale (Mooney et al., 1952; Xu et al., 2000). However, the hydrophobic-hydrophilic character of smectite surfaces has been reexamined and portions of the smectite surface have been shown to have a relatively hydrophobic character (Jaynes and Boyd, 1991). On a molecular scale the uncharged regions between charge sites on siloxane surfaces have been shown to function as hydrophobic nanosites (Johnston, 1996; Laird, 1996).

b. Specific electron donor-electron acceptor interactions and cation complexation (including cation- $\pi$  interactions).

Recent evidence has suggested that electron donor-electron acceptor interactions, cation complexation, or cation- $\pi$  interactions can form between the cations and electron donor groups, e.g., hetero atom or  $\pi$  -electrons of aromatic organics, and such interactions can be strengthened if interactions happen in confined matrices, such as ion channels in cell membranes, the interiors of synthetic receptors, and natural biomolecules in aqueous systems (Chu et al., 1993; Ghidini, 1990; Ma and Dougherty, 1997). The magnitude of enthalpies of these interactions can be quite substantial, which is strongly competitive against the hydrogen bonds, and other non-covalent interactions (Dougherty and Stauffer, 1990; Gokel et al., 2001). Since smectite interlayers are confined spaces that are also rich in cations, the formation of cation- $\pi$  interactions between DD/DF and the exchangeable

cations may affect DD/DF sorption to mineral surfaces (Zhu et al., 2004). The extent to which these interactions are operative on clay surfaces will be strongly influenced by the hydration status of the exchangeable cation, the ionic potential of the cation, and the polarizability of the organic solute.

3) Objective 3: Quantum mechanics studies on the reaction mechanisms and pathways leading to the formation of PCDDs from precursor chlorophenols, and the energetic aspects of the reactions.

Quantum mechanical calculations will be applied to augment the experimental studies (Gu et al., 2009) on dioxin formation on clay minerals using chlorophenols as precursor. Quantum methods, especially DFT methods have been readily used to provide molecular level insights of physical chemical processes in complex systems, with the model acting as a bridge between experimental observations and molecular-scale interactions (Warshel, 2003). In a cluster model, a properly chosen structural moiety representing the most important aspects of the whole chemical structure, is used to evaluate the atomic geometry, electronic structure, and energetics of the entire system. It has been proven by many studies that even a small cluster, such as a single iron cationorganic molecule complex, can provide reliable structural and energetical information on interactions in a complex matrix (Fiedler et al., 1994; Kallies and Meier, 2001; Shiota and Yoshizawa, 2000; Sun et al., 2007). In this research I propose to use an isolated Fe(OH)<sup>2+</sup> or Fe(OH)<sub>2</sub><sup>+</sup> cluster, octahedrally coordinated by water, to represent the chemically active center embedded in clay minerals. The cluster models will be applied to investigate the chemical transformations of PCP. It is hypothesized that a cluster of PCP/Fe(OH)  $(H_2O)_n^{2+}$  with various number of water in the first hydration shell (n=0 to 3) could be useful to characterize the spectroscopic features of PCP chemical transformations on the clay mineral surfaces. The isolated PCP molecule and PCP/H<sub>2</sub>O complexes will also be studied to understand the hydration state of PCP under conditions of high humidity. Furthermore, the interactions of a model neutral clay surface  $(6.5(Al)_2(Si)_4O_{10}(OH)_2 \cdot nH_2O)$  and PCP, the PCP radical cation, and the PCP phenoxy radical will be modeled by ONIOM methods in order to rationalize the stabilization effects of radical cation intermediates on clay surface.

The cluster model will be further extended to explore the entire pathway of PCDD formation from 2,4,5-TCP. Reaction intermediates and transition states can be located using QST3 methods, and the potential energy profile will be constructed to allow a semi-quantitative comparison with available experimental thermodynamic and kinetic data.

LITERATURE CITED

#### LITERATURE CITED

- Aggarwal, V., H. Li, S.A. Boyd, and B.J. Teppen. 2006. Enhanced sorption of trichloroethene by smectite clay exchanged with Cs<sup>+</sup>. Environmental Science & Technology 40:894-899.
- Baker, J.I., and R.A. Hites. 2000. Is combustion the major source of polychlorinated dibenzo-p-dioxins and dibenzo-furans to the environment? A mass balance investigation. Environmental Science & Technology 34:2879-2886.
- Boyd, S.A., G. Sheng, B.J. Teppen, and C.T. Johnston. 2001. Mechanisms for the adsorption of substituted nitrobenzenes by smectite clays. Environmental Science & Technology 35:4227.
- Brzuzy, L.P., and R.A. Hites. 1996. Global mass balance for polychlorinated dibenzopdioxins and dibenzofurans. Environmental Science & Technology 30:1797-1804.
- Bumb, R.R., W.B. Crummett, S.S. Cutie, J.R. Gledhill, R.H. Hummel, R.O. Kagel, L.L. Lamparski, E.V. Luoma, D.L. Miller, T.J. Nestrick, L.A. Shadoff, R.H. Stehl, and J.S. Woods. 1980. Trace chemistries of fire: a source of chlorinated dioxins. Science 210:385-390.
- Chang, F.-R.C., N.T. Skipper, and G. Sposito. 1995. Computer simulation of interlayer molecular structure in sodium montmorillonite hydrates. Langmuir 11:2734-2741.
- Chappell, M.A., D.A. Laird, M.L. Thompson, H. Li, B.J. Teppen, V. Aggarwal, C.T. Johnston, and S.A. Boyd. 2005. Influence of smectite hydration and swelling on atrazine soption behavior. Environmental Science & Technology 39:3150.
- Chiou, C.T. 2002. Partition and adsorption of organic contaminants in environmental systems John Wiley & Sons, Hoboken, NJ.
- Chu, I.-H., H. Zhang, and D.V. Dearden. 1993. Macrocyclic chemistry in the gas phase: intrinsic cation affinities and complexation rates for alkali metal cation complexes of crown ethers and glymes. Journal of the American Chemical Society 115:5736-5744.
- Curtiss, G.P., P.V. Roberts, and M.V. Reinhard. 1986. A natural gradient experiment on solute transport in a sand aquifer. 4. Sorption of organic solutes and its influence on mobility. Water Resources Research 22:2059.
- Dougherty, D.A., and D.A. Stauffer. 1990. Acetylcholine binding by a synthetic receptor: implications for biological recognition. Science 250:1558-1560.

- EPA., U.S. 2007. Pilot survey of levels of polychlorinated dibenzo-p-dioxins, polychlorinated dibenzofurans, polychlorinated biphenyls and mercury in rural soils of the US. National Center for Environmental Assessment, Washington, DC; EPA/600/R-05/048F.
- Ferrario, J.B., and C.J. Byrne. 2002. Dibenzo-p-dioxins in the environment from ceramics and pottery produced from ball clay mined in the United States. Chemosphere 46:1297.
- Ferrario, J.B., D. McDaniel, and C.J. Byrne. 1999. The isomer distribution and congener profile of polychlorinated dibenzo-p-dioxins (PCDDs) in ball clay from the Misssissippi Embayment (Sledge, Mississsippi). Organohalogen compounds 40:1-5.
- Ferrario, J.B., C.J. Byrne, and D.H. Cleverly. 2000. 2,3,7,8-dibenzo-p-dioxins in mined clay products from the United States: Evidence for possible natural origin. Environmental Science & Technology 34:4524-4532.
- Fiedler, A., D. Schroeder, S. Shaik, and H. Schwarz. 1994. Electronic structures and gasphase reactivities of cationic late-transition-metal oxides. Journal of the American Chemical Society 116:10734.
- Fingler, S., B. Tkalcevic, Z. Frobe, and V. Drevenkar. 1994. Analysis of polychlorinated biphenyls, organochlorine pesticides and chlorophenols in rain and snow. Analyst 119:1135-1140.
- Franzblau, A., A. Demond, T. Towey, P. Adriaens, S.-C. Chang, W. Luksemburg, M. Maier, D. Garabrant, B. Gillespie, J. Lepkowski, C.-W. Chang, Q. Chen, and B. Hong. 2009. Residences with anomalous soil concentrations of dioxin-like compounds in two communities in Michigan, USA: A case study. Chemosphere 74:395.
- Gadomski, D., M. Tysklind, R.L. Irvine, P.C. Burns, and R. Andersson. 2004. Investigations into vertical distribution of PCDDs and mineralogy in three ball clay cores from the United States exhibitinh the natural formation pattern. Environmental Science & Technology 38:4956-4963.
- Gaus, C., O. Papke, N. Dennison, D. Haynes, G.R. Shaw, D.W. Connell, and J.F. Muller. 2001. Evidence for the presence of a widespread PCDD source in coastal sediments and soils from Queensland, Australia. Chemosphere 43:549-558.
- Gaus, C., G.J. Brunskill, D.W. Connell, J. Prange, J.F. Muller, O. Papke, and R. Weber. 2002. Transformation processes, pathways, and possible sources of distinctive polychlorinated dibenzo-p-dioxin signatures in sink environments. Environmental Science & Technology 36:3542-3549.
- Ghidini, E.U., F.; Ungaro, R.; Harkema, S.; El-Fadl, A. A.; Reinhoudt, D. N. . 1990. Complexation of alkali metal cations by conformationally rigid, stereoisomeric

- calix [4] arene crown ethers : a quantitative evaluation of preorganization. . Journal of the American Chemical Society 112:6979-6985.
- Gokel, G.W., L.J. Barbour, S.L. De Wall, and E.S. Meadows. 2001. Macrocyclic polyethers as probes to assess and understand alkali metal cation-pi interactions. Coordination Chemistry Reviews 222:127-154.
- Green, N.J.L., A. Hassanin, A.E. Johnston, and K.C. Jones. 2004. Observations on historical, contemporary, and natural PCDD/Fs. Environmental Science & Technology 38:715-723.
- Gu, C., H. Li, B.J. Teppen, and S.A. Boyd. 2008. Octachlorodibenzodioxin formation on Fe(III)-montmorillonite clay. Environmental Science & Technology 42:4758–4763.
- Hays, S.M., and L.L. Aylward. 2003. Dioxin risks in perspective: past, present, and future. Regulatory Toxicology and Pharmacology 37:202.
- Hoekstra, E.J., H. De Weerd, E.W.B. De Leer, and U.A.T. Brinkman. 1999. Natural formation of chlorinated phenols, dibenzo-p-dioxins, and dibenzofurans in soil of a Douglas fir forest. Environmental Science & Technology 33:2543-2549.
- Holmstrand, H., D. Gadomski, M. Mandalakis, M. Tysklind, R. Irvine, P. Andersson, and O. Gustafsson. 2006. Origin of PCDDs in ball clay assessed with compound-specific chlorine isotope analysis and radiocarbon dating. Environmental Science & Technology 40:3730-3735.
- Holt, E., R. Von Der Recke, W. Vetter, D. Hawker, V. Alberts, B. Kuch, R. Weber, and C. Gaus. 2008. Assessing dioxin precursors in pesticide formulations and environmental samples as a source of octachlorodibenzo-p-dioxin in soil and sediment. Environmental Science & Technology 42:1472-1478.
- Horii, Y., B. van Bavel, K. Kannan, G. Petrick, K. Nachtigall, and N. Yamashita. 2008. Novel evidence for natural formation of dioxins in ball clay. Chemosphere 70:1280-1289.
- Huang, G.-L., H. Xiao, J. Chi, W.-Y. Shiu, and D. Mackay. 2000. Effects of pH on the water solubility of selected chlorinated phenols. Journal of Chemical & Engineering Data 45:411.
- Hyun, S., L.S. Lee, and P.S.C. Rao. 2003. Significance of anion exchange in pentachlorophenol sorption by variable-charge soils. Journal of Environmental Quality 32:966-976.
- Israelachvili, J.N. 1992. Intermolecular and surface forces. 2nd ed. Academic Press, San Diego, CA.

- Jaynes, W.F., and S.A. Boyd. 1991. Hydrophobicity of siloxane surfaces in smectites as revealed by aromatic hydrocarbon adsorption from water. Clays and Clay Minerals 39:428-436.
- Jobst, H., and R. Aldag. 2000. Dioxine in Lagerstätten-Tonen. Umweltwissenschaften und Schadstoff-Forschung 12:2.
- Johnston, C.T. 1996. Sorption of organic compounds on clay minerals: A surface functional approach, p. 1-44, *In* B. L. Sawhney, ed. Reactions of organic pollutants with clays. Clay Minerals Society, Boulder, CO.
- Johnston, C.T., G. Sheng, B.J. Teppen, S.A. Boyd, and M.F. De Oliveira. 2002. Spectroscopic study of dinitrophenol herbicide sorption on smectite. Environmental Science & Technology 36:5067-5074.
- Kallies, B., and R. Meier. 2001. Electronic structure of 3d[M(H<sub>2</sub>O)<sub>6</sub>]<sup>3+</sup> ions from Sc(III) to Fe(III): a quantum mechanical study based on DFT computations and natural bond orbital analyses. Inorganic Chemistry 40:3101.
- Kjeller, L.O., K.C. Jones, A.E. Johnston, and C. Rappe. 1991. Increases in the polychlorinated dibenzo-p-dioxin and -furan content of soils and vegetation since the 1840s. Environmental Science & Technology 25:1619-1627.
- Laird, D.A. 1996. Interactions between atrazine and smectite surfaces, p. 86-100 Herbicide Metabolites in Surface Water and Groundwater, Vol. 630.
- Lee, J.-F., M.M. Mortland, C.T. Chiou, D.E. Kile, and S.A. Boyd. 1990. Adsorption of benzene, toluene, and xylene by two tetramethylammonium-smectites having different charge densities. Clays and Clay Minerals 38:113-120.
- Leuenberger, C., M.P. Ligocki, and J.F. Pankow. 1985. Trace organic compounds in rain. 4. identities, concentrations, and scavenging mechanisms for phenols in urban air and rain. Environmental Science & Technology 19:1053-1058.
- Li, H., T.R. Pereira, B.J. Teppen, D.A. Laird, C.T. Johnston, and S.A. Boyd. 2007. Ionic strength-induced formation of smectite quasicrystals enhances nitroaromatic compound sorption. Environmental Science & Technology 41:1251-1256.
- Ma, J.C., and D.A. Dougherty. 1997. The cation-pi interaction. Chemical Reviews 97:1303-1324.
- Mackay, D., W.Y. Shiu, and K.C. Ma. 1992. Illustrated Handbook of physical-chemical properties and environmental fate of organic chemicals. Lewis Publishers Inc., Chelsea, MI.
- Mader, B.T., K. UweGoss, and S.J. Eisenreich. 1997. Sorption of nonionic, hydrophobic organic chemicals to mineral surfaces. Environmental Science & Technology 31:1079-1086.

- Mandal, P.K. 2005. Dioxin: a review of its environmental effects and its aryl hydrocarbon receptor biology. Journal of Comparative Physiology B: Biochemical, Systemic, and Environmental Physiology 175:221-230.
- Means, J.C., S.G. Wood, J.J. Hassett, and W.L. Banwart. 1980. Sorption of polynuclear aromatic hydrocarbons by sediments and soils. Environmental Science & Technology 14:1524.
- Mooney, R.W., A.G. Keenan, and L.A. Wood. 1952. Adsorption of water vapor by montmorillonite. II. Effect of exchangeable ions and lattice swelling as measured by X-ray diffraction. Journal of the American Chemical Society 74:1371-1374.
- Nolan, T., K.R. Srinivasan, and H.S. Fogler. 1989. Dioxin sorption by hydroxy-aluminum-treated clays. Clays and Clay Minerals 37:487-492.
- Rappe, C., R. Anderson, M. Bonner, K. Cooper, H. Fiedler, F. Howell, S.E. Kulp, and C. Lau. 1997. PCDDs and PCDFs in sol and river sediment samples from a rural area in the United States of America. Chemosphere 34:1297-1314.
- Rappe, C.T., Mats; Andersson, Rolf; Burns, Peter C.; Irvine, Robert L. 2001. Dioxin in ball clay and kaolin. Organohalogen Compounds 51:259-263.
- Schmitz, M., G. Scheeder, S. Bernau, R. Dohrmann, and K. Germann. Dioxins in Primary Kaolin and Secondary Kaolinitic Clays. Environmental Science & Technology:null-null.
- Schwarzenbach, R.P., and J. Westall. 1981. Transport of non-polar organic compounds from surface water to groundwater, laboratory sorption studies. Environmental Science & Technology 15:1360-1367.
- Shiota, Y., and K. Yoshizawa. 2000. Methane-methanol conversion by the first-row transition-metal oxide ions: ScO<sup>+</sup>, TiO<sup>+</sup>, VO<sup>+</sup>, CrO<sup>+</sup>, MnO<sup>+</sup>, FeO<sup>+</sup>, CoO<sup>+</sup>, NiO<sup>+</sup>, and CuO<sup>+</sup>. Journal of the American Chemical Society 122:12317.
- Sun, Q., M. Altarawneh, B.Z. Dlugogorski, E.M. Kennedy, and J.C. Mackie. 2007. Catalytic effect of CuO and other transition metal oxides in formation of dioxins: theoretical investigation of reaction between 2,4,5-trichlorophenol and CuO. Environmental Science & Technology 41:5708.
- Tanford, C. 1980. The hydrophobic effect: Formation of micelles and biological membranes. 2nd ed. John Wiley & Sons, NY.
- Teppen, B.J., K. Rasmussen, P.M. Bertsch, D.M. Miller, and L. Schäfer. 1997. Molecular dynamics modeling of clay minerals. 1. Gibbsite, kaolinite, pyrophyllite, and beidellite. Journal of Physical Chemistry B101:1579-1587.

- Van Bladel, R., and A. Moreale. 1974. Adsorption of fenuron and monuron (substituted ureas) by two montmorillonite clays. Soil Science Society of America Journal 38:244-249.
- Voice, T.C., and W.J. Weber. 1983. Sorption of hydrophobic compounds by sediments, soils and suspended solids—I. Theory and background. Water Research 17:1433-1441.
- Waite, D.T., N.P. Gurprasad, A.J. Cessna, and D.V. Quiring. 1998. Atmospheric pentachlorophenol concentrations in relation to air temperature at five Canadian locations 37:2251-2260.
- Warshel, A. 2003. Computer simulations of enzyme catalysis: methods, progress, and insights. Annual Review of Biophysics and Biomolecular Structure 32:425.
- Wild, S.R., S.J. Harrad, and K.C. Jones. 1992. Pentachlorophenol in the Uk Environment .1. a Budget and Source Inventory 24:833-845.
- Xu, W.Z., C.T. Johnston, P. Parker, and S.F. Agnew. 2000. Infrared study of water sorption on Na-, Li-, Ca-, and Mg-exchanged (SWy-1 and SAz-1) montmorillonite. Clays and Clay Minerals 48:120-131.
- Zhu, D.Q., S.H. Hyun, J.J. Pignatello, and L.S. Lee. 2004. Evidence for pi-pi electron donor-acceptor interactions between pi-donor aromatic compounds and pi-acceptor sites in soil organic matter through pH effects on sorption. Environmental Science & Technology 38:4361-4368.

### **CHAPTER II**

# MECHANISMS ASSOCIATED WITH THE HIGH ADSORPTION OF DIBENZO-P-DIOXIN FROM WATER BY SMECTITE CLAYS

#### **ABSTRACT**

Clay minerals may be an important sorptive phase for dioxins in soils, and are often found in natural clay deposits. Sorption experiments demonstrated that smectites, especially Cs-saponite, effectively adsorbed dibenzo-p-dioxin (DD) from water, approaching 0.8 % (wt/wt). Adsorption was promoted by exchangeable cations with low hydration energies, and negative charge in the smectite arising from the tetrahedral siloxane sheets. X-ray diffraction measurements revealed that as DD loading increased to  $\geq 8,000$  mg/kg the clay basal spacing increased abruptly from 12.3 to 15.2 Å demonstrating DD intercalation. The 12.3 Å spacing provides an interlayer distance that closely matches the molecular thickness of DD. In this configuration DD is essentially dehydrated as it interacts with the opposing hydrophobic siloxane sheets and with co-planar Cs<sup>+</sup> via one of the dioxin ring oxygens. Ab initio calculations suggest that geometrical structures form at higher loadings in which intercalated DD molecules adopt a butterfly geometry sandwiched between dehydrated interlayer Cs<sup>+</sup> and the siloxane surface, consistent with the 15.2 Å spacing, wherein Cs<sup>+</sup> interacts with dioxin ring oxygens and benzene ring  $\pi$ -electrons. Fourier transformation infrared measurements confirm that adsorbed DD is present in orientations that are not parallel with the interlayer planar siloxane surfaces of smectite.

## INTRODUCTION

Polychlorinated dibenzo-p-dioxins and dibenzofurans (PCDD/Fs) are among the most toxic organic compounds in the environment due to their potency as aryl hydrocarbon receptor ligands. These carcinogenic and persistent pollutants are ubiquitous in the environment. They are produced by over 20 known anthropogenic processes such as waste incineration and pesticide manufacture (Brzuzy and Hites, 1995; Brzuzy and Hites, 1996; Kjelier et al., 1991), and natural processes such as forest fires (Hoekstra et al., 1999). Among the dioxin congeners, 2,3,7,8tetrachlorodibenzo-p-dioxin (TCDD) is considered most toxic. It is classified by the International Agency for Research on Cancer as a group I carcinogen (known to cause cancer in humans), and as "carcinogenic to humans" by USEPA (Steenland et al., 2004), and poses many other potential adverse health effects (Bertazzi et al., 2001). Since PCDD/Fs have exceptionally low water solubilities, high octanol-water partition coefficients, and high chemical and biological stabilities, sorption by soils and sediments is a predominant environmental fate for these compounds (Laine et al., 1997). As such, soils and sediments are included in the World Health Organization's TEF/TEQ regulations for PCDD/Fs contaminated matrices. The action levels for PCDD/Fs in residential soils are 1 ppb TEQ by the U.S. Agency for Toxic Substances and Disease Registry (De Rosa et al., 1997), and in Michigan, 90 ppt TEQ (2006).

Organic matter is often considered the primary sorptive compartment in soils for PCDD/Fs hence controlling their soil-water distribution and environmental fate (Frankki et al., 2007; Walters and Guiseppi-Elie, 1988). Recent reports have documented high concentrations of PCDD of unknown origin in natural prehistoric

clay mineral deposits such as ball clays which have complex compositions that include smectites and kaolinite. Several incidents of PCDD contaminated meat, baby food, farmed catfish and salmon were linked to such dioxin-contaminated minerals that had been used as animal feed additives (Ferrario et al., 2000; Hayward and Bolger, 2005; Hayward et al., 1999). On a surface area basis clay minerals are the dominant component of soils, subsoils, and aquifer materials, and should be considered potentially important environmental sinks for PCDD/Fs (McBride, 1994). In this context smectites are especially important due to their widespread distribution, large cation exchange capacity, high surface areas (~800 m<sup>2</sup>/g), and water-induced expansibility (Sposito, 1984). Interestingly, dioxins are present at inexplicably high levels even in rural soils isolated from the common known sources of anthropogenic dioxins (Rappe et al., 1997; Rogowski and Yake, 2005). The environmental chemistry of dioxins in surface and subsurface soils and geologic deposits containing smectite clay minerals is poorly understood hence limiting our ability to predict fate and manage risk.

Previous studies on adsorption of neutral organic compounds (NOCs) by smectite clays demonstrated that in general NOC-smectite interactions were strongly influenced by the nature of exchangeable interlayer cations, the magnitude and distribution of clay layer charge, and the structural characteristics of the NOCs (Aggarwal et al., 2006; Boyd et al., 2001; Haderlein and Schwarzenbach, 1993; Haderlein et al., 1996; Johnston et al., 2002). For example, studies on sorption of semipolar nitroaromatic compounds (NACs) and comparatively nonpolar trichloroethene (TCE) from water by a series of alkali or alkali-earth cation exchanged

smectite clays showed that adsorption by Cs<sup>+</sup>- or K<sup>+</sup>-saturated smectites were 10 to 100 times higher than those by the corresponding Na<sup>+</sup>- or Ca<sup>2+</sup>-saturated smectites (Aggarwal et al., 2006; Johnston et al., 2002). The hydration propensity of interlayer cations was a major factor in the intercalation of NOCs. Lower hydration energy and the resultant smaller hydrated radius of exchangeable cations, e.g., K<sup>+</sup>, Cs<sup>+</sup>, would plausibly provide more unobscured hydrophobic planar clay siloxane surface adsorption domains, and manifest an optimal interlayer spacing corresponding to the approximate thickness of the adsorbed molecule, enabling partial dehydration of the sorbate, which is an energetically favorable process (Fedorov et al., 2004). Direct interactions/complexations between weakly hydrated alkali cations such as K+ and  $Cs^+$  and electron donating groups (e.g., oxygen, nitrogen, sulfur) or aromatic  $\pi$ systems of NOC molecules in aqueous solution have been shown to be energetically feasible (Chu et al., 1993; Ghidini et al., 1990; Glendening et al., 1994). Such interactions could further promote the adsorption and intercalation of NOCs by smectite clays, as been shown in the case of NACs (Boyd et al., 2001; Johnston et al., 2002), since the interlayer cations are highly concentrated in the confined sub-aqueous interlayer regions (Aggarwal et al., 2007; Boyd et al., 2001; Johnston et al., 2002).

The present study was initiated to examine the adsorption of an important class of persistent organic pollutants, namely dibenzodioxins and dibenzofurans, by smectite clays of different structures and saturated with different exchangeable cations ( $K^+$ ,  $Cs^+$  and  $Ca^{2+}$ ). A suite of complimentary methods including detailed adsorption

experiments, X-ray diffraction (XRD), infrared spectroscopy and *ab initio* calculations, were used to examine adsorption of representative members, viz, dibenzo-p-dioxin (DD) and dibenzofuran (DF), by smectites. Our results show very high adsorption of DD (~0.8% wt/wt), and provide molecular scale insight into the forces and mechanisms involved in the adsorption process.

# MATERIALS AND METHODS

Clays and Chemicals. Reference smectites (SWy-2, SapCa-2,Upton and SHCa-1), obtained from the Source Clays Repository of the Clay Minerals Society at Purdue University, West Lafayette, IN, were used in this study. Their major physicochemical characteristics are listed in Table II-1. The preparation of cation saturated montmorillonite followed the method of Arroyo *et al.*(Arroyo et al., 2005). Briefly, the <2 μm clay fraction was collected by wet sedimentation, suspended in 0.1 M KCl, CaCl<sub>2</sub> or CsCl for 24h, then centrifuged and resuspended repeatedly to saturate the exchangeable cation sites. Excess salts were removed by rinsing with deionized water. Clays were then quick-frozen, freeze-dried, and ground with a mortar and pestle.

Dibenzo-p-dioxin with purity >99% was purchased from Chem Service Inc. (West Chester, PA), and dibenzofuran with purity >99% was purchased from Aldrich Chemical Co. (Milwaukee, WI), and used as received. The logarithm of octanol-water partition coefficients are 4.3, 4.12 for DD and DF, and their water solubilities are 0.901 and 3.1 mg L<sup>-1</sup>, respectively (Shiu et al., 1988; Yalkowsky and Dannenfelser, 1992).

Table II-1. Characteristics of clay minerals used as adsorbents for dibenzodioxin and dibenzofuran

Sample	Smectite clay type, and octahedral sheet type	Tetrahedral charge (%) <sup>a</sup>	Cation exchange capacity (CEC) (cmol/kg)	Surface area (m <sup>2</sup> /g) <sup>d</sup>	BET N <sub>2</sub> surface area <sup>a</sup>	OC% <sup>e</sup>	Surface charge density (µmol/m <sup>2</sup> ) <sup>f</sup>
SWy-2	montmorillonite, dioctahedral	3.6	83.6	766	31.82	0.07	1.09
Upton	montmorillonite, dioctahedral	1.6	113.3	730	39.8		1.55
SHCa-1	hectorite, trioctahedral	14	86.4	743	63.19		1.16
SapCa-2	saponite, trioctahedral	102	97.4 <sup>c</sup>	750		0.128	1.30

a. Source Clays Repository of the Clay Minerals Society at Purdue University, West Lafayette, IN.

b. Measured by BaCl<sub>2</sub> compulsive exchange method (Gillman, 1979).

c. Measured by qualitative scanning electron microscopy (SEM)/energy dispersive X-ray spectroscopy (EDS) method (Christidis and Dunham, 1997).

d. Calculated from structural formula.

e. Organic C content. Measured by Shimadzu TOC-5000A.

f. Assumed by CEC/surface area.

Table II-2. Computed binding energies ( $\Delta E_{ZPE}$ ) and geometrical parameters for  $Cs^+$ -dibenzodioxin complexes illustrated in Figure II-3.

	ΔΕ <sub>ΖΡΕ</sub> kcal/mol		Cs <sup>+</sup> -oxygen distance, r Å		bending angle between two aromatic rings, α	
	HF	DFT	HF	DFT	HF	DFT
complex I	-6.26	-8.96	3.327	3.263	180.0	180.0
complex II	-10.96	-12.23	3.452	3.421	149.63	152.71
complex III	-10.48	-12.18	4.416	4.469	161.92	169.80
Cs <sup>+</sup> -water	-11.77	-12.35	3.148	3.107		

Sorption Isotherm Measurement. All sorption isotherms were determined using a batch equilibrium method. Freeze-dried clay (8 to 30 mg) was suspended in glass vials containing 4.0 mL (for Ca<sup>2+</sup> and K<sup>+</sup>) or 20.0 mL (for Cs<sup>+</sup>) solutions of various concentrations of DD/DF (0.2 to 0.8 mg L<sup>-1</sup> for DD, 0.28 to 2.8 mg L<sup>-1</sup> for DF); ionic strength was maintained at 0.01M CsCl, 0.01M KCl or 0.005M CaCl<sub>2</sub>. The vials were capped with Teflon-lined septa, shaken reciprocally at 40 rpm for 24 h at room temperature (23±2 °C), then centrifuged at 1667 g for 20 min. Preliminary studies showed that equilibrium was achieved within this time. The concentrations of DD or DF in supernatants were analyzed by high performance liquid chromatography (HPLC, Perkin-Elmer, Norwalk, Connecticut) using an UV-visible detector set at 223 nm for DD and 285 nm for DF. Methanol (0.5 mL) was added to all HPLC vials before

injection to prevent DD or DF adsorption onto glassware during HPLC analysis. A Supelco Discovery reverse phase C18 column was used. The mobile phase was a mixture of 80% methanol and 20% water with a flow rate of 1.0 mL/min. The amount sorbed was calculated from the difference between the concentrations of blanks (no clay) and the supernatants from the clay-containing samples.

**X-Ray Diffraction (XRD)**. Basal spacings of clays were determined by XRD analysis. Loadings of DD or DF on all clays, except DD on Cs-saponite, were too low to show any changes in XRD patterns. The d-spacing remained at 12.4 Å for all K-saponite samples, and at 14.9 Å for the Ca-Saponite samples, hence only XRD data for DD Cs-saponite are presented here. Cs-saponite suspensions (3.0 L) with different DD equilibrium concentrations were filtered through membrane filters (47 mm, 0.45  $\mu$ m pore size, Millipore Co. Bedford, MA). The particles were transferred into vials containing 200  $\mu$ L of 0.01 M CsCl, mixed, dropped on glass slides, and allowed to dry overnight at ambient conditions to obtain oriented clay films. The XRD patterns were recorded as described previously (Johnston et al., 2002).

Computational Methods. The optimized geometries and energies of Cs<sup>+</sup>-DD complexes in the gas phase have been obtained using both Hartree-Fock (HF) and density functional theory (DFT), specifically the Becke three-parameter exchange functional (B3) (Becke, 1993) and the Lee–Yang–Parr correlation functional (LYP) (Lee et al., 1988), incorporated in the GAMAESS ver. 07 (Fedorov et al., 2004) and PCGAMESS 7.15 packages (Granovsky). The aug-cc-pVTZ basis sets were chosen for the carbon, oxygen and hydrogen atoms (Dunning, 1989) and the LANL2DZ basis

set with ECPs augmented by 6d polarization function with energy optimized exponent ( $\alpha_d$ =0.19) was used for cesium (Hay and Wadt). All complexes were fully optimized using a threshold of 0.00003 au, and the equilibrium nature of each stationary point was further investigated by frequency analysis. The binding energies  $\Delta E$  were determined as the difference between the optimized energies of the complexes and the sum of the energies of separate cation and DD. To examine the accuracy of the calculations, the geometry and zero-point energy corrected binding energy ( $\Delta E_{ZPE}$ ) of the Cs<sup>+</sup>-H<sub>2</sub>O complex were calculated using B3LYP. The geometry and resultant binding energy of -12.35 kcal/mol are in good agreement with previous experimental and quantum computational studies of this system, where binding energies are in the range of  $\sim$  -10.23 to -13.69 kcal/mol (Dzidic and Kebarle, 1970; Glendening and Feller, 1995).

FTIR measurements. Polarized FTIR spectral measurements were performed as described previously (Johnston et al., 2002) to determine orientation of the molecular plane of intercalated DD relative to the planar siloxane surface of smectites. A suspension containing 1 mg of Cs-saponite dispersed in 1 mL was allowed to dry on the surface of a ZnSe IRE in a 9-bounce horizontal ATR-FTIR cell (Pike Technology) using a Perkin Elmer 2000/GX FTIR spectrometer equipped with a MCT detector using 2 cm<sup>-1</sup> resolution and co-addition of 64 scans. DD was introduced in 1 mL aliquots, each containing 0.8 ppm of DD, and polarized spectra were recorded of the aqueous deposits. After each aliquot was added, polarized ATR-FTIR spectra were recorded corresponding to the A<sub>s</sub> and A<sub>p</sub> elements. The aqueous portion was carefully

removed from the cell and another aliquot was added. This procedure was repeated twenty times and the corresponding surface concentrations of DD sorbed on Cs-saponite, estimated from parallel sorption experiments, were 6000 to 8000  $\mu$ g/kg.

# RESULTS AND DISCUSSION

Sorption isotherms of DD and DF from water by different Cs-smectites are shown in Figures II-1A-D. Sorption strongly depends on clay type. The strongest adsorption was observed for Cs-saponite, where DD loadings of nearly 0.8% (w/w) were achieved at a relative equilibrium aqueous concentration of 0.5 (aqueous concentration/aqueous solubility). This is by far the largest DD sorption reported for any clay mineral or for soil organic matter (SOM). Other Cs-saturated smectites, i.e., Upton, SHCa and SWy-2 show lower uptake of DD than saponite (about 27%, 9.7%, and 5.8% respectively, with respect to saponite at relative equilibrium aqueous concentration of 0.5), which are still comparable to the amount of estimated sorption by SOM based on partitioning theory and related empirical equations that estimate sorption coefficients from octanol-water partition coefficients (Chiou et al., 1983).

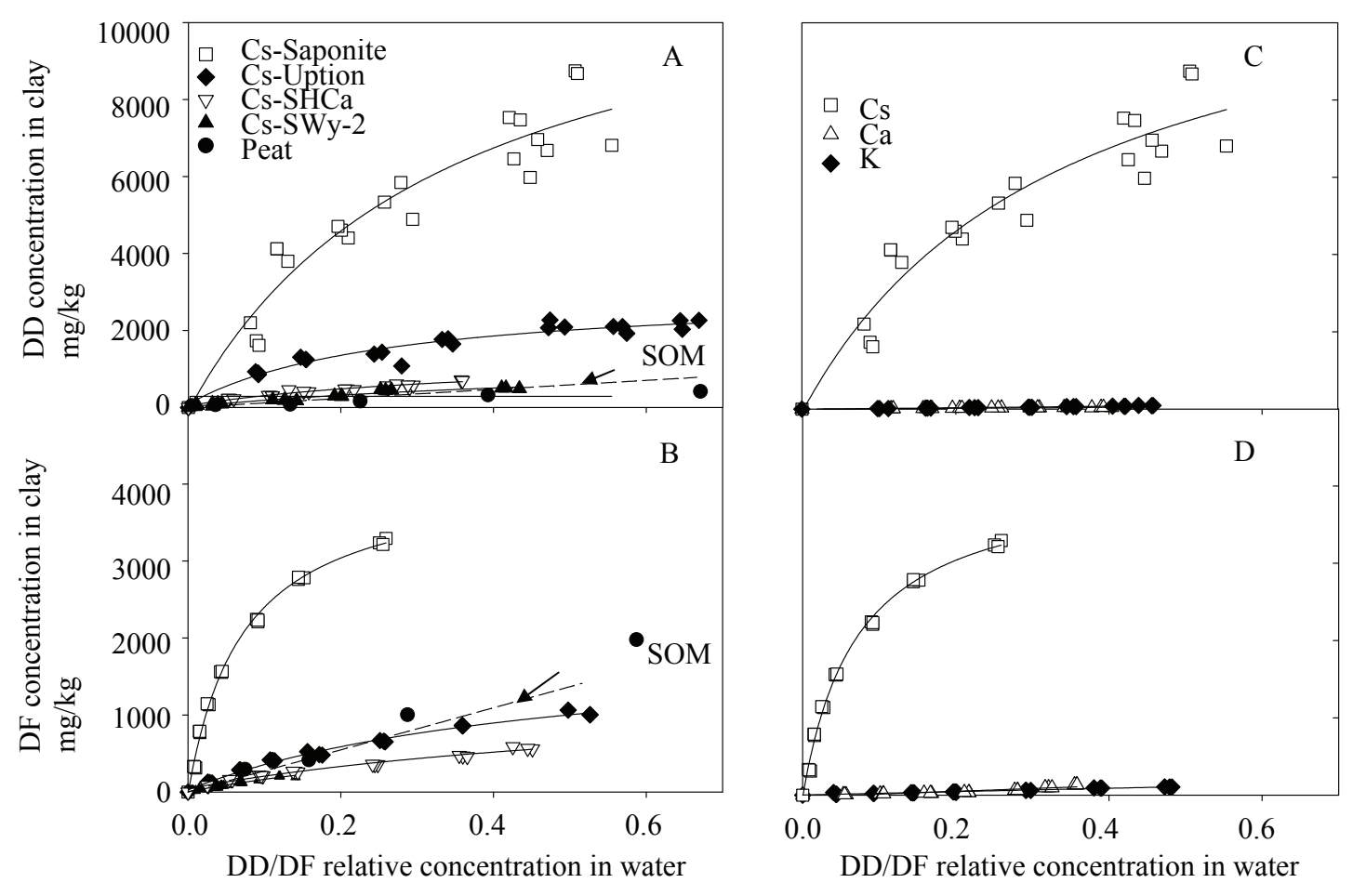


Figure II-1. Adsorption isotherms representing (A) dibenzodioxin (DD) or (B) dibenzofuran (DF) uptake from water by Cs-saturated smectites (saponite, SapCa-2; montmorillonite, Upton and SWy-2; hectorite, SHCa) and comparison of (C) dibenzodioxin (DD) or (D) dibenzofuran (DF) adsorption by homoionic saponite saturated with different exchange cations. The amount sorbed by soil organic matter was estimated using the equation:  $\log K_{OM} = 0.904 \log K_{OW} - 0.779$  (Chiou et al., 1983)

Comparisons among Cs<sup>+</sup>-saturated smectites possessing dominant octahedral charge (Upton, SHCa and SWy-2) show a trend that higher sorption is related to higher CEC (within this relatively narrow range of charge densities), indicating that direct interaction between Cs<sup>+</sup> and dioxin is an important factor in adsorption. This interaction could be favorable compared to the hydration of Cs<sup>+</sup>, since as shown in XRD and NMR studies (Bérend et al., 1995; Laperche et al., 1990), Cs-smectites are poorly hydrated, and contain ≤ one layer of water in the interlayer at 100% relative humidity or in bulk water, with  $\sim 1.4$  water molecules per half unit cell of the smectites. The high DD adsorption by saponite is likely related to its high tetrahedral charge, essentially 100%. In saponite, structural negative charge resides exclusively in the tetrahedral Si-O layers, which form the surfaces of the individual 2:1 clay layers. The negative charge arising from tetrahedral substitution is more localized, being spread over fewer surface oxygens than in octahedrally charged smectites, and resides closer to the planar surfaces of the clays. This manifests strong binding of interlayer Cs<sup>+</sup> cations in the form of inner-sphere complexes with siloxane oxygens, and further limits the number of water molecules in the Cs<sup>+</sup> hydration shell (Sutton and Sposito, 2001). This property seems important for DD sorption, by allowing both more favorable cation-DD interactions and by providing larger adsorption domains consisting of siloxane surface between exchangeable cation either devoid of water or with weakly held water. The same dependence of DF sorption on smectite type is observed (Figure II-1B), but with reduced sorption capacities. Compared to saponite, the amounts of adsorbed DF at the relative aqueous concentration of 0.5 for Upton,

SHCa and SWy-2 are 25%, 14% and 6.4%, respectively. All smectites contain less than 0.15% OM, and the high affinity of DD or DF for Cs-smectite cannot be reconciled based on OM content.

Sorption of DD and DF was substantially affected by the type of exchangeable cation on the clay (Figure II-1C, II-1D). The sorption capacities of DD by saponite are in the order: Cs<sup>+</sup>>>K<sup>+</sup>>Ca<sup>2+</sup>, and the latter two are 91 and 152 times smaller than that by Cs-saponite when compared at a relative concentration of 0.5. These observations are consistent with our earlier results on NAC sorption (Johnston et al., 2002), and with the concept that exchangeable cations, and specifically their hydration properties, strongly influence sorption through direct interactions with adsorbed molecules, and via their influence on exposed hydrophobic planar clay surface domains between exchangeable cations, as well as interlayer swelling (Aggarwal et al., 2006; Boyd et al., 2001; Fedorov et al., 2004; Johnston et al., 2002). The large differences in sorption between Ca-, K-, and Cs-smectites imply both that the clay interlayer is an important sorption site and that the clay itself, rather than any SOM associated with the clay, dominates the sorption of DD and DF.

Regarding specific interactions, our quantum molecular calculations indicate that alkali or alkali earth cations can have strong interactions, i.e. cation- $\pi$  or cation-O, with DD and DF. Such interactions face competition primarily from water molecules in the hydration shell of interlayer cations. The comparatively weak hydration of exchangeable Cs<sup>+</sup> should logically favor such direct Cs-DD/DF interactions. In a previous study (Aggarwal et al., 2006), it was estimated that the hydrated radii of Ca<sup>2+</sup>

or K must overlap in the interlayer regions of homoionic saponite, meaning that DD or DF would have to compete with water for interlayer adsorption sites. In contrast, hydrated Cs<sup>+</sup> cations were projected to occupy only about 67% of the interlayer space (Aggarwal et al., 2006) manifesting less competition with water and greater accessibility to Cs<sup>+</sup> in the Cs-smectite interlayers for adsorption DD/DF. This may help explain why Cs-smectite is a much more effective sorbent for DD/DF than are Kand Ca-smectites. Interestingly, compared to DD or DF, NACs bind more favorably to K-smectites (Boyd et al., 2001; Johnston et al., 2002). Perhaps the comparatively smaller size of single-ring NACs and the comparatively larger negative charge on -NO<sub>2</sub> group oxygens leads to stronger interactions between alkali cations and -NO<sub>2</sub> group oxygens than to the dioxin and furan ring oxygens. Accordingly, NACs may be able to access a greater portion of the interlayer regions of K-smectites by displacing water and forming complexes with K + (Aggarwal et al., 2006; Johnston et al., 2002). Such results do illustrate the remarkably subtle factors that can coalesce to create high affinity smectite-based adsorbents for specific NOCs.

The basal spacing of Cs-saponite increased sharply from 12.3 Å to ~15.3 Å as loadings reach ~8000 mg/kg of adsorbed DD (Figure II-2). There was no sign in the XRD patterns of any crystal DD formation via precipitation on the clay surface during the adsorption process. The expanded spacings demonstrate the intercalation of DD in Cs-saponite. The adsorption process is favored by gaining enthalpic energy from its interactions with both clay surfaces as well as interlayer cations, and entropic energy

by partitioning of DD from bulk water into subaqueous environment of the clay interlayer (Fedorov et al., 2004). However, unlike the gradual increase in d-spacing to ~12.5 Å with increasing amounts NACs adsorbed (Johnston et al., 2002), the discontinuous increase in basal spacing by ~3.0 Å observed here when DD loadings reach approximately 8000 mg/kg suggests at least two different types of interlayer DD molecular orientations involved in adsorption.

The possible orientations and interactions of interlayer DD were evaluated by calculations of Cs<sup>+</sup>-DD complexes in the gas phase. These gas phase calculations are useful because electrostatic interactions are dominant in the smectite interlayers, and other possible interactions such as van der Waals interactions and interactions between the clay surface oxygens and  $\pi$  electron system of DD molecule would be less energetic compared with direct Cs<sup>+</sup>-DD interactions (Pelmenschikov and Leszczynski, 1999). The geometrical structures and parameters of all three possible complexes calculated at the HF and DFT levels are given in Table II-2. The inclusion of electron correlation and exchange effects with the DFT method generally gives more accurate geometries and energy predictions for noncovalent interactions, thus the results of DFT method are used for the comparisons below. Complex I has a planar configuration of C<sub>2v</sub> symmetry; the DD molecular plane is parallel to the siloxane surface, and Cs<sup>+</sup> is co-planar with the two oxygens of the dioxin ring and in close contact (3.263 Å) with one of them (Figure II-3). This is predominantly an electrostatic interaction between Cs<sup>+</sup> and an oxygen on the dioxin ring. The binding energy of Complex I (-8.96 kcal/mol, Table II-2) is about 3.39 kcal/mol smaller than that of Cs<sup>+</sup>-H<sub>2</sub>O complex, and the configuration is a possible transition state which is characterized by possessing one imaginary frequency of -23.04 cm<sup>-1</sup>. However, this planar structure might be stabilized by the planar siloxane surfaces, because DD could fit between the clay interlayers (~3 Å interlayer distance) and interact directly with both opposing siloxane surfaces to minimize unfavorable DD interactions with bulk water. Thus, this interaction is likely promoted by the favorable dehydration entropy gain of the DD molecules. This orientation for Complex I is the type of complex previously documented for NACs (Boyd et al., 2001; Johnston et al., 2002), and provides a structural hypothesis for DD-smectite complexes characterized by ~12.5 Å basal spacings (Figure II-2).

In Complex II,  $Cs^+$  interacts with both oxygen atoms of the DD molecule. It has a butterfly configuration of  $C_{2v}$  symmetry(Figure II-3), with the  $Cs^+$  cation sitting above the dioxin ring of DD. The distance between  $Cs^+$  and the DD oxygens is 3.421 Å (Table II-2). Complex III has  $C_s$  symmetry, with the  $Cs^+$  cation sitting above one of the benzene rings of DD and closely interacting with the  $\pi$ -electrons of the benzene ring and the dioxin ring oxygens (Figure II-3). The distance between  $Cs^+$  and DD oxygen is 4.469 Å (Table II-2). The binding energies for complexes II and III, -12.24 kcal/mol and -12.18 kcal/mol respectively, are both significantly larger than that for Complex I, and similar to that of the  $Cs^+$ -H<sub>2</sub>O complex (-12.35 kcal/mol). As more

DD molecules are adsorbed in the interlayer region, it apparently becomes energetically feasible for DD to displace more water molecules from the Cs<sup>+</sup> hydration shell to form Complex II and/or Complex III. The presumed energy requirement for expansion of the basal spacing to ~15 Å against the electrostatic attractions between clay layers and interlayer cations is apparently provided by the enthalpy gains associated with Complex II and Complex III. The bent DD molecule inserted between Cs<sup>+</sup> and the clay siloxane surfaces as in Complexes II or III would add roughly 3.3 Å to the total thickness (total of 15.4 Å, Figure II-3), which compares favorably to the measured basal spacing (Figure II-2). The conformational transition from entropy-favorable Complex I to the more favorable enthalpies of Complexes II and III with increasing adsorption of DD provides a possible rationale for the discontinuous shift of Cs-saponite basal spacings from 12.3 Å to 15.3 Å observed by XRD.

Polarized ATR-FTIR spectra of DD adsorbed to Cs-saponite in aqueous suspension are shown in Figure II-4. Both the  $A_s$  and  $A_p$  spectra are dominated by the v(Si-O) bands of the Cs-saponite clay in the 950 to 1100 cm<sup>-1</sup> region (Ras et al., 2007). The presence of adsorbed DD is confirmed by the DD bands at 1284, 1298 and 1492 cm<sup>-1</sup>. These bands correspond to in-plane vibrational modes (i.e., vibrational motions that are within the molecular plane of the DD molecule). In prior work, a similar approach has been used to determine the molecular orientation of NACs adsorbed to smectite surfaces (Johnston et al., 2002). The polarization behavior of the in-plane and out-of-plane vibrational modes of dinitro-o-cresol showed that in the adsorbed

state it was oriented with its molecular plane parallel to the siloxane surface. In contrast, the in-plane vibrational modes of DD adsorbed by Cs-smectite have similar intensities in both the A<sub>s</sub> and A<sub>p</sub> polarized ATR-FTIR spectra. These results indicate the adsorbed DD is *not* oriented with its molecular plane parallel to the clay surface but are consistent with the molecular orientation where the molecular plane of DD is tilted with respect to the surface of the clay. These results are consistent the X-ray diffraction results and *ab initio* calculations.

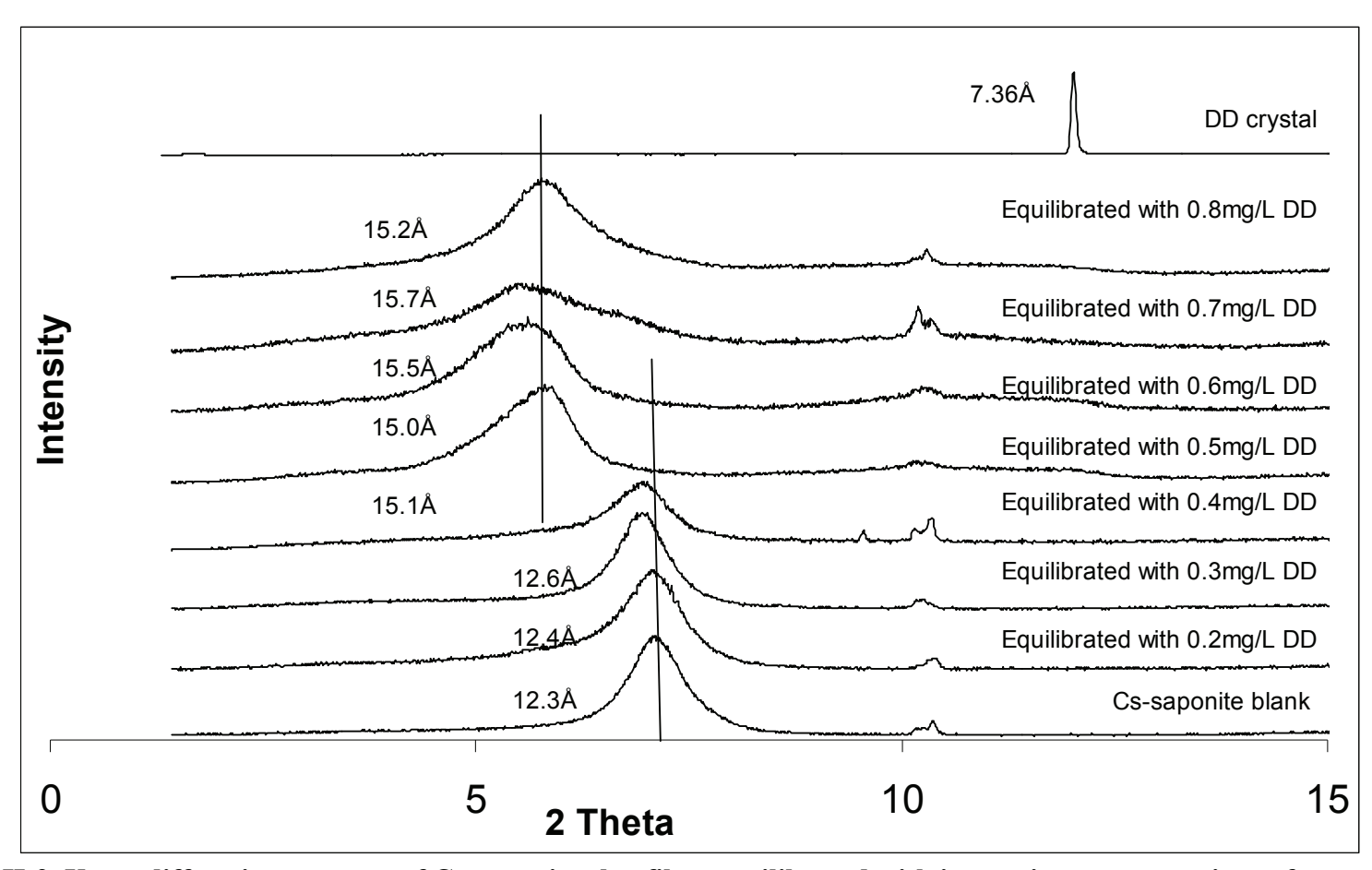


Figure II-2. X-ray diffraction patterns of Cs-saponite clay films equilibrated with increasing concentrations of aqueous dibenzodioxin (DD) solutions, Cs-saponite blank (no DD adsorbed) and crystalline DD. 2 Theta represents the diffracted angle relative to the incident X-ray beam.

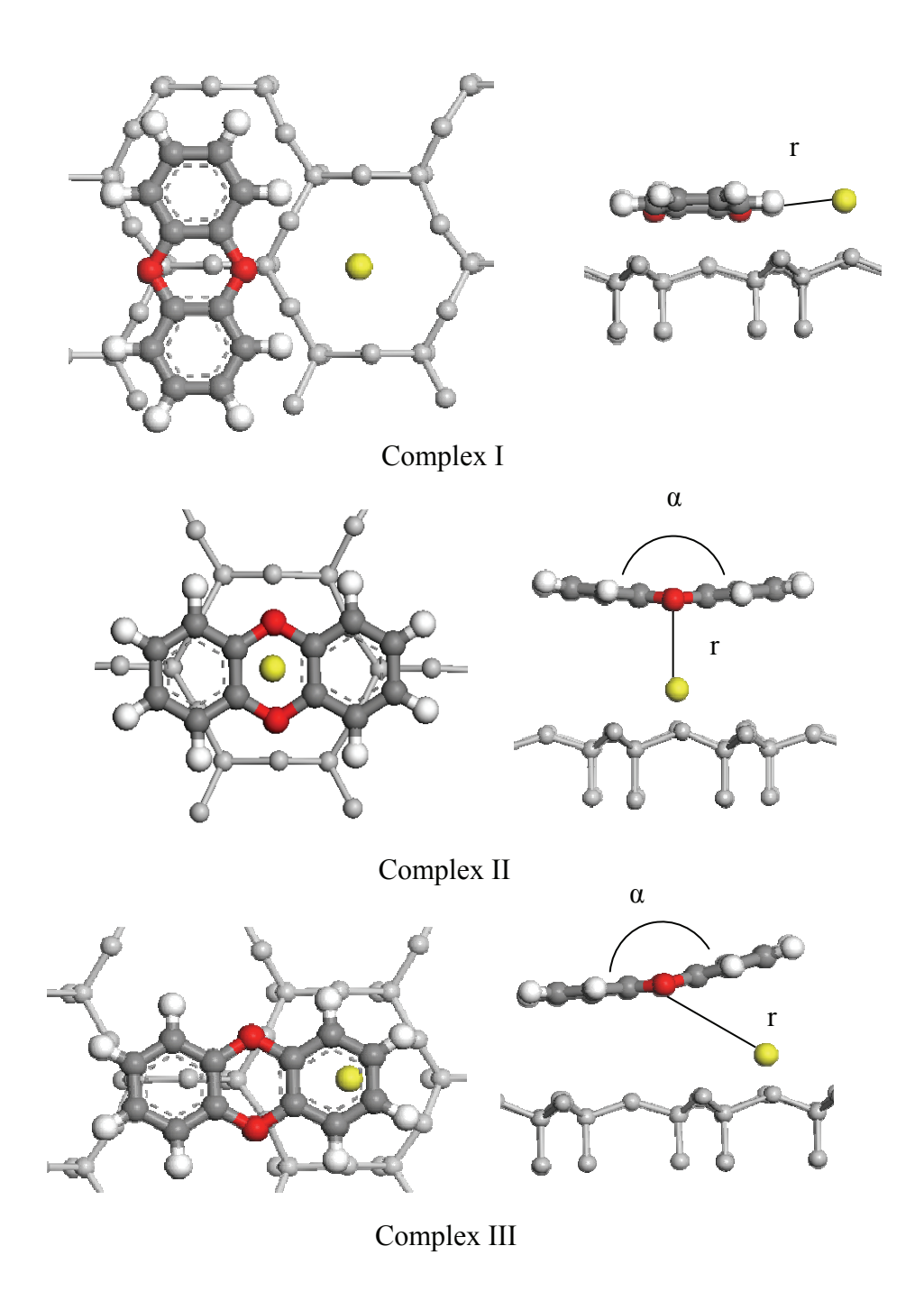


Figure II-3. Schematic views of three possible conformations of  $Cs^+$ -dibenzodioxin complexes with respect to the siloxane surface of smectite clay; top (left) and side views. The atom coloring scheme for atoms is Cs = yellow, O = red, H = white, C = gray, tetrahedral siloxane of clay minerals=light gray. Geometrical parameters are listed in table II-2. (I)  $C_{2v}$  symmetry; (III)  $C_{3v}$  symmetry.

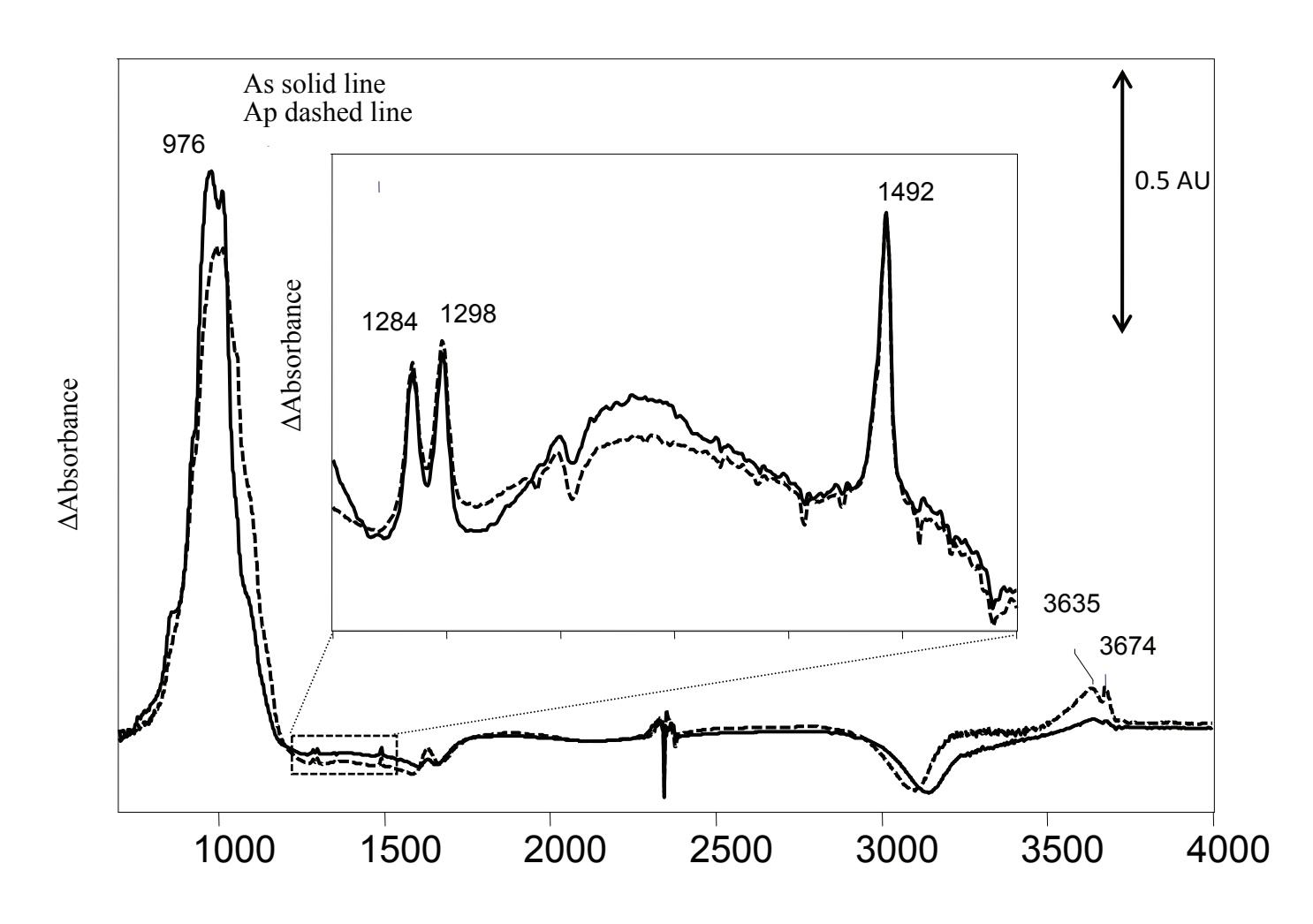


Figure II-4. Polarized ATR-FTIR spectra of dibenzodioxin (DD) sorbed to Cs-saponite in aqueous suspension. The in-plane vibrational bands of DD at 1248, 1298 and 1492 cm<sup>-1</sup> are magnified in the insert.

In summary, a high level of DD adsorption by Cs-saponite was observed by batch adsorption experiments, and intercalation of DD was confirmed by XRD. The influences of different interlayer cations, CEC and clay structural charge location on adsorption of DD revealed that weakly hydrated interlayer cation such as Cs + interact with DD directly in several different geometrical arrangements. Weak interlayer cation hydration, especially for Cs<sup>+</sup>, also provides more dehydrated clay siloxane surface and more vacant interlayer volume to accommodate hydrophobic DD molecules. As suggested by gas phase quantum calculations DD adsorbed at lower loadings in the smectite interlayer orients with its molecular plane parallel to the clay surfaces and coplanar with Cs<sup>+</sup>, retaining an optimal minimum interlayer spacing for the simultaneous interaction with the planar siloxane surfaces of opposing clay layers (and minimal interaction with water) as an entropy favorable configuration. Additionally, DD may intercalate between Cs<sup>+</sup> and clay surface when a sufficient amount of DD accumulates in the interlayer. In the latter configuration, the displacement of hydration water of Cs<sup>+</sup>, and the direct interaction of  $Cs^+$  with the dioxin ring oxygens as well as  $\pi$  electrons of the benzene rings, is apparently energetically favorable enough to cause expansion of the clay layers. The findings presented here are in compliance with our previous adsorption studies on NOCs such as TCE and NACs. All cases emphasize that the hydration state of interlayer cations of smectite clay minerals strongly affects the adsorption of NOCs. The confluence of clay-related factors with the structural properties of the solute can result in unique reaction mechanisms and adsorbate

configurations, leading to high affinity smectitic adsorbents, as illustrated here for DD adsorption by Cs-saponite. Such adsorption mechanisms and forces involving clay mineral interactions should be considered with traditional NOC-SOM partitioning models to give a more comprehensive understanding of the environmental transport and fate of DD/DF in soils, subsoils and aquifer materials, and their association with certain clay mineral deposits.

LITERATURE CITED

### LITERATURE CITED

- 2006. Part 201 generic cleanup criteria tables. Michigan Department of Environmental Quality.
- Aggarwal, V., Y.-Y. Chien, and B.J. Teppen. 2007. Molecular simulations to estimate thermodynamics for adsorption of polar organic solutes to montmorillonite. European Journal of Soil Science 58:945–957.
- Aggarwal, V., H. Li, S.A. Boyd, and B.J. Teppen. 2006. Enhanced sorption of trichloroethene by smectite clay exchanged with Cs<sup>+</sup>. Environmental Science & Technology 40:894-899.
- Arroyo, L.J., H. Li, B.J. Teppen, and S.A. Boyd. 2005. A simple method for partial purification of reference clays. Clays and Clay Minerals 53:511-519.
- Becke, A.D. 1993. Density-functional thermochemistry. III. The role of exact exchange. Journal of Chemical Physics 98:5648-5652.
- Bérend, I., J.-M. Cases, M. François, J.-P. Uriot, L. Michot, A. Masion, and F. Thomas. 1995. Mechanism of adsorption and desorption of water vapor by homoionic montmorillonites: 2. the Li<sup>+</sup>, Na<sup>+</sup>, K<sup>+</sup>, Rb<sup>+</sup>, and Cs<sup>+</sup>-exchanged forms. Clays and Clay Minerals 43:324-336.
- Bertazzi, P.A., D. Consonni, S. Bachetti, M. Rubagotti, A. Baccarelli, C. Zocchetti, and A.C. Pesatori. 2001. Health effects of dioxin exposure: a 20-year mortality study. American Journal of Epidemiology 153:1031-1044.
- Boyd, S.A., G. Sheng, B.J. Teppen, and C.T. Johnston. 2001. Mechanisms for the adsorption of substituted nitrobenzenes by smectite clays. Environmental Science & Technology 35:4227-4234.
- Brzuzy, L.P., and R.A. Hites. 1995. Estimating the atmospheric deposition of polychlorinated dibenzo-p-dioxins and dibenzo-furans from soils. Environmental Science & Technology 29:2090-2098.
- Brzuzy, L.P., and R.A. Hites. 1996. Global mass balance for polychlorinated dibenzop-dioxins and dibenzofurans. Environmental Science & Technology 30:1797-1804.
- Chiou, C.T., P.E. Porter, and D.W. Schmeddlng. 1983. Partition equilibria of nonionic organic compounds between soil organic matter and water. Environmental Science & Technology 17:227-231.

- Christidis, G., and A.C. Dunham. 1997. Compositional variations in smectites; Part II, Alteration of acidic precursors, a case study from Milos Island, Greece. Clay Minerals 32:253-270.
- Chu, I.-H., H. Zhang, and D.V. Dearden. 1993. Macrocyclic chemistry in the gas phase: intrinsic cation affinities and complexation rates for alkali metal cation complexes of crown ethers and glymes. Journal of the American Chemical Society 115:5736-5744.
- De Rosa, C.T., D. Brown, R. Dhara, W. Garrett, H. Hansen, J. Holler, D. Jones, D. Jordan-Izaguirre, R. O'Connor, H. Pohl, and C. Xintaras. 1997. Dioxin and dioxin-like compounds in soil, part 1: ATSDR interim policy guideline. Toxicology and Industrial Health 13:759-768.
- Dunning, J.T.H. 1989. Gaussian basis sets for use in correlated molecular calculations. I. The atoms boron through neon and hydrogen. Journal of Chemical Physics 90:1007-1023.
- Dzidic, I., and P. Kebarle. 1970. Hydration of the alkali ions in the gas phase. Enthalpies and entropies of reactions  $M^+(H_2O)_{n-1} + H_2O = M^+(H_2O)_n$ . Journal of Physical Chemistry 74:1466-1474.
- Fedorov, D.G., R.M. Olson, K. Kitaura, M.S. Gordon, and S. Koseki. 2004. A new hierarchical parallelization scheme: Generalized distributed data interface (GDDI), and an application to the fragment molecular orbital method (FMO). Journal of Computational Chemistry 25:872-880.
- Ferrario, J.B., C.J. Byrne, and D.H. Cleverly. 2000. 2,3,7,8-dibenzo-p-dioxins in mined clay products from the United States: Evidence for possible natural origin. Environmental Science & Technology 34:4524-4532.
- Frankki, S., Y. Persson, A. Shchukarev, M. Tysklind, and U. Skyllberg. 2007.
  Partitioning of chloroaromatic compounds between the aqueous phase and dissolved and particulate soil organic matter at chlorophenol contaminated sites. Environmental Pollution 148:182-190.
- Ghidini, E., F. Ugozzoli, R. Ungaro, S. Harkema, A.A. El-Fadl, and D.N. Reinhoudt. 1990. Complexation of alkali metal cations by conformationally rigid, stereoisomeric calix [4] arene crown ethers: a quantitative evaluation of preorganization. Journal of the American Chemical Society 112:6979-6985.
- Gillman, G.P. 1979. A proposed method for the measurement of exchange properties of highly weathered soils. Australian Journal of Soil Research 17:129-139.
- Glendening, E.D., and D. Feller. 1995. Cation-water interactions. The  $M^+(H_2O)_n$  clusters for alkali metals, M = Li, Na, K, Rb, and Cs. Journal of Physical Chemistry 99:3060-3067.

- Glendening, E.D., D. Feller, and M.A. Thompson. 1994. An ab initio investigation of the structure and alkali metal cation selectivity of 18-crown-6. Journal of the American Chemical Society 116:10657-10669.
- A. Granovsky. 2008. PC GAMESS version 7.15. A. Granovsky.
- Haderlein, S.B., and R.P. Schwarzenbach. 1993. Adsorption of substituted nitrobenzenes and nitrophenols to mineral surfaces. Environmental Science & Technology 27:316-326.
- Haderlein, S.B., K.W. Weissmahr, and R.P. Schwarzenbach. 1996. Specific adsorption of nitroaromatic explosives and pesticides to clay minerals. Environmental Science & Technology 30:612-622.
- Hay, P.J., and W.R. Wadt. 1985. Ab initio effective core potentials for molecular calculations. Potentials for the transition metal atoms Sc to Hg. Journal of Chemical Physics 82:270-283.
- Hayward, D.G., and P.M. Bolger. 2005. Tetrachlorodibenzo-p-dioxin in baby food made from chicken produced before and after the termination of ball clay use in chicken feed in the United States. Environmental Research 99:307-313.
- Hayward, D.G., D. Nortrup, A. Gardner, and M. Clower. 1999. Elevated TCDD in chicken eggs and farm-raised catfish fed a diet with ball clay from a southern United States mine. Environmental Research 81:248-256.
- Hoekstra, E.J., H. De Weerd, E.W.B. De Leer, and U.A.T. Brinkman. 1999. Natural formation of chlorinated phenols, dibenzo-p-dioxins, and dibenzo-furans in soil of a Douglas fir forest. Environmental Science & Technology 33:2543-2549.
- Johnston, C.T., G. Sheng, B.J. Teppen, S.A. Boyd, and M.F. de Oliveira. 2002. Spectroscopic study of dinitrophenol herbicide sorption on smectite. Environmental Science & Technology 36:5067-5074.
- Kjelier, L.O., K.C. Jones, A.E. Johnston, and C. Rappe. 1991. Increases in the polychlorinated dibenzo-p-dioxin and -furan content of soils and vegetation since the 1840s. Environmental Science & Technology 25:1619-1627.
- Laine, M.M., J. Ahtiainen, N. Wagman, L.G. Oberg, and K.S. Jorgensen. 1997. Fate and toxicity of chlorophenols, polychlorinated dibenzo-p-dioxins, and dibenzofurans during composting of contaminated sawmill soil. Environmental Science & Technology 31:3244-3250.
- Laperche, V., J.F. Lambert, R. Prost, and J.J. Fripiat. 1990. High-resolution solid-state NMR of exchangeable cations in the interlayer surface of a swelling mica:

  Na, <sup>111</sup> Cd, and <sup>133</sup> Cs vermiculites. Journal of Physical Chemistry 94:8821-8831.

- Lee, C., W. Yang, and R.G. Parr. 1988. Development of the Colle-Salvetti correlationenergy formula into a functional of the electron density. Physical Review B 37:785.
- McBride, M.B. 1994. Environmental chemistry of soils Oxford University Press, New York.
- Pelmenschikov, A., and J. Leszczynski. 1999. Adsorption of 1,3,5-trinitrobenzene on the siloxane sites of clay minerals: ab initio calculations of molecular models. Journal of Physical Chemistry B 103:6886-6890.
- Rappe, C., R. Andersson, M. Bonner, K. Cooper, H. Fiedler, F. Howell, S.E. Kulp, and C. Lau. 1997. PCDDs and PCDFs in soil and river sediment samples from a rural area in the United States of America. Chemosphere 34:1297-1314.
- Ras, R.H.A., R.A. Schoonheydt, and C.T. Johnston. 2007. Relation between spolarized and p-polarized internal reflection spectra: Application for the spectral resolution of perpendicular vibrational modes. Journal of Physical Chemistry A 111:8787-8791.
- Rogowski, D.L., and W. Yake. 2005. Typical dioxin concentrations in agriculture soils of Washington state and potential sources. Environmental Science & Technology 39:5170-5176.
- Shiu, W.Y., W. Doucette, F.A.P.C. Gobas, A. Andren, and D. Mackay. 1988.

  Physical-chemical properties of chlorinated dibenzo-p-dioxins. Environmental Science & Technology 22:651-658.
- Sposito, G. 1984. The surface chemistry of soils Oxford University Press, Inc., New York, NY.
- Steenland, K., P. Bertazzi, A. Baccarelli, and M. Kogevinas. 2004. Dioxin revisited: developments since the 1997 IARC classification of dioxin as a human carcinogen. Environmental Health Perspectives 112:1265–1268.
- Sutton, R., and G. Sposito. 2001. Molecular simulation of interlayer structure and dynamics in 12.4 A Cs-smectite hydrates. Journal of Colloid and Interface Science 237:174-184.
- Walters, R.W., and A. Guiseppi-Elie. 1988. Sorption of 2, 3, 7, 8-tetrachlorodibenzop-dioxin to soils from water/methanol mixtures. Environmental Science & Technology 22:819-825.
- Yalkowsky, S.H., and R.M. Dannenfelser. 1992. The aquasol database of aqueous solubility College of Pharmacy, University of Arizona, Tucson, AZ.

# **CHAPTER III**

# RELATION OF CLAY STRUCTURAL FACTORS TO DIBENZO-P-DIOXIN ADSORPTION BY SMECTITES: EMPIRICAL EVIDENCE AND MOLECULAR DYNAMICS SIMULATIONS

# **ABSTRACT**

Dibenzo-p-dioxin adsorption by smectite clays can greatly exceed that by soil organic matter when compared on an equal mass basis. Sorption experiments demonstrated that sorption of dibenzo-p-dioxin by smectites depended strongly on the hydration properties of the exchangeable cations, and clay surface charge density, of the smectites. Molecular dynamics simulations of saponites saturated with different exchangeable cations (Na<sup>+</sup>, K<sup>+</sup>, Cs<sup>+</sup> and Ca<sup>2+</sup>) with one, two and three layers of water in the interlayer regions were conducted to establish the extent of, and study the molecular mechanism responsible for, the adsorption of dibenzo-p-dioxin. The simulated radial distribution functions for the spatial correlations between oxygen on dioxin (Odd) and interlayer cations as well as water hydrogen were computed. Comparison among the computed coordination numbers suggested that O<sub>dd</sub>-interlayer cation complexation plays an important role in adsorption and the order of coordination numbers between Oddinterlayer cation follows Cs>K>Na>Ca, which is in good agreement with the observed trend of dibenzo-p-dioxin adsorption to the smectites from water.

# INTRODUCTION

Nonionic organic contaminants (NOCs) encompass many of the most troublesome categories of pollutants found in the soil environment. Over the past 30 years, many studies of NOC sorption by soils have investigated the transport and fate of these chemicals in the environment. During this period, dogma evolved that soil organic matter (SOM) was the primary, if not singular, sorptive phase responsible for the sequestration of NOCs including dioxins (Chiou, 2002; Chiou et al., 1979; Cornelissen et al., 2005; Haderlein et al., 1996; Karickhoff et al., 1979; Nolan et al., 1989; Overcash et al., 1991; Walters and Guiseppi-Elie, 1988; Walters et al., 1989). Sorption of NOCs by SOM was envisioned as solute partitioning into amorphous soil organic matter, with the magnitude of sorption dependent on the relative NOC solubilities in SOM and water. Subsequently, NOC adsorption to chars (produced during combustion of plant materials under oxygen limited conditions) was envisioned as an important and distinct sorptive process, especially at low relative concentrations (NOC concentration in water/ NOC water solubility) (Chiou et al., 1979; Cornelissen et al., 2005). These, literally hundreds of studies, ignored or explicitly excluded the contribution of mineral matter to NOC sorption in soils. However, recent studies have reported very significant adsorption of important structural classes of NOCs such as nitroaromatics (NACs) (Boyd et al., 2001; Haderlein et al., 1996), triazines (Laird et al., 1992), diuron (Sheng et al., 2001), chlorinated solvents such as trichloroethene (TCE) (Aggarwal et al., 2006) and dioxin (Liu et al., 2009) by clay minerals, challenging the dogma that NOCs are sorbed primarily by the organic constituents of soils.

Polychlorinated dibenzo-p-dioxins (PCDDs) are recognized as the most toxic organic contaminants found in soils and sediments. Because they have exceptionally low water solubilities, and are resistant to biodegradation, sorption of these recalcitrant compounds is a primary determinant of their environmental fates. Interestingly, accumulations of dioxins have been found in prehistoric geologic deposits of ball clays which contain a mixture of clay minerals including kaolinite and smectites, suggesting a natural association of clays and dioxins (Holmstrand et al., 2006; Prange et al., 2002). The levels of dioxins in ball clays were high enough to cause several instances of livestock contamination when the clays were used as feed additives (Hayward et al., 1999). A recent survey of dioxin body burdens of people living on dioxin contaminated floodplain soils near Midland, Michigan revealed that the most contaminated individual was a potter with a history of firing ball clays in an unvented in-home kiln (Franzblau et al., 2007), again linking dioxin exposure to ball clays. The association of PCDDs with natural clay deposits, and the documented capability of smectite clays to function as an effective sorbent for many series of organic contaminants, prompted the current study which seeks to document factors influencing the adsorption of dibenzo-p-dioxin (DD) by smectite clays, and to elucidate the molecular scale forces responsible for such interactions.

Among the common clay minerals found in soils, subsoils and ball clays, smectites have been shown to be the most effective adsorbents of NOCs (Schellenberg et al., 1984), with sorptive affinities exceeding that of SOM (Sheng et al., 2001), and sorptive capacities as high as 1 to 10% by weight (Aggarwal et al., 2006; Boyd et al., 2001; Haderlein et al., 1996; Laird et al., 1992; Liu et al., 2009; Sheng et al., 2001).

Smectites are 2:1 aluminosilicates that are widely distributed in soils and sediments. These minerals occur in nature as stacked assemblages of individual planar aluminosilicate layers which have aspect ratios of ~100 to 500. When exposed to water the clay layers separate (clay swelling) exposing a large surface area on the order of 800 m<sup>2</sup>/g. They also possess substantial cation exchange capacities (CEC ~80 to 120 meq/100g) originating from isomorphic substitution within the clay sheets. Inorganic (exchangeable) cations residing between the clay layers neutralize the structural negative charges imbedded in the clay sheets, and hydration of these cations causes clay interlayer swelling. Association of water with siloxane oxygens comprising the surfaces of smectite sheets is comparatively weak, indicating that the interlayer surfaces are relatively hydrophobic, especially those portions not impacted by the imbedded negative charges (Jaynes and Boyd, 1991a; Johnston, 2010; Johnston et al., 2001; Rana et al., 2009). The confluence of certain surface and structural properties of smectites has been shown to manifest high affinity NOC adsorption sites in smectite clays (Li et al., 2004; Li et al., 2007; Sheng et al., 2002). Generally, NOC adsorption is maximized (~1 to 10% w/w) in smectite clays with comparatively low layer charge density (low CEC) originating from the tetrahedral layers, and whose CEC is satisfied by comparatively weakly hydrated cations (e.g. Cs<sup>+</sup>, NH<sub>4</sub><sup>+</sup>, K<sup>+</sup>). These factors optimize the interlayer (vertical) distance between clay layers, and the horizontal distance between exchangeable cations; together this defines the size and nature of adsorption domains in a manner that promotes solute (NOC) dehydration, and direct interactions of NOCs with exchangeable cations as well as with the siloxane sheet, all of which are energetically favorable.

A previous study documented the strong affinity between dioxin and certain clays, and demonstrated that dioxin adsorption by smectite clays can greatly exceed that by soil organic matter when compared on an equal mass basis (Liu et al., 2009; Rana et al., 2009). The sorption of dioxin by smectites depended strongly on the hydration properties of the exchangeable cations, and clay surface charge density, of the smectites, consistent with previous studies (Li et al., 2004; Li et al., 2007; Sheng et al., 2002). The retention of dioxin on montmorillonites and saponites was attributed to a mixed mode of hydrophobic interactions with smectite surfaces, complexation of dioxin ring oxygens with the poorly hydrated interlayer cations, and partial solute dehydration in the sub-aqueous environment of the clay galleries (Li et al., 2004; Liu et al., 2009). In addition to macroscopic experimental techniques such as the batch sorption experiments, X-ray diffraction, FTIR, and simplified gas phase quantum modeling were used in earlier studies to help reveal the operative adsorption mechanism(s). However, the molecular models did not include either the specific effects of clay mineral structure or the hydrated interlayer environment, which have been identified as important factors in dioxin adsorption by smectites (Liu et al., 2009; Rana et al., 2009).

Molecular dynamics has proven to be a successful technique to investigate molecular-scale interactions occurring in large complex systems such as clay minerals (Aggarwal et al., 2007; Chang et al., 1995; Greathouse et al., 2000; Gu et al., 2008; Sutton and Sposito, 2001; Teppen et al., 1998; Teppen et al., 1997), and was used here to pursue insight into the mechanisms and forces involved in dioxin adsorption by smectite clay. The objective of this study was to examine the adsorption of dibenzo-p-dioxin by a systematic set of clay minerals which differed in the amount and source of clay layer

charge, and the hydration propensities of exchangeable cations. Detailed molecular dynamics simulations were conducted to explore the molecular-scale interactions of dibenzo-p-dioxin on hydrated clay surfaces. The extensive modeling results described here agree with macroscopic observations of sorption behavior reported here and in previous studies (Aggarwal et al., 2007; Greathouse et al., 2000; Sutton and Sposito, 2001; Teppen et al., 1998), allowing new insight into the molecular scale mechanisms and forces operative in the adsorption of dioxin in smectite clay interlayers.

# **MATERIALS AND METHODS**

Clays and Chemicals. Reference clay minerals SWy-2, SWa-1 and SAz-1 (montmorillonites), SapCa-2(saponite) and SHCa-1(hectorite), obtained from the Source Clays Repository of the Clay Minerals Society at Purdue University, West Lafayette, IN, were used in this study. Their major physicochemical characteristics are listed in Table III-1. The preparation of cation saturated montmorillonite followed the method of Arroyo *et al.*, (Arroyo et al., 2005). Briefly, the < 2 μm clay size fraction was collected by wet sedimentation, suspended in 0.1 M ionic strength solutions of KCl, CsCl, NH<sub>4</sub>Cl, CaCl<sub>2</sub>, MgCl<sub>2</sub> or FeCl<sub>3</sub> for 24h, then centrifuged and resuspended three times to saturate the exchangeable cation sites of the clays. Excess salts were removed by rinsing repeatedly with deionized water until a negative Cl<sup>-</sup> test was obtained with AgNO<sub>3</sub>. Clays were then

quick-frozen, freeze-dried, and ground with a mortar and pestle. Dibenzo-p-dioxin with purity >99% was purchased from Chem Service Inc. (West Chester, PA) and used as received.

Table III-1. Characteristics of clay minerals used as adsorbents for dibenzodioxin.

Sample	Tetrahedral charge (%)	Ion exchange capacity (cmol/kg)	Surface area (m <sup>2</sup> /g)	BET N <sub>2</sub> Surface area (m <sup>2</sup> /g)	Surface charge density (µmol/m <sup>2</sup> )
SWy-2	3.6	83.6	766	31.82	1.09
SapCa-2	102	78.2	730	197	1.04
SHCa-1	14	86.4	743	63.19	1.16
SWa-1	73	106.1	722	85.5	1.48
SAz-1	12	128.3	768	97.42	1.69

**Sorption Isotherm Measurement.** All sorption isotherms were determined using a batch equilibrium method. Freeze-dried clay (8 to 30 mg) was suspended in glass vials containing 4.0 mL solutions of various dioxin concentrations; ionic strength was maintained using 0.01M or 0.005M cation chloride solutions for clays saturated with monovalent or divalent cations respectively, with the cation chloride salt corresponding to the exchangeable cation. The vials were capped with Teflon-lined septa, shaken reciprocally at 40 rpm for 24 h at room temperature (23±2 °C), then centrifuged at 1667 g for 20 min. Preliminary studies showed that equilibrium was achieved within this time. The concentrations of dioxin in supernatants were analyzed by high performance liquid chromatography (HPLC, Perkin-Elmer, Norwalk, Connecticut) using an UV-visible detector set at 223 nm. Methanol (0.5 mL) was added to all HPLC vials before injection to prevent solute from adsorbing onto glassware during HPLC analysis. A Supelco Discovery reverse phase C18 column was used. The mobile phase was a mixture of 80% methanol and 20% water with a flow rate of 1.0 mL/min. The amount of dioxin sorbed by the clay was calculated from the difference between the dioxin concentrations in blanks (no clay) and in the supernatants from the clay-containing samples.

Computational Methods. Molecular dynamics simulations of dioxin-clay interactions were performed to explore the molecular-scale interactions between dioxin, exchangeable cations and water in the interlayer region. Periodic models for Cs-, K-, Na- and Ca-exchanged saponite clays were created following the procedure described by Aggawal et al. (Aggarwal et al., 2007). The supercell (12 unit cells) of Cs-, K- and Na-saponite clays (which showed the greatest dioxin adsorption among smectites tested) has the

composition (M<sub>0.75</sub>)[Mg<sub>6</sub>][Si<sub>7.25</sub> Al<sub>0.75</sub>]O<sub>20</sub>(OH)<sub>4</sub>. The size for the Ca-saponite supercell was doubled to maintain the same numbers of interlayer cations. Nine exchangeable cations and three molecules of dioxin (six dioxin for Ca-saponite) were all placed at random initial positions within the supercells using a random solvation script. Various numbers of water molecules (ranging from 0 to 300 for Ca-saponite, 0 to 150 for the others) were then added into the supercells using the random solvation script, and these structures were subjected to molecular dynamics simulations of different hydration states of clay minerals. A combination of a force field for aluminosilicate clays (Teppen et al., 1997) with the PCFF force field (Maple et al., 1994) for dioxin and water was applied to the simulation systems. The structure and charges of dioxin were optimized using the COMPASS force field (Sun, 1998). The molecular dynamics module discover in Material Studio software package (Accelrys, 2001-2009) was used to run the simulations of the hydrated clay systems in the NPT ensemble with constant temperature of 298K, constant pressure of 0.1Mpa and step size of 0.5fs. Prior to the production runs, the systems were subjected to simulated annealing from 1000 K to 300 K at a rate of 100 K per 10 ps to avoid the high-energy local minimum problems. Then, equilibrium runs of 0.2 ns at 298K were performed, followed by production runs of 0.3 ns. The trajectories at the final production stage were collected every 1000 steps. The trajectories for three equilibrium hydration states with d-spacings of 12 Å, 15 Å and 17 Å for each of Cs-, K-, Na- and Ca- exchanged saponite system were selected for radial distribution function analysis.

### RESULTS AND DISCUSSION

**Adsorption isotherms.** The cation exchange sites of the montmorillonite (SWy-2) clay were saturated with a series of cations whose enthalpies of hydration increased in the order:  $Cs^{+} < K^{+} < NH_{4}^{+} << Ca^{2+} < Mg^{2+} << Fe^{3+}$  and  $Al^{3+}$ . The resultant homoionic clays were used as sorbents for dibenzo-p-dioxin (dioxin) dissolved in water. Sorption isotherms relating concentrations of clay-sorbed to aqueous-phase dioxin are shown in Figure III-1. Dioxin affinity for the clays demonstrated a strong dependence on the exchangeable cation used to neutralize CEC. To obtain approximate adsorption coefficients for comparative purposes, sorption data were fit to linear equations, which yielded adsorption coefficients (K) of 1517, 346.6, 47.8, 19.1, 15.8, 73.3 and 48.6 for Cs<sup>+</sup>,  $NH_4^+$ ,  $K^+$ ,  $Mg^{2+}$ ,  $Ca^{2+}$ ,  $Fe^{3+}$ , and  $Al^{3+}$  homoionic clays, respectively. Generally, adsorption of dioxin was inversely related to the hydration enthalpy of the exchangeable cation for this series of homoionic smectites. This result is consistent with previous observations on the effect of exchangeable cation type on adsorption of NACs and dinitrophenol herbicides (Aggarwal et al., 2006; Holmstrand et al., 2006; Prange et al., 2002; Sheng et al., 2002). Interlayer cations influence the molecular scale interlayer environment of the clay, where adsorption occurs in a complex fashion to determine the net uptake of dioxin from bulk water.

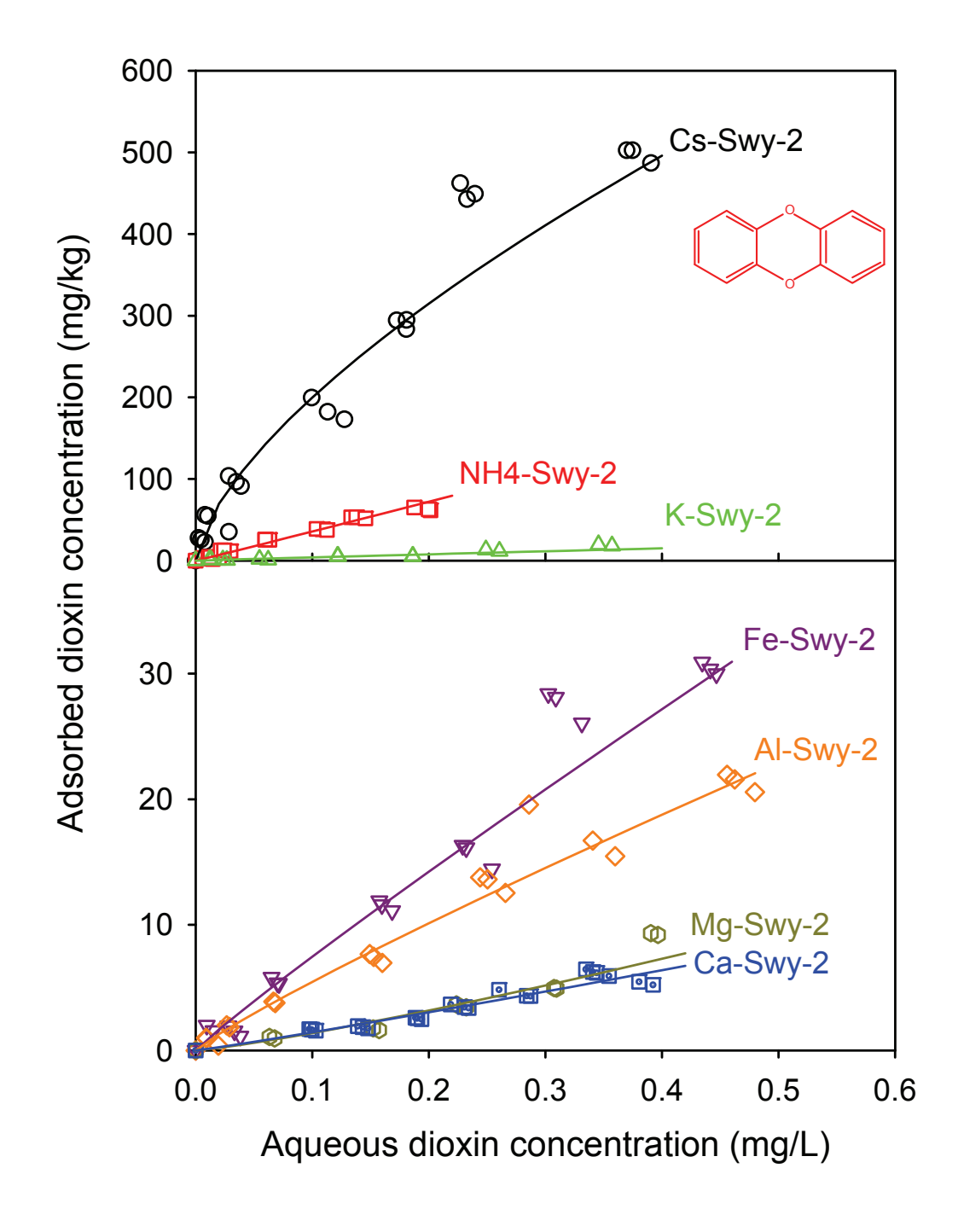


Figure III-1. Adsorption isotherms of dioxin by Cs-, NH<sub>4</sub>, K-, Fe-, Al-, Mg-, and Ca-saturated montmorillonite (SWy-2) from water.

Exchangeable cation hydration acts as a primary determinant of dioxin sorption by smectite clays through influencing a) the interlayer distance, b) the size of adsorption domains on the siloxane sheets, and c) complexation interactions between adsorbed dioxin and interlayer cations. Hydration of the interlayer cation is the primary force that determines the distance between opposing clay layers. Exchangeable cations with higher hydration energies and larger hydrated radii manifest a greater interlayer distance, i.e., the vertical distance between clay layers. For example, Cs<sup>+</sup> is relatively weakly hydrated and contains  $\leq 1$  layer of water in the interlayer of the corresponding homoionic Cs-smectite (suspension in bulk water) manifesting an interlayer distance of  $\sim 3$  Å, and a d001 spacing of  $\sim 12.5$  Å. In Ca-smectite, the exchangeable Ca<sup>2+</sup> ions are much more strongly hydrated and the d001 spacings are always  $\geq$  15 Å; K-smectite is intermediate with d001 spacing of between ~ 12 and 15 Å depending on the surface charge density of the clay. For planar molecules like dioxin, adsorption is generally maximized when the width of the molecule closely matches the interlayer distance. This situation is realized, for instance, in Cs-smectites where the interlayer distance of  $\sim 3$  Å matches the approximate thickness of planar aromatic molecules such as NACs and dioxin. This allows the sorbate (e.g. dioxin) to orient coplanar with the clay layer siloxane surface. In this orientation dioxin interacts simultaneously with the opposing clay layers, providing two energetically favorable manifestations, i.e., maximal hydrophobic interactions between the planar dioxin molecule and the planar siloxane surface (as well as the potential for formation of electron donor acceptor complexes (Haderlein et al., 1996; Jaynes and Boyd, 1991a)), and allowing partial dehydration of dioxin in the subaqueous interlayer region (Liu et al., 2009).

Lower interlayer cation hydration also benefits dioxin adsorption by maximizing the availability of siloxane surfaces for adsorption. A smaller hydration sphere lowers the amount of siloxane surface obscured by strongly bound waters of hydration. Dioxin then has more opportunity to compete with weakly bound water for sites on the siloxane surface, which is thought to be the primary locale for dioxin adsorption. A third way cation hydration affects adsorption is via its influence on cation-dioxin interactions. Water molecules in the primary hydration sphere are less strongly held by ions with larger ionic radii (e.g., Cs<sup>+</sup>, K<sup>+</sup>) compared to those with smaller ionic radii (e.g., Na<sup>+</sup>) or higher valance (e.g., Ca<sup>2+</sup>). The comparatively weakly held water can be more easily displaced by solutes such as dioxin thereby providing greater access to siloxane surface (as described above), and greater potential for direct interactions between interlayer cations and NOCs. These interactions involve polar functional groups possessing negative charge character (e.g., -NO2 groups of NACs) or electronegative elements such as dioxin ring oxygens. The strength of these interactions occurs in an exchangeable cation dependant manner, consistent with the dioxin adsorption trends on the series of different cation-exchanged smectite (Figure III-1), i.e., that dioxin adsorption by smectite clay is inversely related to the magnitude of the cation hydration enthalpy.

Orientation of dioxin in the smectite interlayers is dependent on the amount adsorbed. Previously (Liu et al., 2009; Rana et al., 2009) it was observed that at lower loading dioxin molecules were oriented co-planar with the siloxane surfaces, as evidenced by an interlayer distance of  $\sim$  3 Å corresponding to the approximate width of the dioxin molecule. Sorbed dioxin molecules were expected to occupy positions between

the exchangeable cations where they interacted with the siloxane sheets of opposing clay layers. At higher loadings, XRD measurements demonstrated that the interlayer distance expanded to ~ 5.2 Å, indicating a different orientation. To elucidate this orientation, polarized ATR-FTIR spectra of oriented films of dioxin adsorbed on smectite were obtained. The polarization behavior of the in-plane and out-of-plane vibrational modes indicated that the molecular planes of adsorbed dioxin were tilted with respect to the planar clay surfaces. This orientation seems plausible because it allows direct interactions of Cs<sup>+</sup> with the dioxin ring oxygens (Rana et al., 2009). Apparently, this interaction is sufficiently favorable to cause expansion of the clay interlayer distance.

Adsorption isotherms of dioxin on different smectite clays (saturated with  $K^{+}$  and  $Ca^{2+}$ ) are shown in Figure III-2. The smectites used, SapCa-2 (saponite), SHCa-1 (hectorite), SWy-2 (montmorillonite), SWa-1 (montmorillonite) and SAZ-1 (montmorillonite), varied in their surface charge densities (1.04~1.69  $\mu$ mol/m²), cation exchange capacities (CEC, 78~128 cmol/kg) and origin of structural negative charge (3.6 to 100% originating in the tetrahedral sheets).

Smectites contain negative charges imbedded in the aluminosilicate structure due to isomorphous substitution of higher valence cations by lower valence cations, e.g., Si<sup>4+</sup> by Al<sup>3+</sup> in the tetrahedral layers, or Al<sup>3+</sup> by Mg<sup>2+</sup> in the octahedral layers. The extent of substitutions is variable, and can occur in the tetrahedral Si-O layers or the octahedral Al-O layer, or both. The resultant negative charge created by isomorphous substitution is distributed among some number of siloxane oxygen atoms depending on the origin

(octahedral vs. tetrahedral layers) of charge; and the charge density (number of negative charges per unit surface area) varies in magnitude depending on the degree of isomorphous substitution. Generally, negative charges originating from substitutions in the octahedral sheet are thought to be distributed over many more oxygens in both sheets of tetrahedral siloxane oxygens. In contrast, negative charges originating from substitutions in the tetrahedral sheets are distributed over fewer siloxane surface oxygens, and impact only the siloxane sheet where the substitution occurs. Increased negative charge on siloxane oxygens would be expected to impart a more hydrophilic character to regions of the siloxane sheet that are impacted. Thus, regions of siloxane surface not impacted by isomorphous substitution should be relatively more hydrophobic (as illustrated by Figure 8 in (Rana et al., 2009)) and sorption of NOCs to these hydrophobic siloxane regions should be more favorable.

Dioxin adsorption was higher in clays with a higher percentage of total charge originating from tetrahedral sheets, and inversely related to the magnitude of surface charge density, consistent with the effects of origin and degree of isomorphous substitution. For the set of clay minerals saponite (SapCa-2), hectorite (SHCa-1) and montmorillonite (SWy-2), which have similar CECs of 78, 86 and 84 cmol/kg, respectively, but very different percentages of tetrahedral charge (100%, 14% and 3.6% respectively), dioxin adsorption by both K-and Ca-saturated clays followed the order SapCa> SHCa> SWy2 with corresponding adsorption coefficients (K) of 301.9, 124.8 and 47.8 for K-clays and 144.9, 39.9 and 15.8 for Ca-clays. As such, the magnitude of dioxin sorption among this series of smectites was directly related to the proportion of tetrahedral charge, in agreement with the hypothesis that tetrahedral substitution

manifests a greater proportion of total siloxane surface that is comparatively more hydrophobic in nature.

Rana et al. (Rana et al., 2009) calculated the distribution of charge deficit on the siloxane surfaces of saponite (SapCa-1) and montmorillonite (SWy-2). Saponite is a trioctahedral smectite with negative charge originating exclusively from the tetrahedral sheet. In contrast, montmorillonite is a dioctahedral smectite with > 95% of its charge due to isomorphous substitution in the octahedral sheet. In saponite, the major influence of the charge deficit is restricted to the siloxane sheet where the substitution is located. If all charges in saponite were localized to only the tetrahedra where they originate, then ca. 9% of the siloxane surface would be directly impacted by the isomorphous substitution, i.e., the negative charge would be spread over a comparatively small number of oxygens. In contrast, the charge in montmorillonite, which originates from the octahedral layer, is delocalized over siloxane oxygens of both tetrahedral sheets comprising the 2:1 layer structure. The net result is that a much greater proportion of the siloxane surface of SWy-2 montmorillonite is impacted by the negative charges. The hydrophobic natures of the siloxane surfaces of saponite and montmorillonite are apparently distinct, with the former having a much greater proportion of relatively more hydrophobic siloxane surface, i. e., that surface not impacted by structural negative charge; in montmorillonite the charge is broadly delocalized making these surfaces comparatively more hydrophilic. The resulting hypothesis is that water is held more forcefully on the surface of montmorillonites, making it more difficult for NOCs such as dioxin to access that surface. Hence, montmorillonites are less effective sorbents for aqueous phase dioxin compared to saponite (Figure III-2).

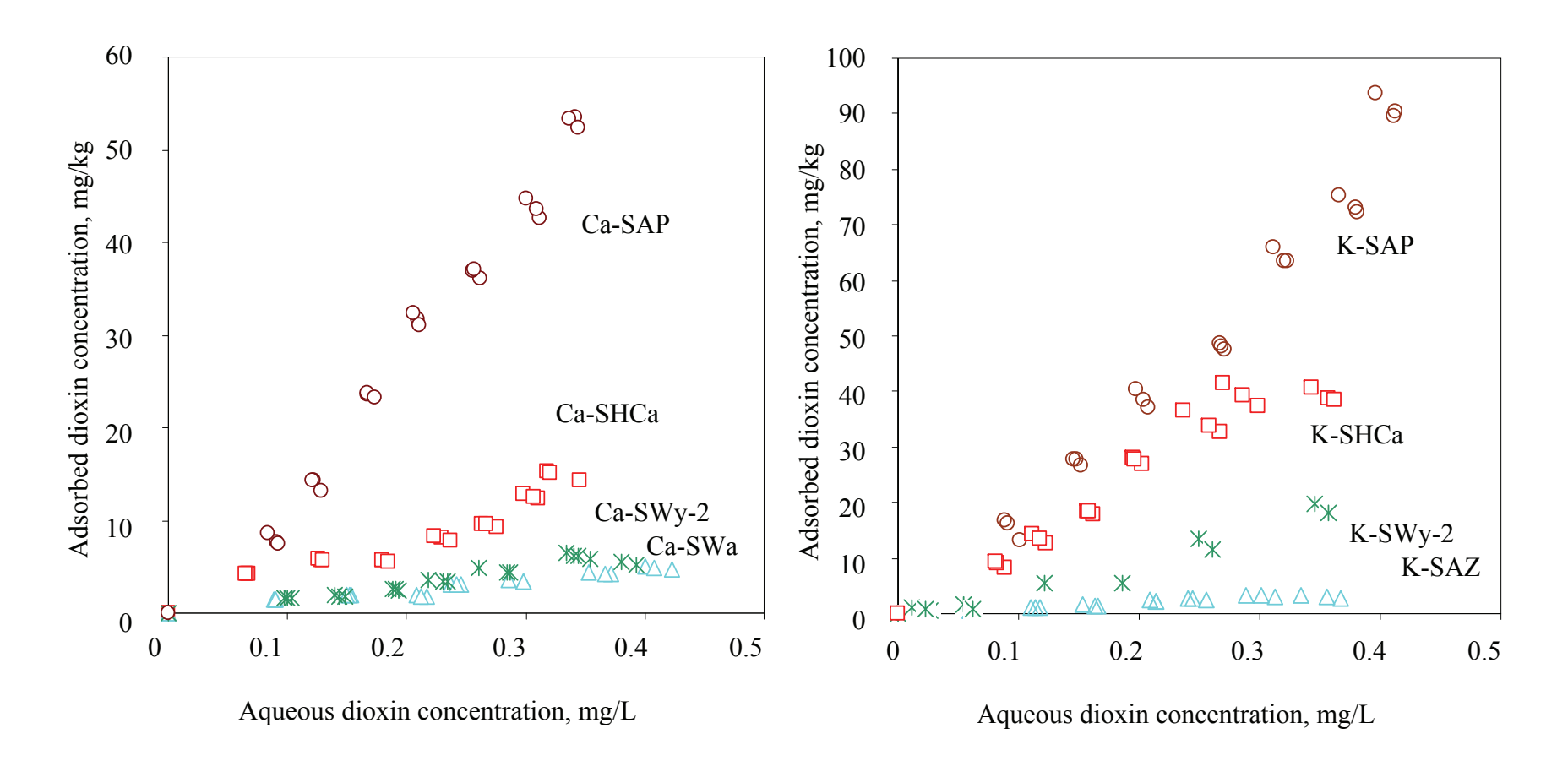


Figure III-2. The comparison of dioxin adsorption by different smectite clays (SapCa-2, SHCa-1, SWy-2, SWa-1 and SAZ-1) in the homoionic  $\operatorname{Ca}^{2+}$  and  $\operatorname{K}^+$  forms. Similar trends in the ordering of clays as adsorbents for dioxin are observed for both  $\operatorname{Ca}^{2+}$  (left) and  $\operatorname{K}^+$  (right) saturated clays. Higher adsorption generally is related (directly) to higher tetrahedral charge and (inversely) to clay surface charge density.

High surface charge density (or higher CEC) smectites such as SAZ-1 montmorillonite (surface charge 1.69 μmol/m<sup>2</sup>; CEC 123 cmol/kg) or SWa-1 nontronite (surface charge 1.48 µmol/m<sup>2</sup>; CEC 107 cmol/kg) showed diminished adsorption of dioxin (e.g. K=9.8 for K-SAZ-1 and 11.8 for Ca-SWa-1), compared to smectites with lower charge density. The observation that higher surface charge density (or higher CEC) results in diminished dioxin adsorption has been shown in previous studies on sorption of NOCs, including NACs by smectite clays exchanged with inorganic cations such as Cs<sup>+</sup>,  $K^{+}$  and  $NH_{4}^{-+}$  (Li et al., 2004; Li et al., 2007; Sheng et al., 2002). The same cause and effect relationship has been observed for adsorption of aromatic hydrocarbons in smectites exchanged with tetramethyl- or trimethyl-ammonium cations (Jaynes and Boyd, 1991b; Lee et al., 1990). It has also been demonstrated that reducing the charge of a highcharge clay (like SAZ-1) chemically (using the Li-charge reduction method) produces similar effects of surface charge on NOC adsorption, i.e., that chemical charge reduction resulted in higher adsorption by the clay (Jaynes and Boyd, 1991a; Sheng et al., 2002). The effects of cation hydration (inverse), percent tetrahedral charge (direct) and surface charge density and CEC (inverse) on adsorption that have been documented for NACs are also seen for the adsorption of dioxin, suggesting their broad applicability to NOCs that demonstrate affinity for smectite clays. The theoretical basis of these effects will be addressed below using molecular dynamics, which provides an independent means to explore the molecular scale forces and mechanisms involved in the adsorption of dioxin by smectite clays.

**Molecular dynamics.** In order to investigate the underlying mechanisms leading to these experimental results, a series of molecular dynamics simulations of dioxin intercalated in hydrated saponite clays were carried out. The key variables in the series were different interlayer cations (monovalent or divalent, i.e., Na<sup>+</sup>, K<sup>+</sup>, Cs<sup>+</sup> and Ca<sup>2+</sup>) and different water contents. Equilibrium d001 spacings of 12 Å, 15 Å and 17 Å were chose for radial distribution analysis as they correspond approximately to the metastable states with one, two and three layers of interlayer water observed during the multistep swelling of saponite clays (Liu et al., 2009; Rana et al., 2009). The 12 Å and 15 Å approximate very closely the interlayer spacing measured by XRD for Cs-smectite at different dioxin loadings, and both of the hydration states are stable in the wet environments (Liu et al., 2009; Rana et al., 2009). A d001 spacing of 17 Å well represents the hydration states of Na- and Ca-saponites, and the hydration state of K-smectites is usually a mixed layer of Cs-type and Na-type. A typical snapshot of a 12 Å Cs-saponite hydrate containing dioxin molecules in the interlayer region at equilibrium shows dioxin molecules oriented parallel or at a small angle with respect to the clay siloxane surface (Figure III-3), and the dioxin ring oxygens form hydrogen bonds with water molecules or coordinate directly to interlayer cations.

Radial distribution function (RDF) analyses were conducted for the hydrates of Na-, K-, Cs- and Ca-saponites between the following atomic pairs: The electron donor oxygens (O<sub>dd</sub>) on the dioxin ring and their possible electron acceptors, namely interlayer cations or hydrogen atoms of interlayer water molecules (Figure III-4). The coordination number for each pair (Table III-2) was determined by integrating the first peak of each

RDF in an attempt to quantify the durability of each type of interaction as a function of cation type and water content. Due to the relative weakness of many interactions, some of the RDFs are not highly structured, indicating that the hydration shell of dioxin likely has a dynamic character. The fine details of the RDFs could of course be improved by extending simulation time; however it is not expected that the main features of the distributions would change significantly.

For the O<sub>dd</sub>-H<sub>w</sub> pair (oxygen of dioxin and hydrogen of water) which contributes to the hydration of dioxin in the interlayer region, a comparatively weak first peak centered at about 2.3 Å, and a second broader and weaker peak at about 4.5 Å, can be observed for all hydrates. However, the coordination numbers (that is, the average number of water molecules hydrating dioxin ring oxygens) obtained by integrating the first peak in each RDF are significantly smaller for the one-layer hydrates than for the two- and three-layer hydrates. This makes sense, since there is less water in the one-layer hydrates and the water molecules only have access to O<sub>dd</sub> atoms from nearly coplanar orientations in the narrow interlayer galleries.

In comparing systems with different cations, the coordination numbers for the O<sub>dd</sub>-H<sub>w</sub> pair derived were: 0.32, 0.19, 0.30 and 0.67 for Cs-, K-, Na- and Ca- systems, respectively, in the 12 Å hydrates, and 0.82 ~1.50, 1.20~1.40, 1.21~1.68 and 1.50~1.67 for Cs-, K-, Na- and Ca- systems, respectively, in the 15 or 17 Å hydrates. The smaller coordination numbers derived from the Cs-15 or 17 Å hydrates, compared to those from the corresponding K-, Na- and Ca- saponite systems suggests that dioxin molecules in Cs-saponite interlayers are relatively more dehydrated.

Table III-2. Values of the first neighbor distance(r) and corresponding coordination number  $(C_N)$  for dioxin oxygen  $(O_{dd})$  with water hydrogen  $(H_w)$  and interlayer cation  $(C_s^+, K^+, N_a^+)$  and  $(C_s^2, K^+, N_a^+)$ 

	Cs-			K-			Na-			Са-		
d-spacing (Å)	12.2	15.1	16.9	12.1	14.8	16.8	12.2	14.7	16.6	12.1	14.5	16.4
CN (Odd-Cation)	0.35	0.63	0.34	0.60	0.28	0.010	0.62	0.13	0.049	0.17	0.0060	0.0004
cutoff	4.5	4.5	4.5	4	4	4	4	4	4	4	4	4
r* (Å)	3.3	3.4	3.4	2.8	2.9	-	2.6	2.6	-	2.6	-	-
r (2nd neighbor peak <sup>*</sup> )						5.6			5.3		4.5	4.9
$C_{\mathbf{N}}$	0.32	0.82	1.50	0.19	1.20	1.40	0.30	1.21	1.68	0.67	1.50	1.67
$(O_{dd}$ - $H_{water})$												
int cutoff	3.0	3.0	3.0	3.0	3.0	3.0	3.0	3.0	3.0	3.0	3.0	3.0
r (Å)	2.2	2.3	2.3	2.3	2.2	2.3	2.3	2.3	2.3	2.1	2.2	2.2
Total C <sub>N</sub>	0.68	1.45	1.84	0.79	1.49	1.41	0.92	1.34	1.73	0.84	1.50	1.67

<sup>\*</sup> For the 17 Å K-, Na- and Ca-hydrates, the peaks for the first neighbor  $O_{dd}$ -cation pair are too weak to show the accurate r, and the peaks for the second neighbor  $O_{dd}$ -cation pair are dominant peaks and the values are shown in the table.

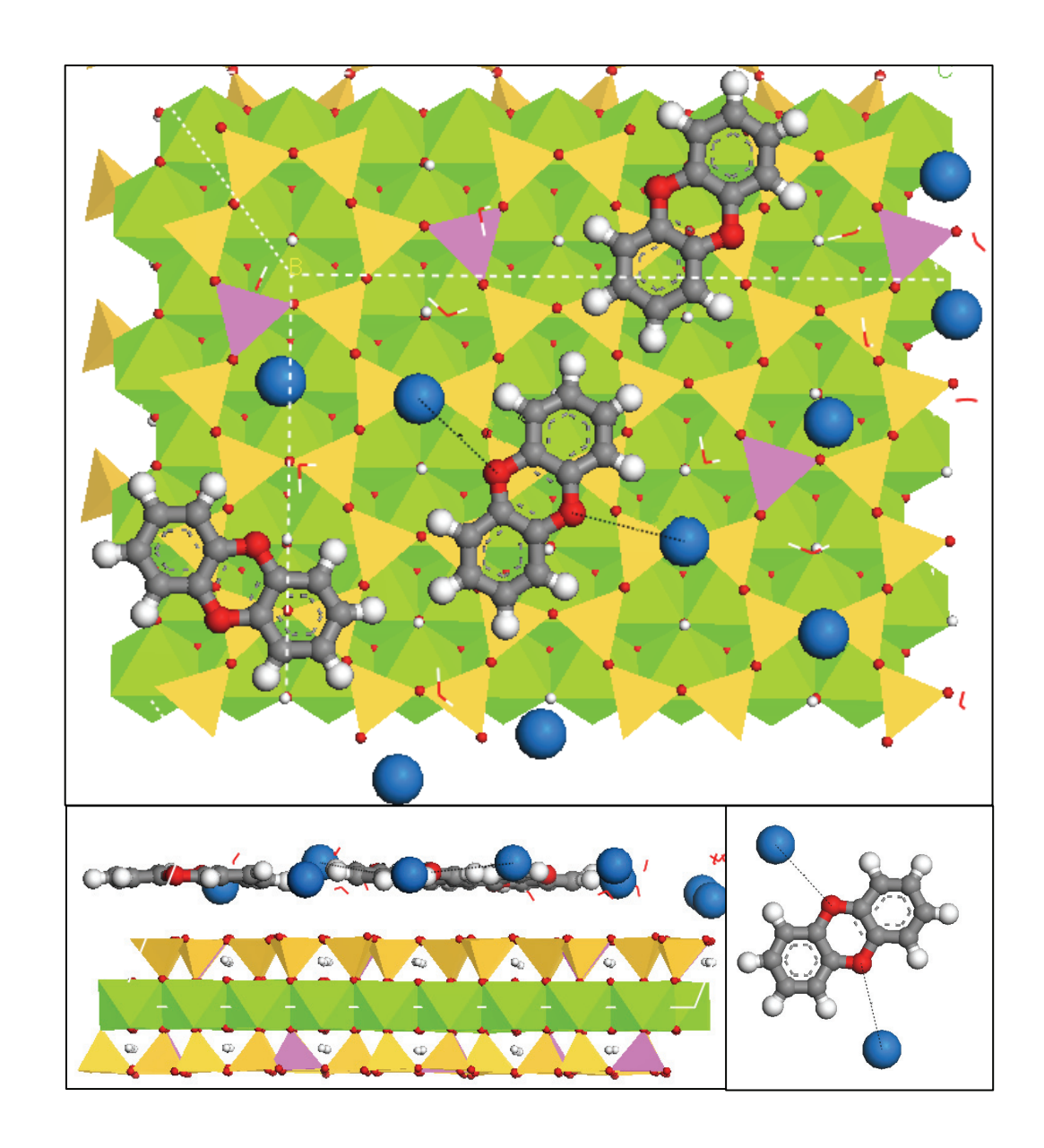


Figure III-3. A snapshot of molecular dynamics simulations for 12 Å Cs-saponite hydrates containing 3 dioxin molecules per supercell. The color scheme for dioxin molecules is: red=O; gray=C; white=H. The Cs<sup>+</sup> interlayer exchangeable cations are shown in blue. The distances shown (in Å) are the Cs<sup>+</sup>-O bond distances for complexes formed between Cs<sup>+</sup> and dibenzo- ring oxygens of dioxin. Upper panel: top surface view of Cs-saponite; lower left: cross-sectional view; lower right: enlarge of a typical interlayer Cs-dioxin complex.

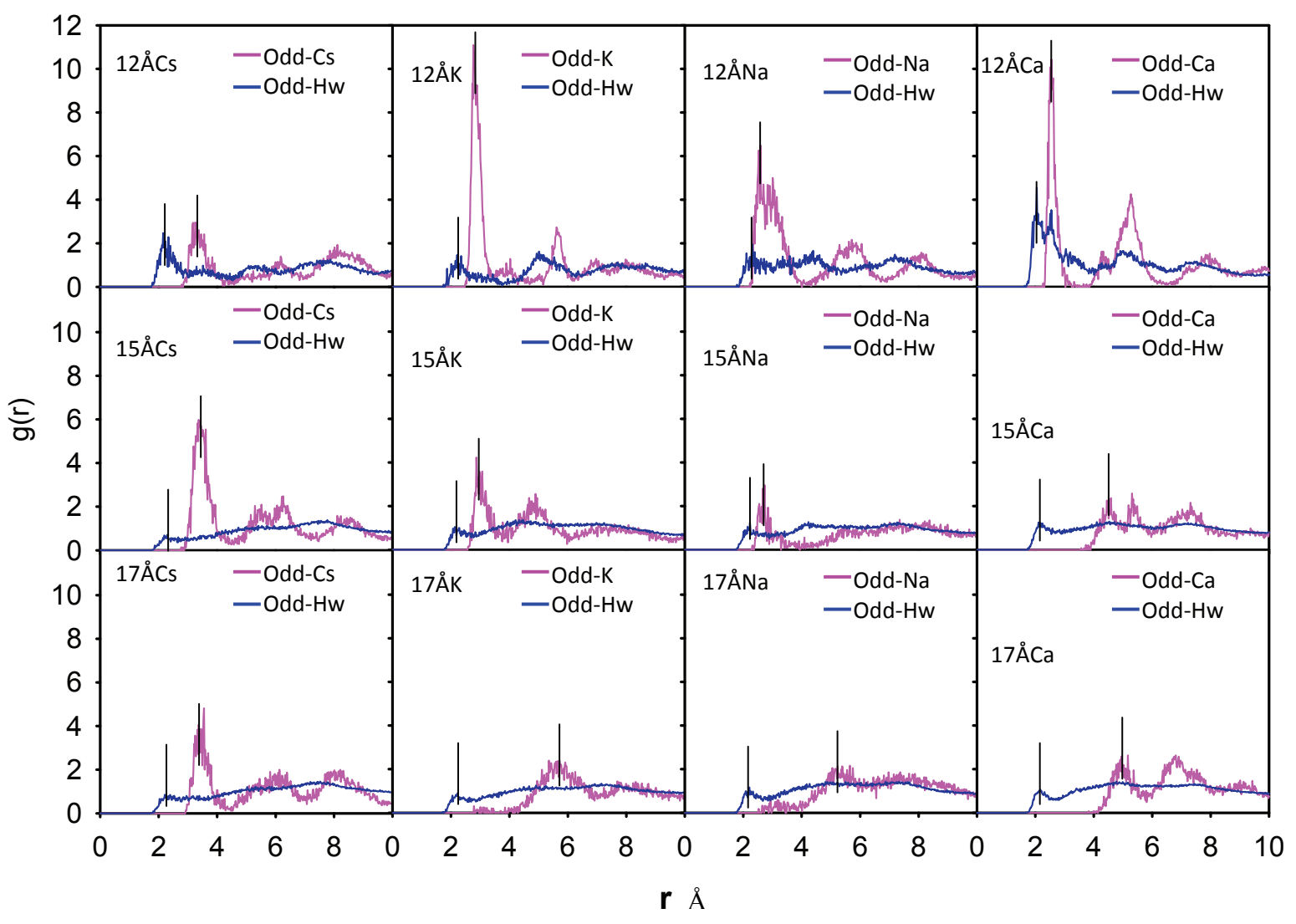


Figure. III-4 Radius distribution function for Odd-Hw,Odd-Hdd and Odd-cation for Cs, K, Na and Ca-Saponite at different water contents. (purple: Odd-exchangeable cation, blue: Odd-Hw)

In contrast, the RDFs for O<sub>dd</sub>-cation pairs (oxygen of dioxin and exchangeable cation) vary significantly depending on both the water contents and interlayer cations. In the case of Cs-saponite, a well-defined and pronounced first peak located at 3.2-3.4 Å, due essentially to direct Cs-dioxin complexation, remains relatively stable with coordination numbers of 0.35, 0.63 and 0.34 for 12 Å, 15 Å and 17 Å hydrates respectively. The K- Na- and Ca-saponites, however, show a sharp decrease in the first peak height as the systems become wetter. The coordination numbers dropped from 0.60 to 0.28 to 0.01 for K-saponite hydrates of 12 Å, 15 Å and 17 Å, from 0.62 to 0.13 to 0.05 for Na-saponite hydrates, and from 0.17 to 0.006 and 0.0004 for Ca-saponite hydrates, respectively.

The RDF analysis shows that the direct Cs-O<sub>dd</sub> complexation for Cs-saponite hydrates remains strong even if the clay layers have expanded beyond the monolayer hydrate. In contrast, complexation decreases rapidly for K-, Na-, and Ca-saponites as the clays become more hydrated. For the two-layer hydrate (~ 15 Å), the likelihood of Odd-cation complexation follows the trend Cs>K>Na>Ca, which is very similar to the trend of dioxin adsorption to the smectites from water (Liu et al., 2009; Rana et al., 2009). The simulations thus support the hypothesis that cation-dioxin complexation interactions play a role in dioxin adsorption by smectites.

The trajectory analysis also suggests relatively low mobility of Cs<sup>+</sup> cations in the interlayer, thereby forming stable spatial domains where dioxin molecules can simultaneously reside upon relatively hydrophobic, unsubstituted portions of the siloxane surface and yet retain close proximity to Cs<sup>+</sup> cations (Figure III-3). This

promotes Cs-dioxin complexation involving the dioxin ring oxygens, and provides a rationale for the observation that Cs-saponites display high affinity for dioxin.

In summary, the molecular dynamics methods were used to provide detailed trajectory analysis of dioxin sorption by smectite clays saturated with different exchangeable cations. These new methods supplement traditional macroscopic experimental techniques by providing molecular-scale analogues of the macroscopic systems. Here, the molecular dynamics support our hypothesis that the hydration status of the exchangeable cation is the central factor in determining dioxin sorption affinity with a particular smectite clay type. The bulk adsorption affinity correlates with molecular-scale phenomena including a) The ability of dioxin to out-compete water for complexation with the interlayer cation, and b) The ability of dioxin to out-compete water for sites on the siloxane surface. These results provide a clear rationale for the observation that Cs-saturated smectites display the highest sorption affinity for dioxin; i.e., because Cs<sup>+</sup> is the most weakly hydrated exchangeable cation among those tested. This allows maximal dehydration of dioxin, and direct Cs-dioxin complexation, which are both energetically favorable.

LITERATURE CITED

### LITERATURE CITED

- Accelrys Software Inc. 2001-2009. Materials Studio 4.1. Accelrys Software Inc.
- Aggarwal, V., Y.-Y. Chien, and B.J. Teppen. 2007. Molecular simulations to estimate thermodynamics for adsorption of polar organic solutes to montmorillonite. European Journal of Soil Science 58:945–957.
- Aggarwal, V., H. Li, S.A. Boyd, and B.J. Teppen. 2006. Enhanced sorption of trichloroethene by smectite clay exchanged with Cs<sup>+</sup>. Environmental Science & Technology 40:894-899.
- Arroyo, L.J., H. Li, B.J. Teppen, and S.A. Boyd. 2005. A simple method for partial purification of reference clays. Clays and Clay Minerals 53:511-519.
- Boyd, S.A., G. Sheng, B.J. Teppen, and C.T. Johnston. 2001. Mechanisms for the adsorption of substituted nitrobenzenes by smectite clays. Environmental Science & Technology 35:4227-4234.
- Chang, F.-R.C., N.T. Skipper, and G. Sposito. 1995. Computer simulation of interlayer molecular structure in sodium montmorillonite hydrates. Langmuir 11:2734-2741.
- Chiou, C.T. 2002. Partition and adsorption of organic contaminants in environmental systems Wiley-Interscience, Hoboken, New Jersey.
- Chiou, C.T., L.J. Peters, and V.H. Freed. 1979. A physical concept of soil-water equilibria for nonionic organic compounds. Science 206:831-832.
- Cornelissen, G., O. Gustafsson, T.D. Bucheli, M.T.O. Jonker, A.A. Koelmans, and P.C.M. van Noort. 2005. Extensive sorption of organic compounds to black carbon, coal, and kerogen in sediments and soils: mechanisms and consequences for distribution, bioaccumulation, and biodegradation. Environmental Science & Technology 39:6881-6895.
- Franzblau, A., E. Hedgeman, Q. Chen, L. S., P. Adriaens, A. Demond, D. Garabrant, B. Gillespie, B. Hong, O. Jolliet, J. Lepkowski, W. Luksemburg, M. Maier, and W. Y. 2007. Case Report: Human exposure to dioxins from clay. Environmental Health Perspectives 116:238-242.
- Greathouse, J.A., K. Refson, and G. Sposito. 2000. Molecular dynamics simulation of water mobility in magnesium-smectite hydrates. Journal of the American Chemical Society 122:11459-11464.

- Gu, C., H. Li, B.J. Teppen, and S.A. Boyd. 2008. Octachlorodibenzodioxin formation on Fe(III)-montmorillonite clay. Environmental Science & Technology 42:4758-4763.
- Haderlein, S.B., K.W. Weissmahr, and R.P. Schwarzenbach. 1996. Specific adsorption of nitroaromatic explosives and pesticides to clay minerals. Environmental Science & Technology 30:612-622.
- Hayward, D.G., D. Nortrup, A. Gardner, and M. Clower. 1999. Elevated TCDD in chicken eggs and farm-raised catfish fed a diet with ball clay from a southern United States mine. Environmental Research 81:248-256.
- Holmstrand, H., D. Gadomski, M. Mandalakis, M. Tysklind, R. Irvine, P. Andersson, and O. Gustafsson. 2006. Origin of PCDDs in ball clay assessed with compound-specific chlorine isotope analysis and radiocarbon dating. Environmental Science & Technology 40:3730-3735.
- Jaynes, W.F., and S.A. Boyd. 1991a. Hydrophobicity of siloxane surfaces in smectites as revealed by aromatic hydrocarbon adsorption from water. Clays and Clay Minerals 39:428-436.
- Jaynes, W.F., and S.A. Boyd. 1991b. Clay mineral type and organic compound sorption by hexadeclyltrimethlyammonium-exchanged clays. Soil Science Society of America Journal 55:43-48.
- Johnston, C.T. 2010. Probing the nanoscale architecture of clay minerals. Clay Minerals 45:245-279.
- Johnston, C.T., M.F. De Oliveira, B.J. Teppen, G. Sheng, and S.A. Boyd. 2001. Spectroscopic study of nitroaromatic-smectite sorption mechanisms. Environmental Science & Technology 35:4767-4772.
- Karickhoff, S.W., D.S. Brown, and T.A. Scott. 1979. Sorption of hydrophobic organic pollutants on natural sediments. Water Research 13:241-248.
- Laird, D.A., E. Barriuso, R.H. Dowdy, and W.C. Koskinen. 1992. Adsorption of atrazine on smectites. Soil Science Society of America Journal 56:62–67.
- Lee, J.F., M.M. Mortland, C.T. Chiou, D.E. Kile, and S.A. Boyd. 1990. Adsorption of benzene, toluene, and xylene by two tetramethylammonium-smectites having different charge densities. Clays and Clay Minerals 38:113-120.
- Li, H., B.J. Teppen, C.T. Johnston, and S.A. Boyd. 2004. Thermodynamics of nitroaromatic compound adsorption from water by smectite clay. Environmental Science & Technology 38:5433-5442.
- Li, H., T.R. Pereira, B.J. Teppen, D.A. Laird, C.T. Johnston, and S.A. Boyd. 2007. Ionic strength-induced formation of smectite quasicrystals enhances

- nitroaromatic compound sorption. Environmental Science & Technology 41:1251-1256.
- Liu, C., H. Li, B.J. Teppen, C.T. Johnston, and S.A. Boyd. 2009. Mechanisms associated with the high adsorption of dibenzo-p-dioxin from water by smectite clays. Environmental Science & Technology 43:2777-2783.
- Maple, J.R., M.-J. Hwang, T.P. Stockfish, U. Dinur, M. Waldman, E. C.S., and A.T. Hagler. 1994. Derivation of class II force fields. I. methodology and quantum force field for the alkyl functional group and alkane molecules. Journal of Computational Chemistry 15:162-182.
- Nolan, T., K.R. Srinivasan, and H.S. Fogler. 1989. Dioxin sorption by hydroxyaluminum-treated clays. Clays and Clay Minerals 37:487-492.
- Overcash, M.R., A.L. McPeters, E.J. Dougherty, and R.G. Carbonell. 1991. Diffusion of 2,3,7,8-tetrachlorodibenzo-p-dioxin in soil containing organic solvents. Environmental Science & Technology 25:1479-1485.
- Prange, J.A., C. Gaus, O. Papke, and J.F. Muller. 2002. Investigations into the PCDD contamination of topsoil, river sediments and kaolinite clay in Queensland, Australia. Chemosphere 46:1335-1342.
- Rana, K., S.A. Boyd, B.J. Teppen, H. Li, C. Liu, and C.T. Johnston. 2009. Probing the microscopic hydrophobicity of smectite surfaces. A vibrational spectroscopic study of dibenzo-p-dioxin sorption to smectite. Physical Chemistry Chemical Physics 11:2976-2985.
- Schellenberg, K., C. Leuenberger, and R.P. Schwarzenbach. 1984. Sorption of chlorinated phenols by natural sediments and aquifer materials. Environmental Science & Technology 18:652-657.
- Sheng, G., C.T. Johnston, B.J. Teppen, and S.A. Boyd. 2001. Potential contributions of smectite clays and organic matter to pesticide retention in soil. Journal of Agricultural and Food Chemistry 49:2899-2907.
- Sheng, G.Y., C.T. Johnston, B.J. Teppen, and S.A. Boyd. 2002. Adsorption of dinitrophenol herbicides from water by montmorillonites. Clays and Clay Minerals 50:25-34.
- Sun, H. 1998. COMPASS: an ab initio force-field optimized for condensed-phase applications overview with details on alkane and benzene compounds. Journal of Physical Chemistry B 102:7338-7364.
- Sutton, R., and G. Sposito. 2001. Molecular simulation of interlayer structure and dynamics in 12.4 Å Cs-smectite hydrates. Journal of Colloid and Interface Science 237:174-184.

- Teppen, B.J., C.-H. Yu, D.M. Miller, and L. Schäfer. 1998. Molecular dynamics simulations of sorption of organic compounds at the clay mineral/aqueous solution interface. Journal of Computational Chemistry 19:144-153.
- Teppen, B.J., P.M. Bertsch, K. Rasmussen, D.M. Miller, and L. Schaefer. 1997.

  Molecular dynamics modeling of clay minerals. 1. Gibbsite, kaolinite,
  pyrophyllite, and beidellite. Journal of Physical Chemistry B 101:1579-1587.
- Walters, R.W., and A. Guiseppi-Elie. 1988. Sorption of 2, 3, 7, 8-tetrachlorodibenzo-p-dioxin to soils from water/methanol mixtures. Environmental Science & Technology 22:819-825.
- Walters, R.W., S.A. Ostazeski, and A. Guiseppi-Elie. 1989. Sorption of 2,3,7,8-tetrachlorodibenzo-p-dioxin from water by surface soils. Environmental Science & Technology 23:480-484.

# **CHAPTER IV**

# PENTACHLOROPHENOL RADICAL CATIONS GENERATED ON FE(III)MONTMORILLONITE INITIATE OCTACHLORODIBENZO-p-DIOXIN FORMATION IN CLAYS

### **ABSTRACT**

Octachlorodibenzodioxin (OCDD) forms spontaneously from pentachlorophenol (PCP) on the surfaces of Fe(III)-saturated smectite clay (Gu et al., 2008). Here, *in situ* FTIR methods and quantum mechanical calculations were used to determine the mechanism by which this reaction is initiated. As the clay was dehydrated, vibrational spectra showed new peaks that grew and then reversibly disappeared as the clay rehydrated. First principle DFT calculations of hydrated Fe-PCP clusters reproduced these transient FTIR peaks when inner-sphere complexation and concomitant electron transfer produced Fe(II) and PCP radical cations. Thus, our experimental (FTIR) and theoretical (quantum mechanical) results mutually support the hypothesis that OCDD formation on Fe-smectite surfaces is initiated by the reversible formation of metastable PCP radical cations via single electron transfer from PCP to Fe(III). The negatively charged clay surface apparently selects for this reaction mechanism by stabilizing PCP radical cations.

### INTRODUCTION

Polychlorinated dibenzo-p-dioxins (PCDDs) and furans (PCDFs) are formed and found as a group of chlorinated congeners generated as by-products of human activities. such as waste incineration, metal smelting, and pesticide manufacture, and by natural processes such as forest fires. Each of these known sources produces a mixture of PCDDs distinguishable by their congener profiles. However, recent studies have reported high levels of PCDDs in otherwise pristine soils and pre-industrial clay deposits, with a typical congener profile characterized by the predominance of octachlorodibenzodioxin (OCDD) and low levels of PCDFs, which does not match any known anthropogenic or natural source (Ferrario et al., 2000; Holmstrand et al., 2006; Horii et al., 2008). Global PCDD budgets fail to account for the observed levels of these compounds in soils, and OCDD presents the greatest imbalance (Baker and Hites, 2000). Based on bulk radiocarbon, compound-specific chlorine isotope and black carbon analysis, Holmstrand et al. (Holmstrand et al., 2006) proposed that the unusual congener profile of PCDDs in a ball clay deposit from the Mississippi Embayment could result from in situ clay mineralfacilitated synthesis of PCDDs. Congener-specific carbon isotopic analysis showed that the carbon isotope composition of OCDD found in ball clays was significantly different from known anthropogenic OCDD, further supporting the hypothesis of natural PCDD formation mechanism(s) on clay surfaces (Horii et al., 2008). The use of ball clays as animal feed additives has led to several instances of livestock contamination with PCDDs (Hayward et al., 1999). A recent survey of PCDD/PCDF levels among a population living on or near dioxin-contaminated floodplain soils in Midland, Michigan revealed that the individual with the highest body burden was a potter who had a history of firing ball

clays in an in-home unvented kiln (Franzblau et al., 2008). These examples document the potential for dioxin exposure directly related to PCDD contaminated clays.

Recently a direct evidence has been provided to show that OCDD can be formed on the clay mineral montmorillonite, under environmentally relevant conditions (Gu et al., 2008). Montmorillonite is a member of the smectite group of 2:1 aluminosilicate clay minerals, which occur naturally and are widely distributed in soils/subsoils, sediments, and geologic clay deposits (Allen and Hajek, 1989). Negative charges embedded in the aluminosilicate layers due to isomorphous substitution are balanced by inorganic cations commonly found in nature, e.g., Ca<sup>2+</sup>, Na<sup>+</sup>, Mg<sup>2+</sup>, and Fe<sup>3+</sup> among others. The aluminosilicate layers of smectites are planar with aspect ratios of ~500 manifesting high surface areas of ~800 m<sup>2</sup> g<sup>-1</sup>. Smectite clays commonly occur as assemblages of stacked clay layers, resulting in large amounts of internal, interlayer surface where the exchangeable inorganic cations and water reside.

When the precursor molecule pentachlorophenol (PCP) was mixed with homoionic Fe(III)-montmorillonite at room temperature, OCDD rapidly formed at environmentally relevant levels (Gu et al., 2008). It has been proposed that the reaction was initiated by one electron transfer from PCP to Fe(III)-montmorillonite to form the PCP radical cation, followed by dimerization, dechlorination, and ring closure reactions (Boyd and Mortland, 1985; Boyd and Mortland, 1986; Gu et al., 2008; Sawhney et al., 1984). Formation of the reactive PCP radical cation would then be the crucial step that initiates the proposed reaction pathway to OCDD. Accordingly, the hypothesis proposed was that the PCP radical cation was stabilized by the planar negatively charged smectite clay layers. By comparison, hydrated transition metal ions in aqueous solution are

incapable of inducing the electron transfer so that the radical cation species is not formed, indicating the unique role played by the planar silicate surface (Boyd and Mortland, 1986). The electron transfer reaction is influenced by the presence of water, as the organic molecules must compete with water for the coordination sites of the metal cation (Gu et al., 2008). Thus, yields of OCDD from the Fe(III)-montmorillonite catalyzed reaction were inversely related to the relative humidity (RH) of the system (Gu et al., 2008). However, anhydrous conditions were not required for the reaction to proceed. Formation of organic radicals on smectites have been observed by various techniques, such as electron spin resonance (Boyd and Mortland, 1985; Boyd and Mortland, 1986; Sawhney et al., 1984), Fourier transform infrared (FTIR) (Hinedi et al., 1993) and resonance Raman spectroscopy (Soma et al., 1985; Soma, 1986). Johnston et al. (Johnston et al., 1992a; Johnston et al., 1991) used FTIR to monitor *in situ* chemisorption of p-dimethoxybenzene on Cu-smectite clay. Concomitant with a decrease in RH, several IR vibrational modes were significantly perturbed and new peaks were observed, which were attributed to the formation of radical cations (Johnston et al., 1992a; Johnston et al., 1991).

Recently, first principle calculations based on density functional theory (DFT), using both cluster models and periodic boundary conditions, have been applied to studies of clay or hydrated clay structural properties (Cygan et al., 2009; Skipper et al., 1991), and clay mineral adsorption/catalytic reactions involving organic molecules (Chatterjee et al., 2003; Gorb et al., 2006; Teppen et al., 2002; Zilberberg et al., 2004). Cluster models have proven to provide accurate geometric and electronic structures of transition metals interacting with organics, at modest computational costs (Fiedler et al., 1994; Shiota and

Yoshizawa, 2000; Sun et al., 2007). Due to constraints in computational resources, in the current study a cluster model of hydrated Fe(III) complexed with PCP was applied to investigate the electronic/spectroscopic properties of interlayer Fe(III)/PCP complexes. The choice of the hydrated iron cation model was based on the observation that in Fesmectites and low-Fe-zeolites the dominant Fe(III) species identified by Mossbauer and EXAFS studies were isolated Fe(OH)<sup>2+</sup> or Fe(OH)<sub>2</sub><sup>+</sup> octahedrally coordinated by water (Choi et al., 2003; Helsen and Goodman, 1983; Wasserman et al., 1998). Also, ESR has been used to show that partial dehydration of iron-exchanged zeolites (achieved by applying vacuum or heat) results in removal of water molecules from Fe(III) hydration shells, and a reduced coordination number around Fe(III) (Wloch et al., 1996). Since the observed Fe-catalyzed dimerization of PCP was sensitive to clay hydration (Gu et al., 2008), calculations of gas-phase PCP/Fe(OH)(H<sub>2</sub>O)<sub>n</sub><sup>2+</sup> with various numbers of water molecules in the first hydration shell (n=0 to 3) were selected as feasible structural models to characterize the electronic (and hence spectroscopic) features of PCP radical formation in Fe(III)-smectite.

The objective of this study was to couple spectroscopic evidence with quantum mechanical calculations to investigate the critical step that initiates the proposed OCDD formation mechanism (Gu et al., 2008). The hypothesis was that the reaction is initiated via a one electron transfer from PCP to Fe(III) of Fe(III)-montmorillonite to form the central reactive intermediate, i.e., the PCP radical cation, which is favored by stabilization effects of the clay surface. The surface IR spectra were collected *in situ* in a controlled humidity IR cell to correlate formation of the putative PCP radical cation with changes in the vibrational spectra as a function of water content in the system. Quantum

mechanical calculations on the reaction of PCP with Fe(III)-montmorillonite clay using different levels of models were conducted in concert and compared with experimental FTIR data. The theoretical and experimental results were found to be mutually consistent.

### MATERIALS AND METHODS

Preparation of Self-supporting Clay films. Smectite clay (Wyoming montmorillonite, SWy-2) was obtained from the Source Clays Repository of the Clay Minerals Society (Purdue University, West Lafayette, IN). The preparation of Fe(III)-montmorillonite followed the method of Arroyo *et al.* (Arroyo et al., 2005). Briefly, the clay suspension was first titrated to pH 6.8 with 0.5 M sodium acetate buffer (pH 5) to remove carbonate impurities. Clay-sized particles (<2 μm) were obtained by centrifugation for 6 min at 60 g, then treated with 0.1 M FeCl<sub>3</sub> solution six times. The Fe(III)-saturated Swy-2 was washed using Milli-Q water until free of chloride as indicated by a negative test with AgNO<sub>3</sub>, then freeze-dried.

Self-supporting clay films were prepared by the procedures developed previously (Fernandes de Oliveira et al., 2005; Johnston et al., 1992b). Twenty ml of clay-PCP aqueous suspension containing 35 mg of the Fe(III)-Swy-2 clay and 0.35 mmol L<sup>-1</sup> of PCP (Aldrich, Milwaukee, WI, purity >98%) were passed through a 0.45 μm hydrophilic polyethersulfone membrane filters (47 mm in diameter). To maximize the PCP loading, the filtered solution was passed through the membrane three more times. The resulting clay-PCP deposit on the filter was allowed to air-dry overnight and then removed from

the filter by running the filter and clay deposit over a knife edge (Johnston and Aochi, 1996).

*In Situ* FTIR Analysis. Infrared spectra were obtained on a Perkin-Elmer GX2000 FTIR spectrometer equipped with deuterated triglycine and mercury-cadmium-telluride detectors, and a KBr beam splitter. A self-supporting clay film was mounted in a vacuum cell, which was connected to a gas/vacuum manifold to control and monitor the pressure in the cell. The unapodized resolution for the FTIR spectra was 2.0 cm<sup>-1</sup>, and a total of 64 scans were collected for each spectrum.

Dehydration of the clay films was accomplished by placing the films under vacuum, and the surface reactions were monitored *in situ* using the FTIR spectrometer. After the system stabilized (approximately 2 h), the vacuum was removed, water was added to the cell, and FTIR spectra were collected until a new equilibrium was achieved, as indicated by no further change in spectra. To estimate the water content on the clay film, the FTIR absorptivity of the HOH bending band at 1630cm<sup>-1</sup> was determined by integrating the area of the band.

Computational Methods. In this study, DFT methods were applied to investigate the electronic and vibrational spectroscopic features associated with interactions between PCP and clay interlayer Fe(III) during dehydration/hydration cycles by modeling interlayer Fe(III) as Fe(OH)(H<sub>2</sub>O)<sub>n</sub><sup>2+</sup> (n=0 to 3). The total coordination number of the Fe(III) center, including coordinated H<sub>2</sub>O and PCP, ranged from two to six. The geometries of all complexes in the gas phase were fully optimized using the Becke three-parameter exchange functional (B3) (Becke, 1993) and the Lee–Yang–Parr correlation

functional (LYP) (Lee et al., 1988), implemented in the Gaussian 03 package (Frisch et al., 2004), followed by calculations of harmonic vibrational frequencies. The LANL2DZ basis set with effective core potentials (ECP) was used for Fe, while the 6-31G\* basis set was used for all other atoms in the PCP/Fe(OH)(H<sub>2</sub>O)<sub>n</sub><sup>2+</sup> complexes. Combining B3LYP methods and LANL2DZ ECPs has been found to produce reasonably accurate vibrational frequencies for a wide range of transition-metal complexes (Bytheway and Wong, 1998). The numbering scheme used for PCP atoms is shown in Figure IV-1. A scaling factor of 0.98 was used to compare the computed frequencies with experimental data in the present study based on previous literature (Curtiss et al., 2000). Further normal mode decomposition analysis was carried out to interpret the vibrational spectra and peak shifts, and thereby infer the initial steps in the reaction mechanism for clay-catalyzed conversion of PCP to OCDD. The adsorption of PCP radicals to a clay surface fragment was modeled in order to estimate the relative stabilization of each radical intermediate by the clay surface. A neutral aluminosilicate fragment was used as a model for the clay because only weak electrostatic interactions between PCP and clay siloxane surfaces have been observed (Zielke and Pinnavaia, 1988). In the two-layered ONIOM model, a neutral smectite cluster model interacting with PCPs was constructed as the real system and the adsorbate PCP species were taken as the model system. The HF method and basis sets of 3-21G and 6-31G were applied to the outer and inner layers, respectively. The clay structure was derived from full relaxation of a periodic model for the neutral clay mineral pyrophyllite. The cluster consisted of 6.5 half unit cells with a formula 6.5(Al)<sub>2</sub>(Si)<sub>4</sub>O<sub>10</sub>(OH)<sub>2</sub>·nH<sub>2</sub>O, containing exactly three ditrigonal hexasiloxane rings on each tetrahedral sheet.

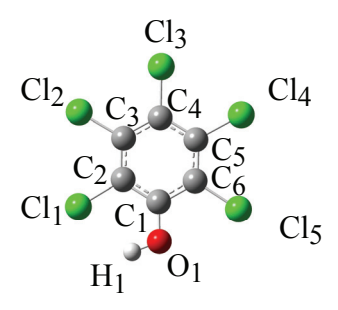


Figure IV-1. Atom numbering scheme for pentachlorophenol (PCP).

## RESULTS AND DISCUSSION

**FTIR Analysis.** Several *in situ* FTIR spectra of the Fe(III) montmorillonite-PCP system (Fe(III)-Swy2/PCP) are shown in Figure IV-2. Since clays strongly absorb infrared (IR) radiation below frequencies of 1250 cm<sup>-1</sup>, and most PCP vibrational bands except the OH-stretching mode v(OH) occur below 1700 cm<sup>-1</sup>, the IR data in the 1250-1700 cm<sup>-1</sup> region are displayed. The spectrum (Figure IV-2a) corresponding to the Fe(III)-Swy2/PCP clay film exposed to ambient air displayed peaks at 1278, 1381 and 1420 cm<sup>-1</sup>, which are assigned to the combination of benzene ring breathing and C-OH stretching v(C-OH) and bending δ(C-OH) modes (Czarnik-Matusewicz et al., 1999; Rao and Rao, 2002). The 1631 cm<sup>-1</sup> peak (Figure IV-2a) corresponds to the HOH angle bending δ(HOH) of water present on clay surface (Johnston et al., 1992a; Johnston et al., 1991).

As vacuum was applied, the intensity of the  $\delta$ (O-H) water band diminished (Figure IV-2a-d and IV-3), indicating dehydration of the clay. Also, the peak at 1420 cm

<sup>1</sup> shifted to 1411 cm<sup>-1</sup>, and peaks at 1278 and 1381 cm<sup>-1</sup> shifted to 1288 and 1385 cm<sup>-1</sup>, respectively, indicating the dehydration of PCP (as discussed below). Importantly, as the clay film was dried two new peaks at 1360 and 1334 cm<sup>-1</sup> appeared (Figure IV-2b-e and IV-3) which are attributed to the main ring-breathing peaks for the PCP radical cation. They have shifted to a lower frequency  $\sim$ 50 cm $^{-1}$  compared to molecular PCP because loss of an electron weakens C-C bonds within the ring. The FTIR spectra strongly support radical cation formation on Fe(III)-montmorillonite surface as evidenced by the peaks at 1360 and 1334 cm<sup>-1</sup> and their response to water. Formation of the PCP radical cation via one electron transfer from PCP to Fe(III) of Fe(III)-smectite has been proposed as the critical step that initiates the clay-facilitated synthesis of OCDD (Boyd and Mortland, 1985; Gu et al., 2008), and the reaction yield is known to be sensitive to the water content of the clay (Gu et al., 2008). Accordingly, a prerequisite for the proposed one electron transfer is inner sphere complexation of PCP, which requires prior removal of some waters of hydration from Fe(III). The PCP radical cation thus formed is plausibly stabilized by the negatively charged clay surface, which is also supported by the calculations on PCP/PCP radicals interacting with clay surface (See ONIOM method discussion below).

A reversal of these changes in the FTIR spectra occurred as the vacuum was released and the system was again exposed to water vapor. As shown in Figure IV-2f, after 2 min exposure to water vapor, the water peak (1631 cm<sup>-1</sup>) was restored and the peaks at 1288, 1385 and 1411 cm<sup>-1</sup> all shifted back to their original positions.

Additionally, the two new peaks at 1360 and 1334 cm<sup>-1</sup> disappeared. Upon further exposure of the clay/PCP complex to water vapor, the water peak continued to increase in intensity, while little further change occurred for the other peaks (Figure IV-2f-i).

To quantify the relation between water content and radical cation formation, the peaks at 1630, 1360 and 1334 cm<sup>-1</sup> were integrated and plotted as a function of exposure time to vacuum and to water vapor (Figure IV-3). It is clearly shown that dehydration of clay, indicated by a decrease in the 1630 cm<sup>-1</sup> band, promoted the formation of radical cations as indicated by the appearance and increase in the intensity of the 1360 and 1334 cm<sup>-1</sup> bands. The apparent radical cation formation reaction was reversible; as the clay was rehydrated the 1360 and 1334 cm<sup>-1</sup> bands diminished rapidly, indicating loss of the radical cation species. This interpretation of the FTIR results is supported by theoretical calculations presented below.

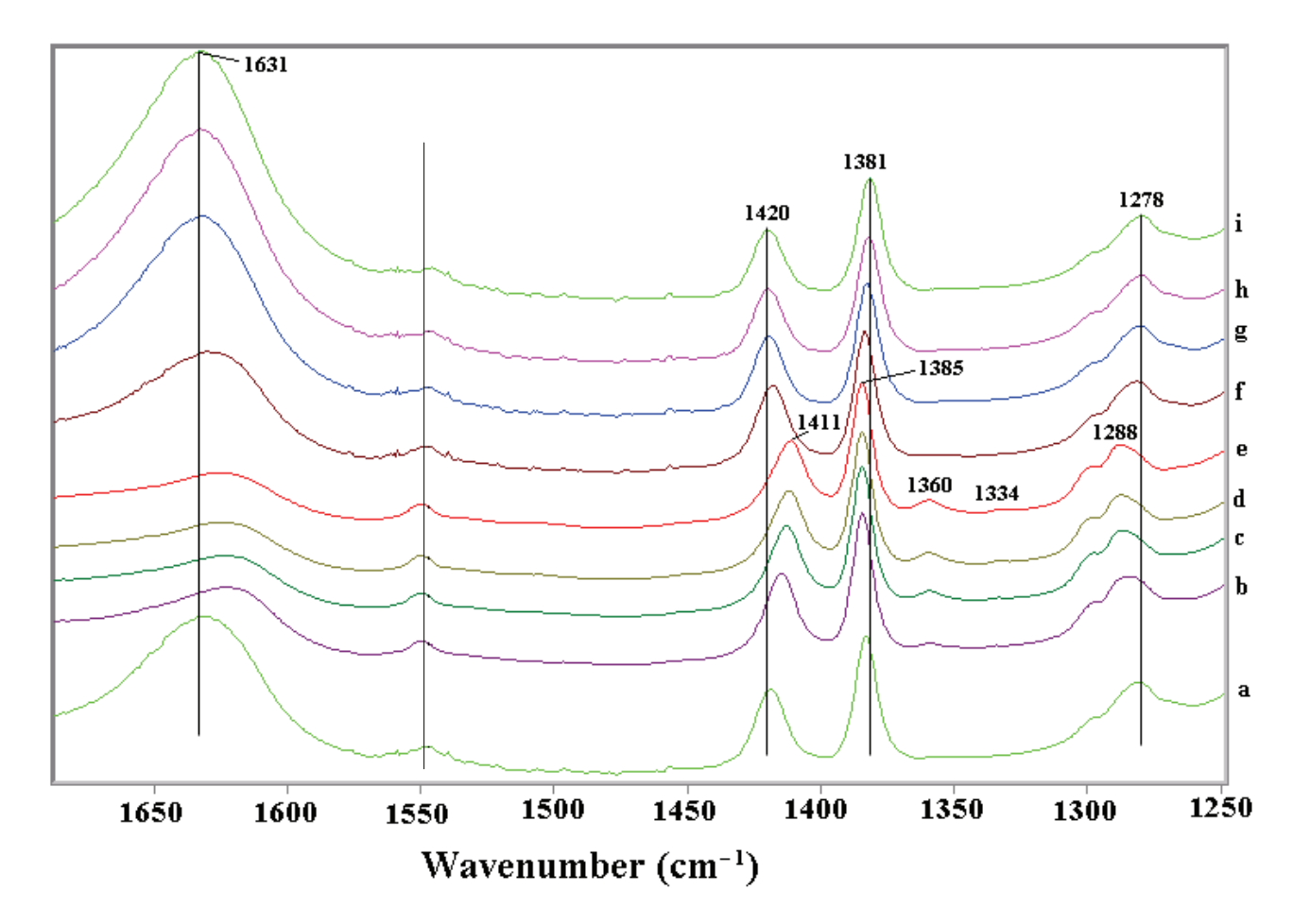


Figure IV-2. FTIR spectra of homoionic Fe(III)-montmorillonite clay/pentachlorophenol self-supporting clay film exposed to vacuum as a function of time: 0 (a), 10 (b), 20 (c), 50 (d) and 120 min (e). After obtaining spectrum at t = 120 min, vacuum was closed and water was added to the cell, spectra were collected at 2 (f), 10 (g), 22 (h) and 35 (i) min after exposure to water vapor.

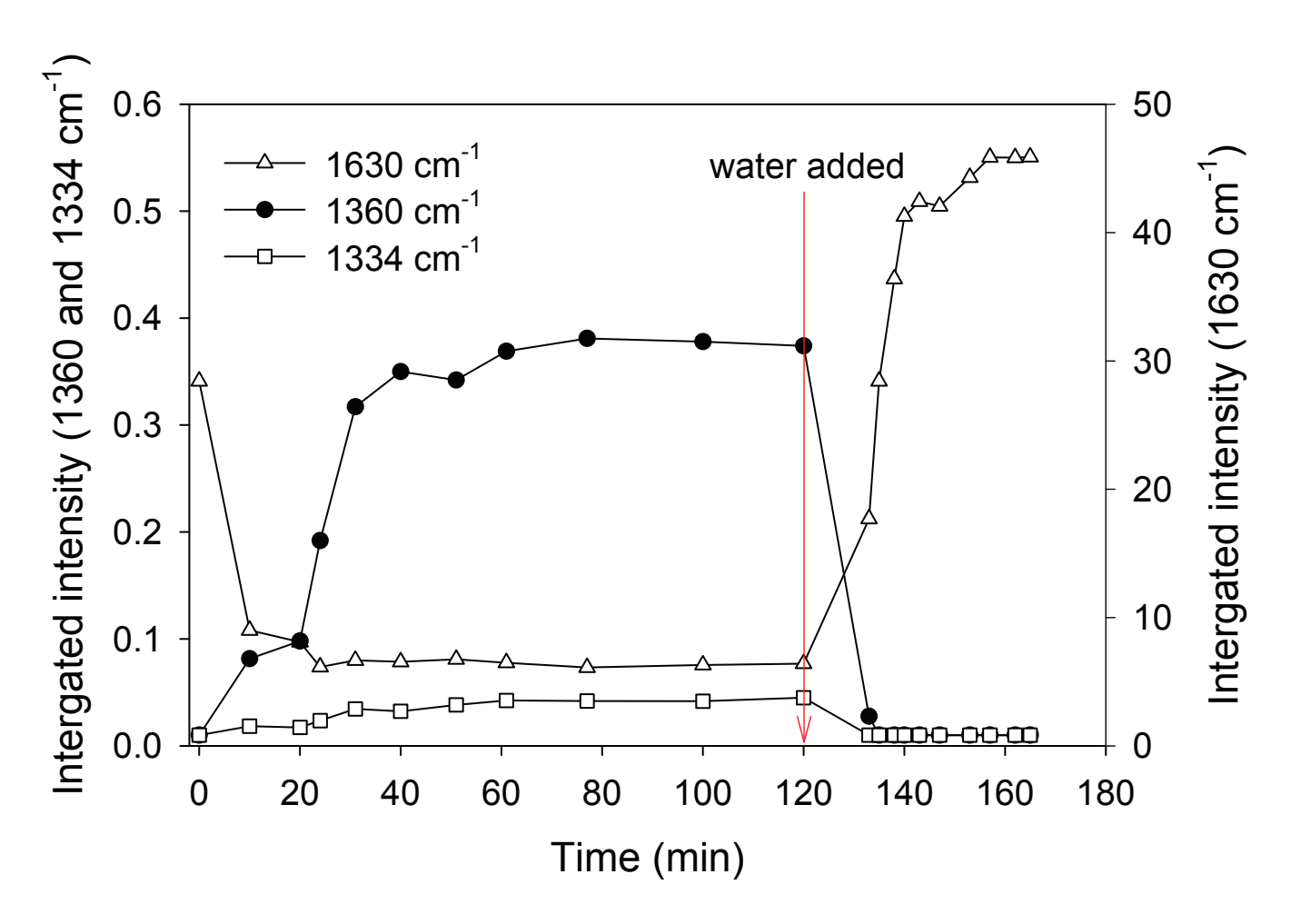


Figure IV-3. Integrated intensities of selected IR bands in homoionic Fe(III)-montmorillonite clay/pentachlorophenol as a function of exposure time to vacuum (0 < t < 120 min) and water vapor (t > 120 min).

**DFT Calculations.** To further understand the IR spectral peak shifts that occurred upon exposure of the FeSWy-2/PCP clay film to vacuum, theoretical spectra of proposed PCP complexes were calculated and compared with the experimental results. The optimized geometries of the gas-phase systems PCP, PCP/H<sub>2</sub>O, and PCP/Fe(OH)(H<sub>2</sub>O)<sub>n</sub><sup>2+</sup> are shown in Figure IV-4, and selected optimized structural parameters are presented in Table IV-1. Due to the size and complexity of PCP/Fe(OH)(H<sub>2</sub>O)<sub>n</sub><sup>2+</sup>, and limitations in computing resources, it was not possible to fully calculate the potential energy profile and locate all energy minima for each complex (Figure IV-5). Instead, geometry optimizations were performed within the low-energy regions where iron directly contacted the PCP hydroxyl group and all water molecules were in the first hydration shell of iron. Such structural configurations were confirmed to have the lowest energies in a previous study (Sun et al., 2007).

Among the optimized structures in the present study, complexes 0a, 1a, 2a and 3a (Figure IV-4) all featured similar structural characteristics in that both  $O_1$  and  $Cl_5$  of the PCP molecule coordinate the iron center as a bidentate ligand, and the hydroxyl group of  $Fe(OH)(H_2O)_n^{2+}$  is located opposite the position at which  $O_1$  of PCP coordinates the Fe center (the angle of  $O_1$ -Fe-OH ranges from  $138^\circ$  to  $163^\circ$ ). These four complexes generally have the lowest energies (Table IV-2) for their respective water contents, apparently due to stabilization of the  $2\sigma$  bonding orbital ( $d_z^2+p_z$ ) for each complex. When  $O_1$ -Fe-OH is roughly collinear, this geometry allows strong overlap of  $p_z$  orbitals from these two oxygens with the two lobes of the iron  $d_z^2$  orbital (Figure IV-6).

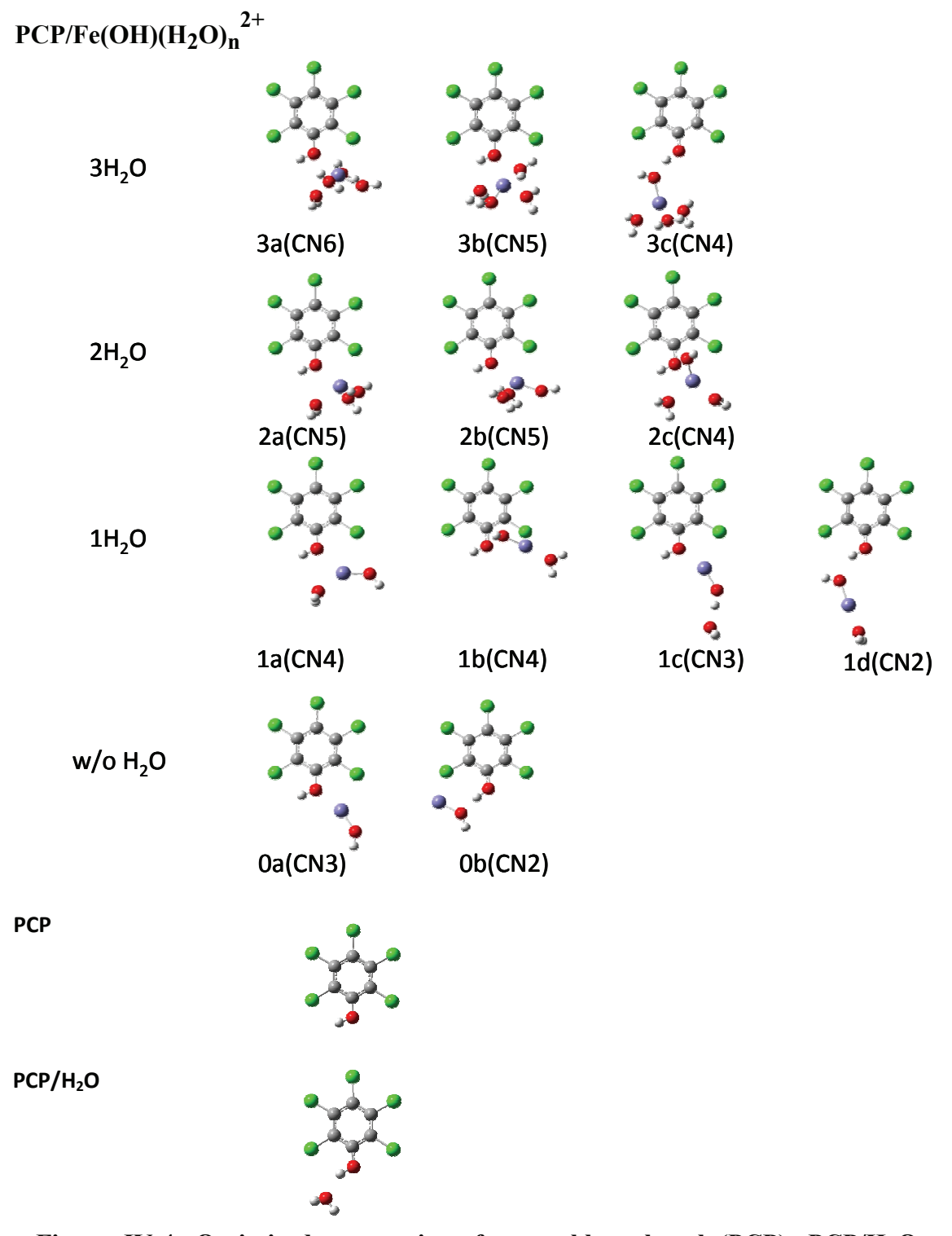


Figure IV-4. Optimized geometries of pentachlorophenol (PCP), PCP/ $H_2O$  and PCP/ $Fe(OH)(H_2O)_n^{2+}$  in the gas phase. Color scheme is: dark gray=carbon; green=chlorine; red=oxygen; light gray=hydrogen.

Table IV-1. Selected computed geometrical parameters of pentachlorophenol (PCP), PCP/H<sub>2</sub>O and PCP/Fe(OH)(H<sub>2</sub>O) $_{n}^{2+}$  in the gas phase (units: distances (Å) and angles (degree) ).

Parameter		PCP complexes				
	PCP	PCP/H <sub>2</sub> O	PCP/Fe(OH)(H <sub>2</sub> O) <sub>n</sub> <sup>2+</sup>			
			0a	1a	2a	3a
bond length						
$C_1$ - $O_1$	1.347	1.335	1.359	1.346	1.360	1.374
$O_1$ - $H_1$	0.974	0.990	0.990	0.986	0.987	0.986
C <sub>3</sub> -C <sub>4</sub>	1.403	1.402	1.439	1.444	1.433	1.420
C <sub>4</sub> -C <sub>5</sub>	1.407	1.406	1.461	1.450	1.437	1.428
H <sub>1</sub> -O <sub>water</sub>		1.793				
O <sub>1</sub> -Fe			2.173	2.404	2.210	2.182
Fe-Cl <sub>5</sub>			2.653	2.929	2.800	2.722
angle						
$C_1$ - $O_1$ - $H_1$	109.0	115.1	110.2	109.9	110.4	109.6
O <sub>1</sub> -Fe-OH			162.6	138.5	138.0	162.1
dihedral angle						
benzenering-O <sub>1</sub> -H <sub>1</sub>	0	0.17	0.07	0.02	4.48	0.05
spin on PCP			1.04	1.04	0.74	0.46
spin on Fe			3.58	3.61	3.73	3.84
Fe coordination number			3	4	5	6

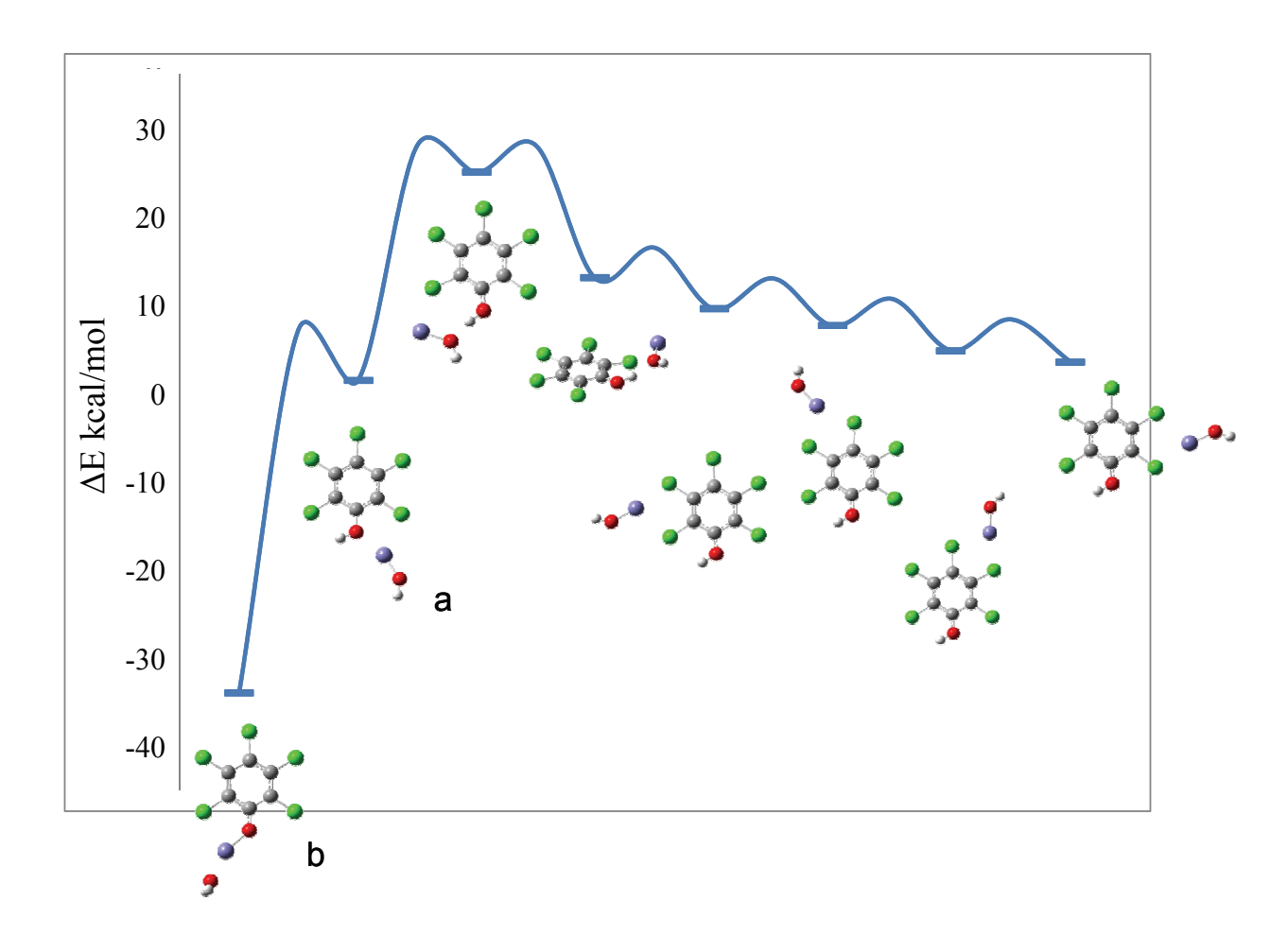


Figure IV-5. Potential energy profile for the stable conformers of PCP/FeOH $^{2+}$  complexes. The configuration a is the collinear structure of the pentachlorophenol (PCP) cation radical with FeOH $^{+}$ , and the configuration b is the PCP phenoxy radical with FeOH $^{2+}$ .

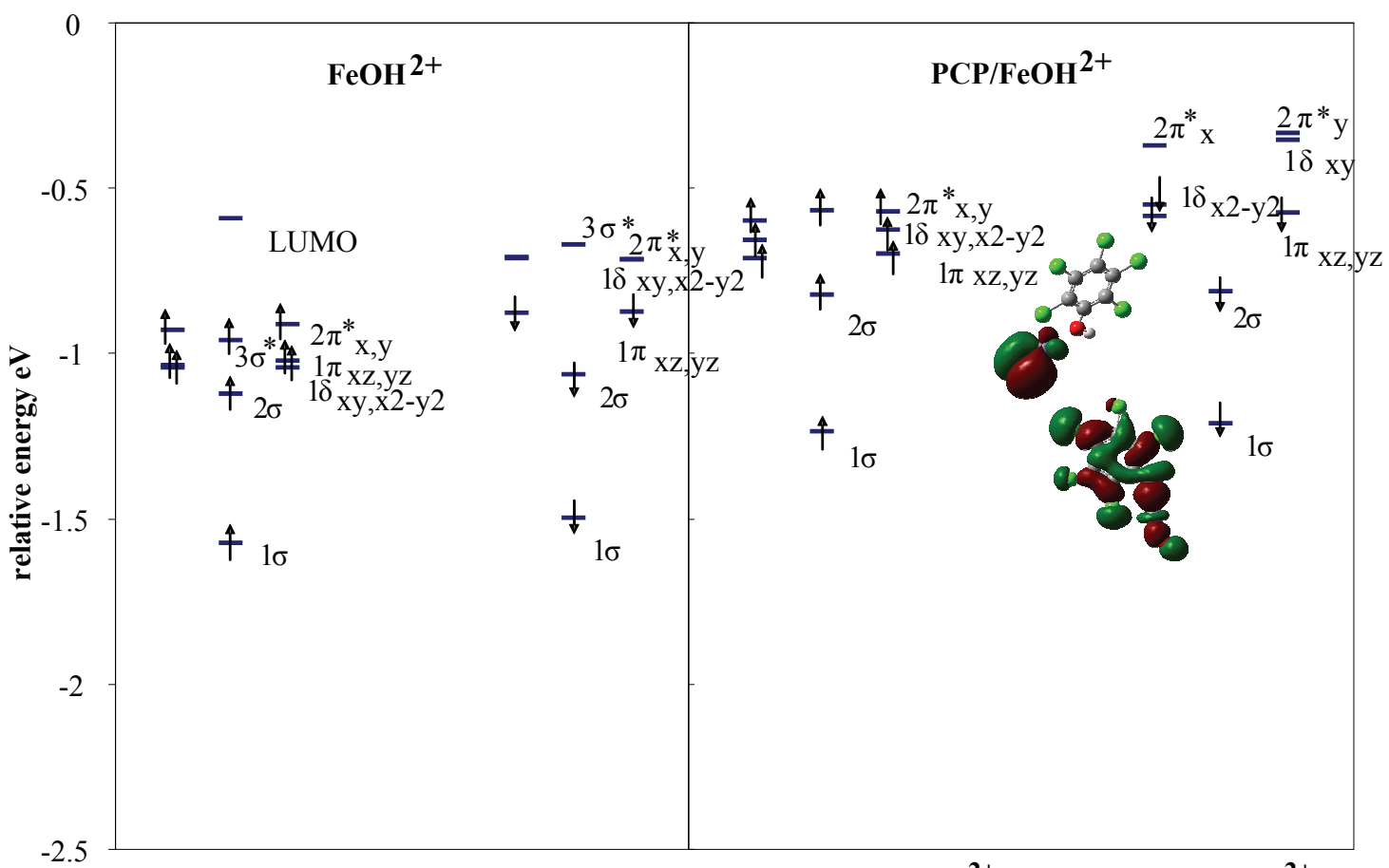


Figure IV-6. Molecular orbital energy level diagrams (the d block) for bare FeOH $^{2+}$  (left) and PCP/FeOH $^{2+}$  (right) systems. The insets on the right panel show the 1 $\delta$  and 2 $\sigma$  molecular orbitals. One electron transferred from PCP molecule fills into the non-bonding 1 $\delta$  orbital, which is localized primarily on the Fe  $d_x^2$  orbital. The 2 $\sigma$  molecular orbital consists of collinear overlaps between Fe  $d_z^2$  and PCP oxygen  $p_z$  orbitals.

Table IV-2. Additional geometry parameters of PCP/Fe(OH)( $H_2O$ ) $_n^{\ 2+}$  in gas phase. (unit: distances (Å), angles (degree) and energies (kcal/mol))

Complex ID	$C_{\mathbf{N}}$	Spin on pcp	spin on Fe	Relative energy*	Angle O-Fe-O	Distance Fe-O
3a	6	0.46	3.84		162.11	2.18
3b	5	0.6	3.83	5.17	135.64	2.31
3c	4	1	3.72	-21	32.30	3.88
2a	5	0.74	3.73		138.03	2.21
2b	5	0.6	3.80	2.78	160.51	2.22
2c	4	0.99	3.68	-1.62	84.98	2.48
1a	4	1.04	3.61		138.54	2.40
1b	4	1.03	3.66	-5.15	61.42	3.88
1c	3	0.92	3.60	20.51	156.89	2.15
1d	2	1	3.72	-9.66	36.64	4.04
0a	3	1.04	3.58		162.62	2.18
0b	2	1.07	3.69	21.06	36.25	3.79

<sup>\*</sup> Relative energy was calculated by assigning the total energy of the optimized "a" structure as zero.

Some configurations in which PCP forms outer-sphere hydrogen bonds with  $Fe(OH)(H_2O)_n^{2+}$  (e.g., complexes 3c and 1d of Figure IV-4) have even lower energies (Table IV-2), but these complexes are intermediates on a different reaction path toward

the low-energy phenoxy radical. They would rapidly convert into the phenoxy radical, which is proposed as the major pathway in the gas phase (Qu et al., 2009), but apparently do not do so in the clay interlayer, plausibly because of the favorable electrostatic interactions afforded to the radical cation by the negative energy field of the clay mineral (Cygan et al., 2009; Govindaraj et al., 1987; Johnston et al., 1992a; Sawhney et al., 1984). Also, their simulated IR spectra do not match with the experimental data (Figure IV-7). Thus, despite the somewhat lower energy of the phenoxy-radical complex in the gas phase, the radical-cation reaction pathway seems to be selected in the clay. Therefore, the series of 'a' complexes (Figure IV-4) was the focal point of the current study. In the simplest PCP/Fe(OH)(H<sub>2</sub>O)<sub>n</sub><sup>2+</sup> complex that has been studied, PCP/FeOH<sup>2+</sup> (structure 0a of Figure IV-4), PCP is coplanar with the FeOH 2+ cation and the Fe-O1 and Fe-Cl5 bond lengths are 2.173 and 2.653 Å, respectively (Table IV-1). The complexation increases the lengths of the O<sub>1</sub>-H<sub>1</sub> and C<sub>1</sub>-O<sub>1</sub> bonds, but dramatically increases the C-C bond lengths that are opposite the phenol position (C<sub>3</sub>-C<sub>4</sub> and C<sub>4</sub>-C<sub>5</sub>, Table IV-1) from  $1.402\sim1.407$  Å to 1.439 Å and 1.461 Å. This effect is due to the extraction by Fe of one  $\pi$ electron from the benzene ring, which causes weakening of the C-C bonds (Qin and Wheeler, 1996). Thus, the PCP radical cation is formed automatically as PCP complexes with FeOH<sup>2+</sup>, while the precomplex (that is, a complex in the absence of electron transfer) cannot be located in this study due to the negligible energy barrier between the radical cation complex and the precomplex. The reversibility of radical cation complex formation observed by FTIR (Figure IV-2) implies that this energy barrier is small in both directions.

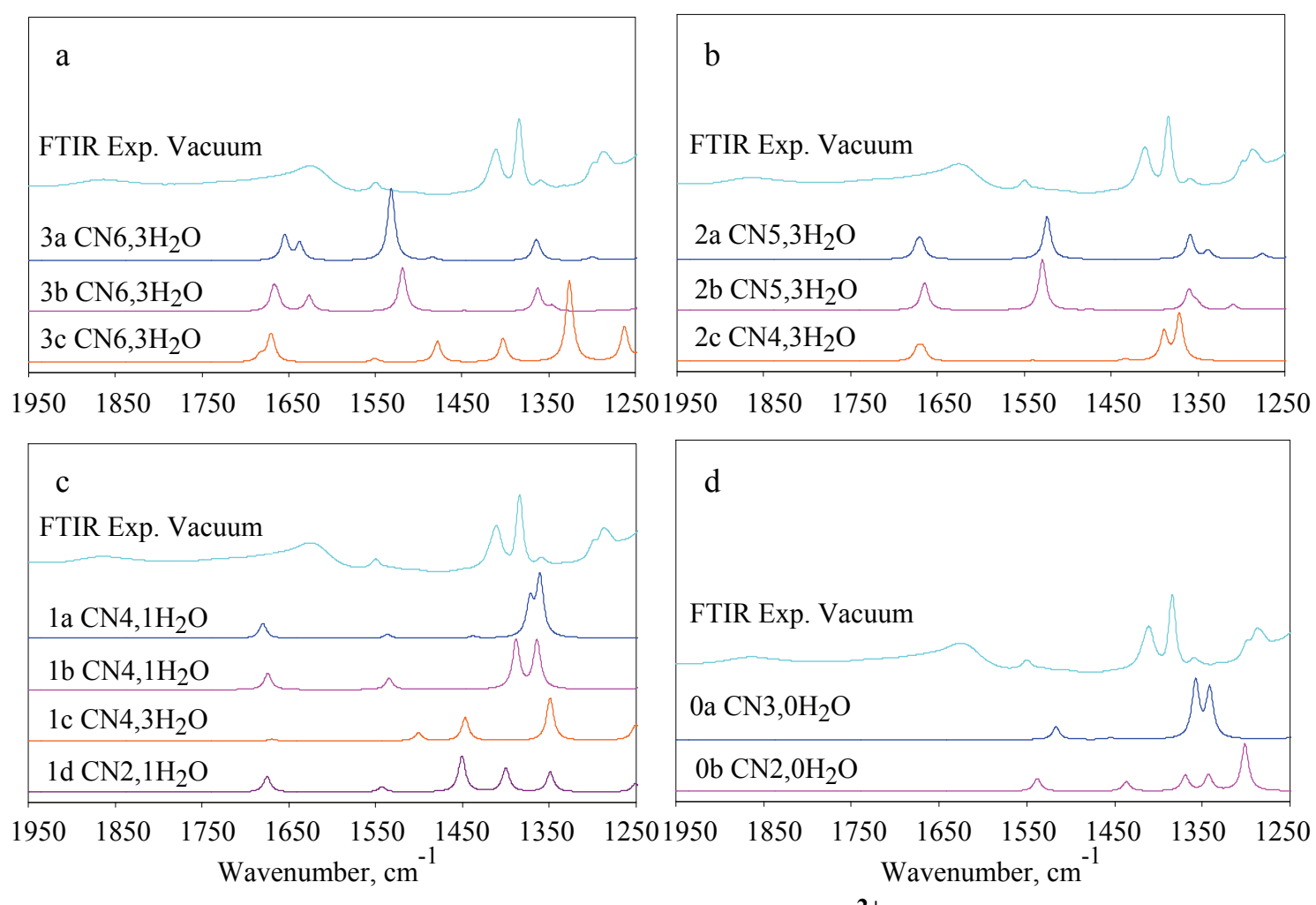


Figure IV-7. DFT calculated infrared spectra of selected PCP/Fe(OH)( $H_2O$ )<sub>n</sub><sup>2+</sup> systems with the number of coordination water n equal to 3(a), 2(b), 1(c) and 0(d).

As the coordination number of iron increases from 3 to 6 when water molecules are added into the iron hydration shell (structures 1a, 2a, 3a of Figure IV-4), the C<sub>3</sub>-C<sub>4</sub> and C<sub>4</sub>-C<sub>5</sub> bond lengths of PCP gradually decrease to 1.42 Å and 1.428 Å (Table IV-1) in the octahedrally coordinated PCP/Fe(OH)(H<sub>2</sub>O)<sub>3</sub><sup>2+</sup> (structure 3a of Figure IV-4). This weakening of the C-C bonds is still profound and the PCP radical cation is formed automatically in all cases. However, the radical cation character of PCP is less pronounced as hydration increases, which is in excellent agreement with the lower yields observed experimentally (Gu et al., 2008), and the FTIR results showing that as the water content increased, radical cation bands diminished (Figure IV-3).

The spin density on the PCP molecule in each PCP/Fe(OH)( $H_2O$ )<sub>n</sub><sup>2+</sup> complex was calculated by natural population analysis (NPA) (Table IV-1). For the simplest PCP/FeOH<sup>2+</sup> complex (structure 0a of Figure IV-4), an excess positive spin density of 1.04 is spread over the PCP molecule. One electron has been transferred from a  $\pi$  orbital of PCP to the nonbonding  $\delta_{x-y}^{2-2}$  orbital of the iron center (as shown in Figure IV-6) and the iron has been reduced from Fe(III) to Fe(II) (Table IV-1). When water molecules were sequentially added into the iron hydration shell (structures 1a, 2a, 3a of Figure IV-4), the spin density on PCP decreased from 1.04 to 0.74 to 0.46, due to spin delocalization to the ligand water molecules (Table IV-1). Although these model PCP/Fe(OH)( $H_2O$ )<sub>n</sub><sup>2+</sup> complexes lack any interaction with clay mineral surfaces, the calculations do yield changes in both PCP structure and electron density that support the hypothesized PCP radical cation formation (Gu et al., 2008), and also reproduce the

correct trend of hydration effects on the radical cation formation. Furthermore, these first principle calculations help explain the spectroscopic features of the radical cation complex, as shown below.

Adding more water into the system would presumably cause displacement of PCP from the inner-sphere coordination sites of iron, due to the stronger binding affinity of water (Fein, 1996). Therefore, the properties of PCP adsorbed on clay minerals at high water content might be simulated by the simplest PCP/water complex. Optimization of the PCP/water geometry (Figure IV-4) shows a strong hydrogen bond between H<sub>1</sub> and the water oxygen, with a bond length of 1.79 Å (Table IV-1). In this case the distance between the PCP donor oxygen and the water receptor oxygen is 2.70 Å. The O<sub>1</sub>-H<sub>1</sub> bond is elongated from 0.974 Å (for isolated PCP) to 0.990 Å for the complex, while the C<sub>1</sub>-O<sub>1</sub> bond is shortened from 1.347 Å (in isolated PCP) to 1.335 Å (Table IV-1). The hydroxyl group of PCP tilts slightly (0.17 degree) out of the aromatic molecular plane, and the C<sub>1</sub>-O<sub>1</sub>-H<sub>1</sub> angle increases from 109.0 degree to 115.1 degree (Table IV-1). These significant changes in the geometries induced by hydrogen bonding would be expected to cause vibrational peak shifts, especially for the modes involved C-O-H bending and C-O stretching, as observed for the 1411cm<sup>-1</sup>  $\delta$ (C-OH) and 1385 cm<sup>-1</sup>  $\nu$ (C-OH).

The calculated infrared spectral patterns for PCP, PCP/ $H_2O$ , and PCP/ $Fe(OH)^{2+}$  (structure 0a of Figure IV-4) are compared with the observed spectra in Figure IV-8. Three frequencies in the experimental spectra of PCP-clay show pronounced shifts in the presence of  $H_2O$  vapor versus vacuum, and are labeled 1, 2, and 3 in Figure IV-8. These

modes are all dominated by ring breathing, C<sub>1</sub>-O<sub>1</sub> stretching, and C<sub>1</sub>-O<sub>1</sub>-H<sub>1</sub> bending, according to their potential energy decompositions (PED) (Table IV-3). Due to the strong hydrogen bonding between O<sub>1</sub> of PCP and water, the calculated peak of 1381.3 cm<sup>-1</sup> in the absence of water red-shifts 5.9 cm<sup>-1</sup> toward lower frequencies for the PCP/H<sub>2</sub>O complex (Figure IV-8d), and the peak at 1426.8 cm<sup>-1</sup> (dry) exhibits a 15.9 cm<sup>-1</sup> blue shift when hydrated, compared to calculated peak positions in the absence of water (Figure IV-8e). All these shifts are in good agreement with the magnitudes and directions of the corresponding experimental shifts (-4, 9, and 10 cm<sup>-1</sup>, respectively, from comparison of Figure IV-2e versus IV-2i).

The appearance of computed vibrational peaks at 1358 and 1343 cm<sup>-1</sup> (lines 4 and 5 of Figure IV-8c) for the radical cation PCP/Fe(OH)<sup>2+</sup> complex (structure 0a of Figure IV-4) agrees well with the experimental spectrum (Figures IV-2e, IV-8b and Figure IV-3). This provides strong independent support for the hypothesis that the new peaks in the experimental spectrum (Figures IV-2e and IV-8b) emanate directly from the formation of PCP radical cations. For the radical cation with its longer and weaker C-C bonds (as described above), it is expected that the ring-breathing C-C vibrational modes would shift dramatically to a lower frequency. Experimentally, each peak shifted 51 cm<sup>-1</sup> (1411-1360=51 and 1385-1334=51, Table IV-3), and the first principle models show very similar shifts (55 and 33 respectively, Table IV-3). The two calculated peaks are only -3 and 9 cm<sup>-1</sup> wavenumbers different from the observed peaks, and are assigned as ring

breathing modes according to the potential energy distribution analysis shown in Table IV-3. The intensities of the two peaks are significantly enhanced by factors of 3.00 and 2.78, compared with the dominant peak at 1412 cm<sup>-1</sup> for the isolated PCP molecule. Based on these calculated peak area ratios and the experimental spectrum for the sample under vacuum (Figures IV-2e and IV-8b), the experimental yield of radical cations after 120 min in vacuum was approximately 3%.

This pattern of the ring-breathing C-C vibrational modes shifting to dramatically lower frequency upon radical cation formation is sustained when more water molecules are added to the first hydration shell of iron (Figure IV-9, left). However, as discussed above, the radical character of the PCP cation decreases somewhat with increasing hydration, and this manifests a linear decrease in the intensity of the radical cation ring-breathing mode at 1360 cm<sup>-1</sup> as the Fe(OH)<sup>2+</sup>-PCP complex becomes more hydrated (Figure IV-9, right). It is important to note that, compared to the 1360 cm<sup>-1</sup> peak, the mode at 1334 cm<sup>-1</sup> diminishes much faster with increasing hydration, which explains why the observed peak at 1334 cm<sup>-1</sup> is weaker than the peak at 1360 cm<sup>-1</sup>. Increasing numbers of water molecules strongly disrupt the favorable energy with which PCP binds to the Fe center (Figure IV-9, right) hence suppressing the electron-transfer reaction. The binding energy of PCP to the Fe-center linearly decreases as the complex becomes more hydrated.

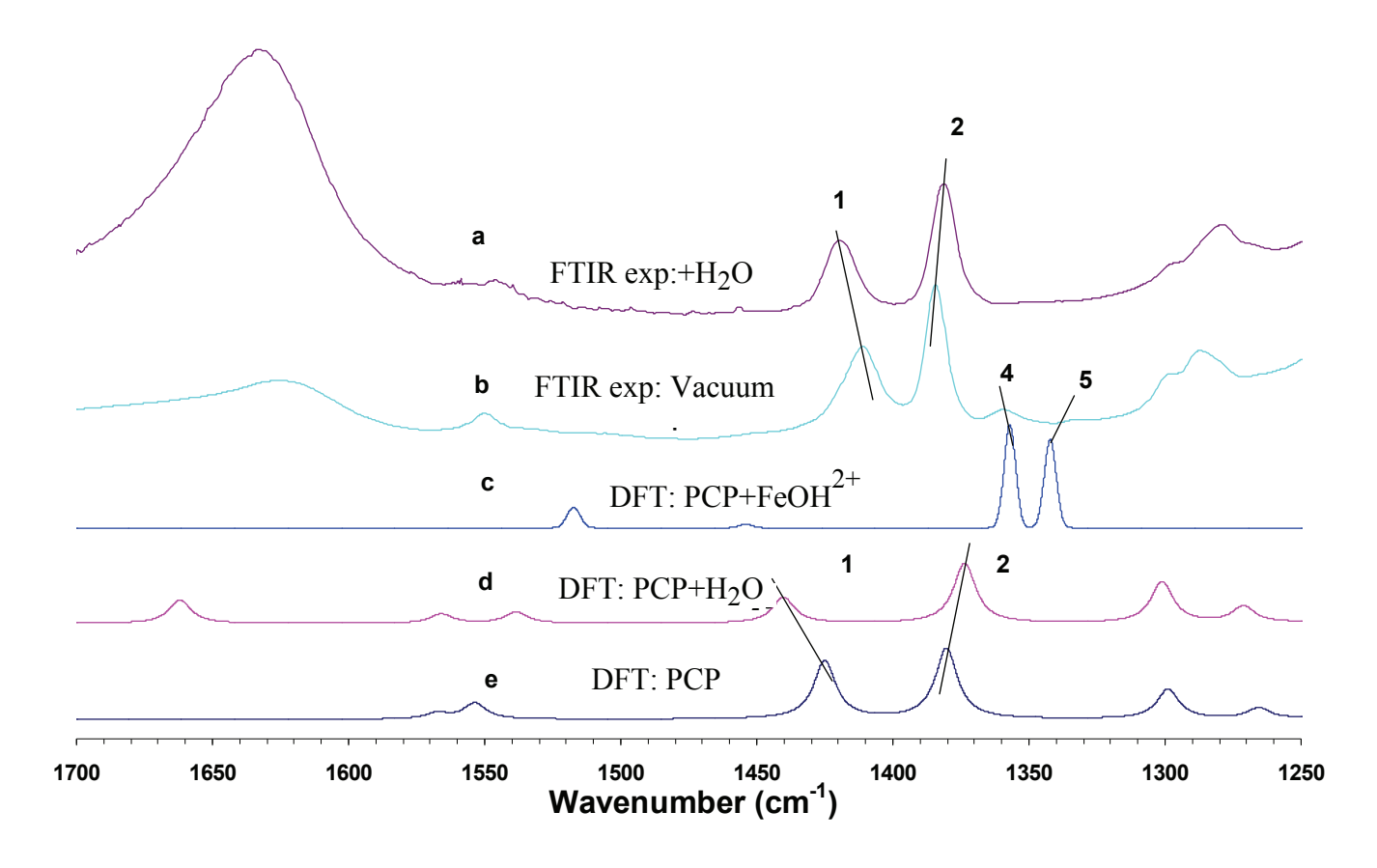


Figure IV-8. Comparison of experimental infrared spectra of Fe(III)-montmorillonite clay/pentachlorophenol (PCP) system: (a) observed spectrum after exposure to water vapor, (b) observed spectrum under vacuum, and calculated spectra (c) (d) and (e) for PCP/FeOH<sup>2+</sup> (structure 0a of Figure IV-4), PCP/H<sub>2</sub>O and PCP respectively. Lines 1, 2 indicate the peak shifts of 1420 and 1381cm<sup>-1</sup>. Lines 4 and 5 indicate new peaks due to formation of radical cation in experimental (b) and calculated (c) spectra. The scaling factor was 0.98.

Table IV-3. The calculated FTIR frequencies of all pentachlorophenol (PCP) species compared with experimental results, and the corresponding potential energy distribution analysis (PED) (percentages, in parentheses).

Species	v <sub>exp</sub>	v <sub>cal</sub>	Δ	Assignments and %PED
	(cm <sup>-1</sup> )	(cm <sup>-1</sup> )	$(v_{cal}-v_{exp})$	
PCP	1411	1426.8	+15.8	C-O str (31)+C-O-H bend (3)+ring breathing (54)
	1385	1381.3	-3.7	C-O str (3)+C-O-H bend (13)+ring breathing (65)
	1288	1301.4	+13.4	C-O-H bend (24)+ring breathing (74)
PCP/H <sub>2</sub> O	1420	1442.7	+22.7	C-O str (1)+ring breathing (91)
	1381	1375.4	-5.6	C-O str (2)+ring breathing (83)
	1278	1302.5	+24.5	ring breathing (91)
PCP/FeOH <sup>2+</sup>	1360	1357.3	-2.7	ring breathing (82)
(0a)	1334	1342.7	+8.7	ring breathing (84)
	-	1237.2	-	ring breathing (78)

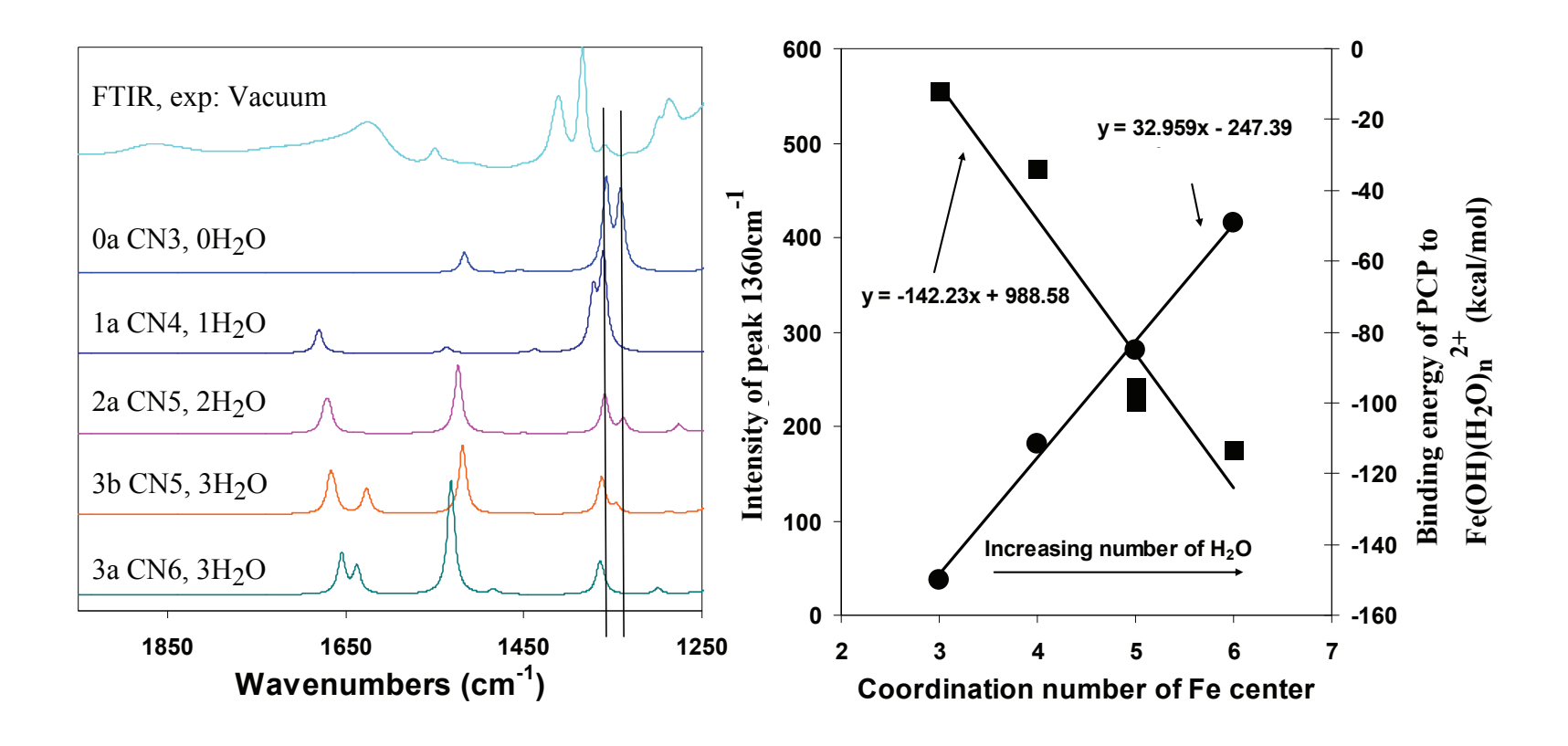


Figure IV-9. Left: Calculated infrared spectra of selected PCP/Fe(OH)( $H_2O$ )<sub>n</sub><sup>2+</sup> systems (for structures refer to Figure IV-4) with the number of coordinated water molecules increasing from 0 to 3. Right: Correlations of intensity of the simulated infrared peak at 1360 cm<sup>-1</sup> ( $\blacksquare$ ), and the binding energies of pentachlorophenol (PCP) onto Fe(OH)( $H_2O$ )<sub>n</sub><sup>2+</sup> ( $\bullet$ ) versus the total coordination number of the Fe center.

ONIOM calculations on PCP/PCP radicals interacting with clay surface. To explore the apparent role of clay surfaces in stabilizing radical cation intermediates, comparisons were made among PCP, its radical cation, and the phenoxy radical on a clay mineral surface as modeled by the ONIOM method. Resulting configurations and structure parameters of PCP are shown in Figure IV-10 and Table IV-4. The calculated bond lengths of a single PCP molecule adsorbed on clay mineral surface were uniformly ~0.2 Å shorter than those of isolated PCP, which results from overestimation of bond strength by the Hartree-Fock method used in the ONIOM model. The average C-C bonds in the PCP radical cation on the clay mineral surface were elongated by 0.026 Å compared with those of neutral PCP on the clay, due to the loss of one  $\pi$  electron (as observed in the absence of clay, Table 1). Both PCP and the PCP radical cation formed hydrogen bonds with the surface oxygen with the H<sub>1</sub>-O<sub>surface</sub> bond length equal to 1.724 Å and 1.535 Å, respectively (Table IV-4), and the benzene plane of each molecule tilted about 30-31 degrees toward the clay mineral surface due to the hydrogen bond. The PCP phenoxy radical adopted a conformation parallel to the clay mineral surface with a distance of 3.06 Å (from O<sub>1</sub> to the surface oxygen plane) which is longer than those of 2.67 Å and 2.69 Å for PCP and the PCP radical cation (Table IV-4), suggesting a weaker adsorption of the PCP phenoxy radical. The calculated adsorption energies were -14.6 kcal/mol, -56.4 kcal/mol and -6.9 kcal/mol for PCP, PCP radical cation and PCP phenoxy radical, respectively (Table IV-4), and compared to the isolated PCP in gas phase the ionization energy of PCP on clay was decreased by 39.2 kcal/mol showing a much stronger stabilization of the PCP radical cation compared to the other species, due to more favorable electrostatic interactions with the (negatively charged) clay mineral surface.

The relatively weak interaction between the neutral PCP molecule and the clay mineral surface supports our usage of Fe(III)/PCP complexes alone (not explicitly accounting for the effects of clay mineral surfaces) to predict the spectroscopic properties of the complicated PCP interactions with interlayer iron in smectite. That is, the role of clay may not be to influence any local structural interactions between Fe and PCP, but the electrostatic field in the clay interlayer may strongly direct the reactivity along the radical cation pathway rather than the phenoxy radical pathway that might otherwise be favored in the absence of clay.

Table IV-4. Selected computed geometry parameters of ONIOM pentachlorophenol (PCP)-smectite clay clusters (units: distances (Å) and angles (degree) energies (kcal/mol)).

Parameter	ONIOM PCP-smectite cluster			
	PCP	PCP cation radical	PCP phenoxy radical	
bond length				
$C_1$ - $O_1$	1.345	1.270	1.292	
$O_1$ - $H_1$	0.966	1.014		
$C_1$ - $C_2$	1.387	1.437	1.428	
$C_2$ - $C_3$	1.381	1.373	1.390	
C <sub>3</sub> -C <sub>4</sub>	1.382	1.419	1.409	
C <sub>4</sub> -C <sub>5</sub>	1.387	1.417	1.409	
C <sub>5</sub> -C <sub>6</sub>	1.379	1.376	1.391	
C <sub>6</sub> -C <sub>1</sub>	1.390	1.440	1.429	
distance of PCP-H···O <sub>surface</sub>	1.724	1.548		
angle between PCP ring and surface oxygen plane	29.91	31.41	2.71	
distance between PCP-O and surface oxygen plane	2.67	2.29	3.06	
adsorption energy	-14.6	-56.4	-6.9	

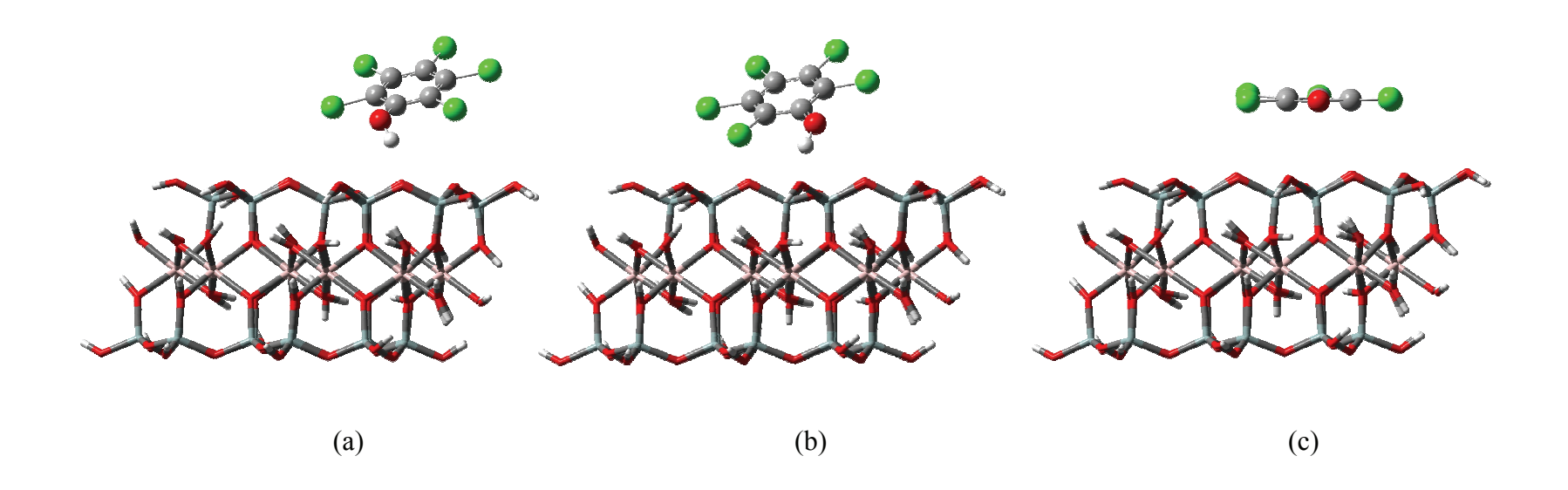


Figure IV-10. ONIOM models of the pentachlorophenol (PCP) molecule (a) PCP radical cation (b) and PCP phenoxy radical adsorbed on smectite clay surface. Color scheme for PCP: red=O; green=Cl; dark gray=C; light gray=H. The 2:1 aluminosilicate clay layer is shown below the PCP structures. Color scheme for the clay layer: red=O; dark gray=Si; light gray=H; pink=Al.

In summary, the critical step that initiates the clay-facilitated formation of OCDD from PCP is the formation of PCP radical cations on Fe(III)-montmorillonite surfaces. This conclusion is strongly supported by independent experimental and theoretical results: (1) The *in situ* FTIR observation of new peaks at 1360 and 1334 cm<sup>-1</sup> that appear (reversibly) upon dehydration, and (2) first principle DFT calculations of models for PCP/Fe(OH)(H<sub>2</sub>O)<sub>n</sub><sup>2+</sup> complexes that reproduce the experimentally observed IR vibrational features, and demonstrate that they are a direct result of single electron transfer from PCP to Fe(III). Detailed atomic and electronic structures of PCP complexes with interlayer Fe(III) species also illuminate the role of water in the reversible formation of the PCP radical cations.

The reactive PCP radical cation described herein initiates a series of reactions that together form OCDD. Pentachlorophenol falls with rains across the world (Baker and Hites, 2000), and many soils contain swelling clay minerals that could catalyze the formation of OCDD from these PCP inputs. Hence the clay facilitated OCDD formation reaction could plausibly be an important ongoing environmental process.

LITERATURE CITED

#### LITERATURE CITED

- Allen, B.L., and B.F. Hajek. 1989. Mineral occurrence in soil environments, p. 199-278, *In* J. B. Dixon and S. B. Weed, eds. Minerals in Soil Environments, 2nd ed. Soil Science Society of America, Madison, WI.
- Arroyo, L.J., H. Li, B.J. Teppen, and S.A. Boyd. 2005. A simple method for partial purification of reference clays. Clays and Clay Minerals 53:511-519.
- Baker, J.I., and R.A. Hites. 2000. Is combustion the major source of polychlorinated dibenzo-p-dioxins and dibenzo-furans to the environment? A mass balance investigation. Environmental Science & Technology 34:2879-2886.
- Becke, A.D. 1993. Density-functional thermochemistry. III. The role of exact exchange. Journal of Chemical Physics 98:5648-5652.
- Boyd, S.A., and M.M. Mortland. 1985. Dioxin radical formation and polymerization on Cu(II)-smectite. Nature 316:532-535.
- Boyd, S.A., and M.M. Mortland. 1986. Radical formation and polymerization of chlorophenols and chloroanisole on copper(II)-smectite. Environmental Science & Technology 20:1056-1058.
- Bytheway, I., and M.W. Wong. 1998. The prediction of vibrational frequencies of inorganic molecules using density functional theory. Chemical Physics Letters 282:219-226.
- Chatterjee, A., T. Ebina, T. Iwasaki, and F. Mizukami. 2003. Intermolecular reactivity study to scale adsorption property of para- and meta-substituted nitrobenzene over 2:1 dioctahedral smectite. Journal of Chemical Physics 118:10212-10220.
- Choi, S.H., B.R. Wood, J.A. Ryder, and A.T. Bell. 2003. X-ray absorption fine structure characterization of the local structure of Fe in Fe-ZSM-5. Journal of Physical Chemistry B 107:11843.
- Curtiss, L.A., K. Raghavachari, P.C. Redfern, and J.A. Pople. 2000. Assessment of Gaussian-3 and density functional theories for a larger experimental test set. Journal of Chemical Physics 112:7374.
- Cygan, R.T., J.A. Greathouse, H. Heinz, and K.A. J. 2009. Molecular models and simulations of layered materials. Journal of Materials Chemistry 19:2470-2481.
- Czarnik-Matusewicz, B., A.K. Chandra, M. Tho Nguyen, and T. Zeegers-Huyskens. 1999. Theoretical and experimental (400-10 000 cm<sup>-1</sup>) study of the vibrational spectrum of pentachlorophenol. Journal of Molecular Spectroscopy 195:308-316.

- Fein, J.B. 1996. The effect of aqueous metal-chlorophenolate complexation on contaminant transport in groundwater systems. Applied Geochemistry 11:735.
- Fernandes de Oliveira, M., C.T. Johnston, G.S. Premachandra, B.J. Teppen, H. Li, D.A. Laird, D. Zhu, and B.S. A. 2005. Spectroscopic study of carbaryl sorption on smectite from aqueous suspension. Environmental Science & Technology 39:9123-9129.
- Ferrario, J., C. Byrne, and D. Cleverly. 2000. 2,3,7,8-dibenzo-p-dioxins in mined clay products from the United States: Evidence for possible natural origin. Environmental Science & Technology 34:4524–4532.
- Fiedler, A., D. Schroeder, S. Shaik, and H. Schwarz. 1994. Electronic structures and gasphase reactivities of cationic late-transition-metal oxides. Journal of the American Chemical Society 116:10734.
- Franzblau, A., E. Hedgeman, Q. Chen, S.-Y. Lee, P. Adriaens, A. Demond, D. Garabrant, B. Gillespie, B. Hong, O. Jolliet, J. Lepkowski, W. Luksemburg, M. Maier, and Y. Wenger. 2008. Case report: Human exposure to dioxins from clay. Environmental Health Perspectives 116:238-242.
- In Gaussian, Inc., Wallingford CT. 2004. In Gaussian, Inc., Wallingford CT.
- Gorb, L., R. Lutchyn, Y. Zub, D. Leszczynska, and J. Leszczynski. 2006. The origin of the interaction of 1,3,5-trinitrobenzene with siloxane surface of clay minerals. Journal of Molecular Structure 766:151-157.
- Govindaraj, N., M.M. Mortland, and S.A. Boyd. 1987. Single electron transfer mechanism of oxidative dechlorination of 4-chloroanisole on copper(II)-smectite. Environmental Science & Technology 21:1119.
- Gu, C., H. Li, B.J. Teppen, and S.A. Boyd. 2008. Octachlorodibenzodioxin formation on Fe(III)-Montmorillonite clay. Environmental Science & Technology 42:4758-4763.
- Hayward, D.G., D. Nortrup, A. Gardner, and M. Clower. 1999. Elevated TCDD in chicken eggs and farm-raised catfish fed a diet with ball clay from a southern United States mine. Environmental Research 81:248-256.
- Helsen, J.A., and B.A. Goodman. 1983. Characterization of iron(II)-and iron(III)-exchanged montmorillonite and hectorite using the Moessbauer effect. Clay Minerals 18:117-125.
- Hinedi, Z.R., C.T. Johnston, and C. Erickson. 1993. Chemisorption of benzene on Cumontmorillonite as characterized by FTIR and <sup>13</sup>C MAS NMR. Clays and Clay Minerals 41:87-94.

- Holmstrand, H., D. Gadomski, M. Mandalakis, M. Tysklind, R. Irvine, P. Andersson, and O. Gustafsson. 2006. Origin of PCDDs in ball clay assessed with compound-specific chlorine isotope analysis and radiocarbon dating. Environmental Science & Technology 40:3730-3735.
- Horii, Y., B. van Bavel, K. Kannan, G. Petrick, K. Nachtigall, and N. Yamashita. 2008. Novel evidence for natural formation of dioxins in ball clay. Chemosphere 70:1280-1289.
- Johnston, C.T., and Y.O. Aochi. 1996. Fourier transform infrared and Raman spectroscopy, p. 269-321, *In* D. L. Sparks, ed. Methods of Soil Analysis Part 3 Chemical Methods. Soil Science Society of America: Madison, WI.
- Johnston, C.T., G. Sposito, and C. Erickson. 1992a. Vibrational probe studies of water interactions with montmorillonite. Clays and Clay Minerals 40:722-730.
- Johnston, C.T., T. Tipton, D.A. Stone, C. Erickson, and S.L. Trabue. 1991. Chemisorption of p-dimethoxybenzene on copper-montmorillonite. Langmuir 7:289-296.
- Johnston, C.T., T. Tipton, S.L. Trabue, C. Erickson, and D.A. Stone. 1992b. Vapor-phase sorption of p-xylene on Co- and Cu-exchanged SAz-1 montmorillonite. Environmental Science & Technology 26.
- Lee, C., W. Yang, and R.G. Parr. 1988. Development of the Colle-Salvetti correlationenergy formula into a functional of the electron density. Physical Review B 37:785-789.
- Qin, Y., and R.A. Wheeler. 1996. Density-functional-derived structures, spin properties, and vibrations for phenol radical cation. Journal of Physical Chemistry 100:10554-10563.
- Qu, X., H. Wang, Q. Zhang, X. Shi, F. Xu, and W. Wang. 2009. Mechanistic and kinetic studies on the homogeneous gas-phase formation of PCDD/Fs from 2,4,5-trichlorophenol. Environmental Science & Technology 43:4068-4075.
- Rao, P.V.R., and G.R. Rao. 2002. Vibrational analysis of substituted phenols: Part I. Vibrational spectra, normal coordinate analysis and transferability of force constants of some formyl-, methoxy-, formylmethoxy-, methyl- and halogenophenols. Spectrochimica Acta Part A 58:3039-3065.
- Sawhney, B.L., R.K. Kozloski, P.J. Isaacson, and M.P.N. Gent. 1984. Polymerization of 2,6-dimethylphenol on smectite surfaces. Clays and Clay Minerals 32:108-114.
- Shiota, Y., and K. Yoshizawa. 2000. Methane-to-methanol conversion by first-row transition-metal oxide ions: ScO<sup>+</sup>, TiO<sup>+</sup>, VO<sup>+</sup>, CrO<sup>+</sup>, MnO<sup>+</sup>, FeO<sup>+</sup>, CoO<sup>+</sup>, NiO<sup>+</sup>, and CuO<sup>+</sup>. Journal of the American Chemical Society 122:12317.

- Skipper, N.T., K. Refson, and J.D.C. McConnell. 1991. Computer simulation of interlayer water in 2:1 clays. Journal of Chemical Physics 94:7434-7445.
- Soma, Y., M. Soma, and I. Harada. 1985. Reactions of aromatic molecules in the interlayer of transition-metal ion-exchanged montmorillonite studied by resonance Raman spectroscopy. 2. Monosubstituted benzenes and 4,4'-substituted biphenyls. Journal of Physical Chemistry 89:738-742.
- Soma, Y.S., M.; Harada, I. 1986. The oxidative polymerization of aromatic molecules in the interlayer of montmorillonites studied by resonance Raman spectroscopy. Journal of Contaminant Hydrology 1:95-106.
- Sun, Q., M. Altarawneh, B.Z. Dlugogorski, E.M. Kennedy, and J.C. Mackie. 2007. Catalytic effect of CuO and other transition metal oxides in formation of dioxins: theoretical investigation of reaction between 2, 4, 5-trichlorophenol and CuO. Environmental Science & Technology 41:5708.
- Teppen, B.J., C.H. Yu, S.Q. Newton, D.M. Miller, and L. Schäfer. 2002. Quantum molecular dynamics simulations regarding the dechlorination of trichloro ethene in the interlayer space of the 2:1 clay mineral nontronite. Journal of Physical Chemistry A 106:5498-5503.
- Wasserman, S.R., L. Soderholm, and U. Staub. 1998. Effect of surface modification on the interlayer chemistry of iron in a smectite clay. Chemistry of Materials 10:559.
- Wloch, E., B. Sulikowski, R. Dula, and E.M. Serwicka. 1996. Cation environment and migration in iron-exchanged zeolite Na---Y studied by ESR. Colloids and Surfaces A 115:257.
- Zielke, R.C., and T.J. Pinnavaia. 1988. Modified clays for the adsorption of environmental toxicants: binding of chlorophenols to pillared delaminated, and hydroxyl-interlayered smectites. Clays and Clay Minerals:403-408.
- Zilberberg, I., M. Ilchenko, O. Isayev, L. Gorb, and J. Leszczynski. 2004. Modeling the gas-phase reduction of nitrobenzene to nitrosobenzene by iron monoxide: A density functional theory study. Journal of Physical Chemistry A 108:4878-4886.

# **CHAPTER V**

# CLAY MEDIATED ROUTE TO NATURAL FORMATION OF POLYCHLORODIBENZO-p-DIOXINS: A DFT STUDY

#### **ABSTRACT**

Recent studies have documented the ubiquitous occurrence of polychlorodibenzop-dioxins and dibenzofurans (PCDD/Fs) of unknown origin in soils and clay deposits. One concern in terms of human exposure to dioxins in soils is the direct ingestion of contaminated soils by children. Interestingly, the PCDD/F congener profiles do not match any known natural or anthropogenic source, and global PCDD/F budgets fail to account for the observed levels in soils. To reconcile these observations, clay minerals were hypothesized to play a central role in the natural *in-situ* synthesis of PCDD/Fs. Recent study has confirmed the clay-facilitated formation of the most prevalent PCDD congener in soils, octachlorodibenzo-p-dioxin (OCDD), supporting the hypothesis. The objective of this study was to investigate whether the most toxic PCDD congener 2,3,7,8tetrachlorodibenzo-p-dioxin (2,3,7,8-TCDD) could form via the same clay-catalyzed mechanism that produced OCDD. Density functional theory calculations of the precursor 2,4,5-trichlorophenol (2,4,5-TCP) interacting with iron(III) species (represent the Fe(III)montmorillonite clay) were carried out to evaluate the possible reaction pathways and the associated reaction energies and activation energies.

The calculations support the formation of the direct precursors of the most toxic PCDD congener, 2,3,7,8-TCDD, and of 1,2,4,7,8-pentachlorodizenzodioxin, and two additional dimers, from the reaction of 2,4,5-TCP with Fe(III)-montmorillonite clay, which imply that soil contaminated with 2,4,5-trichlorophenol may have the potential risk for 2,3,7,8-TCDD contamination.

#### INTRODUCTION

Polychlorodibenzo-*p*-dioxins are among the most toxic environmental contaminants due to their potency as aryl hydrocarbon receptor ligands. Polychlorinated dioxins are formed, and occur in the environment, as mixtures of congeners with different degrees of chlorination and substitution patterns. The known sources of PCDD/Fs, e.g. pesticide manufacture, waste incineration, forest fires, are matched with known congener distribution profiles. Each of 75 congeners has been assigned a toxicity equivalency factor (TEF), and these are summed to generate an aggregate toxic equivalents quotient (TEQ) which is used as the regulatory basis for PCDD/Fs in soils. The 2,3,7,8-TCDD congener is considered most potent (TEF=1) and OCDD is considered much less potent. The TEF for OCDD was raised to 0.0003 in 2005, and there was discussion about revising it upward to 0.001(Van den Berg et al., 2006), or even to 0.0025 (Samara et al., 2009), which is almost 10 times its current level.

There is an established discrepancy between PCDD emissions versus actual PCDD levels in soils, and OCDD presents the greatest imbalance (Baker and Hites, 2000), viz. about 40 times greater than the expected amount, suggesting an *in-situ* process of PCDD formation favoring OCDD. The predominance of OCDD in residential and rural soils is illustrated by an EPA study where of the 1585 ppt (average on mass basis) total dioxins, 1482 ppt were from OCDD (EPA, 2007). As a result, any significant increase in the TEF assigned to OCDD would immediately make many soils in residential and rural areas of the U.S. out of compliance with the proposed EPA limit of 72 ppt TEQ for PCDD/PCDFs (EPA, 2010). The inexplicably high PCDD levels in soils, and the unique congener profiles dominated by OCDD, are also observed in certain clay deposits such as

ball clays (Gadomski et al., 2004). These clays have caused several instances of livestock contamination when used as feed additives (Hayward and Bolger, 2005). Direct ingestion of contaminated soils by children, for example at residences on the Tittabawasee River floodplain soils, is another likely route of human exposure to dioxins, as demonstrated for Pb and DDT in historically contaminated soils (Franzblau et al., 2008).

Recently, direct evidence of OCDD formation via reaction of pentachlorophenol (PCP) with montmorillonite clay was reported (Gu et al., 2008). This gave substance to the hypothesis of *in-situ* clay-facilitated formation of PCDDs (Holmstrand et al., 2006; Horii et al., 2008), and raised the question of whether the most toxic PCDD congener 2,3,7,8-TCDD could form on clays via the same mechanism that produced OCDD.

The overall goal of this study was to expand the understanding on the reactions of chlorophenols with naturally occurring montmorillonite in the context of forming PCDDs using quantum mechanical methods. 2,4,5-Trichlorophenol (2,4,5-TCP) was used as the logical precursor to 2,3,7,8-TCDD. Recent quantum mechanical calculations for PCDD formation from 2,4,5-TCP showed that dimerization of this chemical could progress to form several PCDD congeners, i.e. 2,3,7,8-TCDD and 1,2,4,7,8-pentachlorodibenzo-*p*-dioxin (1,2,4,7,8-PeCDD) (Okamoto and Tomonari, 1999; Qu et al., 2009). However, the estimated energy barriers indicated the reactions without any catalyst can only proceed at high temperatures (Okamoto and Tomonari, 1999; Qu et al., 2009). Here, quantum mechanical calculations were employed to evaluate the whole reaction energy profiles for PCDD formation with Fe(III)/Fe(II) species representing the catalysts imbedded in clay mineral interlayers, and the formation of four major reaction products was reported from

the surface catalyzed dimerization of 2,4,5-TCP on Fe(III)-saturated montmorillonite at ambient temperature.

### MATERIALS AND METHODS

**Computational Methods.** Density functional theory (DFT) calculations were carried out to evaluate the reaction energies and activation energies associated with the proposed reaction pathway with and without iron using Gaussian03 software package (Frisch et al., 2004). As suggested in earlier studies (Okamoto and Tomonari, 1999; Shiota and Yoshizawa, 2000; Sun et al., 2007), Fe(III)O<sup>+</sup> was used to represent the interlayer iron species responsible for the catalytic oxidation of 2,4,5-TCP to 2,4,5-TCP radicals and the following hydrogen abstraction during the dimerization process: Fe(II)(OH)<sup>+</sup> was used in chlorine atom abstraction, since a reductant was needed in this catalytic reduction process to eliminate Cl. The geometry optimizations of all intermediate and transition state structures had been performed using the Becke three-parameter exchange functional (B3) (Becke, 1993) and the Lee-Yang-Parr correlation functional (LYP) (Lee et al., 1988) with 6-31G\* basis set for C, H and O atoms and LANL2DZ ECP basis set for Fe and Cl. The total multiplicity of system was assigned a value of 2 for the system containing only 2,4,5-TCP radicals, 6 for the system containing high spin Fe(III) and 5 for the system containing high spin Fe(II). To determine the activation energy of a specific path for 2,4,5-TCP reactions, the transition state that connects two immediate stable structures

through a minimum energy path was identified by quadratic synchronous transit (QST3) search methods (Peng and Schlegel, 1993).

## RESULTS AND DISCUSSION

The experimental studies conducted at room temperature and a relative low relative humidity showed that 2,4,5-TCP can rapidly undergo dimerization reactions in presence of Fe(III)-saturated montmorillonite (Boyd and Mortland, 1985; Gu et al., 2008). Four major products were identified as: product A, a dimer of 2,4,5-TCP coupled by C-C bond formation leaving the two phenolic -OH groups intact, and three products B, C and D, all diphenylethers with the C-O-C bond formed at various positions on the ring, leaving one phenolic -OH group intact. Based on the previous results (Gu et al., 2008) and similar structures reported in the literature (Okamoto and Tomonari, 1999), the proposed structures for products A, B, C and D are: 3,3',5,5',6,6'-hexachloro-(1,1'biphenyl)-2,2'-diol; 4,5-dichloro-2-(2,4,5-trichlorophenoxy)phenol; 3,4,6-trichloro-2-(2,4,5-trichlorophenoxy)phenol; and 3,4,6-trichloro-3-(2,4,5-trichlorophenoxy)phenol, respectively. The reported yield of product B, the predioxin (precursor) of 2,3,7,8-TCDD was about one-half that of the other three products. Formation of 2,3,7,8-TCDD and 1,2,4,7,8-PeCDD were reported in the range of  $0.067 \sim 0.16 \,\mu\text{mol/g}$  clay ( $22 \sim 51 \,\mu\text{g/g}$  clay) and 0.090~0.19 μmol/g clay (32~68 μg/g clay), respectively at elevated temperature over 140 °C. It is noteworthy that OCDD formed from pentachlorophenol spontaneously at

room temperature under the same reaction conditions (Gu et al., 2008). The reactions reported do not proceed with ferric salts, or in the absence of Fe-montmorillonite, and only minor yields of products (< 5%) are obtained with homoionic Ca-montmorillonite.

A proposed reaction pathway for the four major products is shown in Figure V-1. Insight into the operative reaction mechanisms was gained from DFT calculations for the individual reactions in the presence and absence of FeO<sup>+</sup>/FeOH<sup>+</sup>, which served as a simplified model of the Fe(III)-montmorillonite clay used in our study. The predicted energy profiles, with optimized structures for each proposed intermediate, are presented in Figure V-2. The reaction is initiated by a single electron transfer from 2,4,5-TCP to Fe(III) to form the 2,4,5-TCP radical cation, as previously shown for pentachlorophenol (Boyd and Mortland, 1986; Gu et al., 2008). The 2,4,5-TCP radical cation deprotonates to form the more stable 2,4,5-TCP phenoxy radical. In the absence of Fe(III), the proton/electron dissociation reactions to form 2,4,5-TCP radicals are highly endothermic, with calculated energies of 186.21 and 87.57 kcal/mol, respectively (Table V-1, reactions 0 and 1), suggesting that a proper electron acceptor is required for the reaction to proceed at ambient temperature. In our calculations, isolated Fe(III)O<sup>+</sup>/Fe(II)(OH)<sup>+</sup> was used to represent the redox activity of Fe(III)-montmorillonite. When added to the simulated system, FeO<sup>+</sup> strongly binds 2,4,5-TCP inducing immediate proton/electron transfer to form the 2,4,5-TCP cation radical and subsequently the phenoxy radical without an activation barrier; the reaction energies are -69.55 and -113.47 kcal/mol, respectively (Table V-1, reactions 0' and 1'). The energy benefits afforded by FeO<sup>+</sup>/FeOH<sup>+</sup> are of sufficient magnitude to promote formation of the highly reactive radicals, and allow the energy barrier for the subsequent dimerization reactions to be overcome.

Dimerization of 2,4,5-TCP on Fe(III)-montmorillonite can occur via C-C or C-O bond formation. In the absence of iron, the reaction forming the dimer via C-C linkage (Figure V-1, Product A) is endothermic with an overall reaction energy of 43.54 kcal/mol and a total activation barrier of 52.90 kcal/mol. Addition of FeO<sup>+</sup> to the system (Figure V-2a) significantly reduces the energy barrier to 40.96 kcal/mol by activating the intermediate C-H bond. In addition, the FeO<sup>+</sup> makes the reaction exothermic by -35.13 kcal/mol as a result of forming FeOH<sup>+</sup> rather than eliminating an isolated hydrogen radical (Figure V-2a).

Formation of diphenylethers via C-O coupling accounts for three of the four major products including the two predioxins (Figure V-1, Products B-D). The ether oxygen of the initially formed dimer is strongly bound to iron, which destabilizes reaction barriers such that only a single transition state was located (Figure V-2b-d) and the reaction/activation energies were reported in Table V-1. Several different isomers were produced depending on the ring position of 2,4,5-TCP that is attacked by the 2,4,5-TCP phenoxy radical. Attack at the ortho-chloro position of 2,4,5-TCP, followed by elimination of chlorine, rearomatizes the ring forming 2,3,7,8-predioxin (Figure V-1, Product B). Elimination of chlorine is exothermic with a low activation barrier, so that formation of chloride coupled to reoxidation of Fe(II) to Fe(III)-montmorillonite (Gu et al., 2008) is not a strict requirement, but a distinct possibility. The primary effect of iron

is to lower the overall activation energy which is 15.68 kcal/mol less than the reaction without FeOH<sup>+</sup> (Figure V-2b).

Products C and D (Figure V-1) are formed via attack of the chlorophenoxy radical at the (nonchlorinated) ortho- or meta- positions of 2,4,5-TCP with subsequent elimination of H. Absent Fe(III), the overall reaction energies for formation of products C and D are 50.29 and 53.09 kcal/mol, and the calculated activation barriers are 55.90 and 60.09 kcal/mol, respectively (Figure V-2c, 2d). The presence of Fe(III) species (e.g. FeO<sup>+</sup>) lowers the reaction barriers and energies by circumventing the H· radical through a proton-coupled electron transfer to Fe(III). This results in an overall exoergic reaction. The resultant reaction energies are -46.09 and -32.43 kcal/mol and activation energies are reduced to 31.2 and 38.76 kcal/mol, respectively, for products C and D.

Based on the semi-quantitative calculations of the reaction energy profiles, if all reactions start with a chlorophenoxy radical and Fe-montmorillonite, then reactions A, C and D have similar overall energies (-35.13, -46.09 and -32.43 kcal/mol, respectively) and activation barriers (40.96, 31.20 and 38.76 kcal/mol, respectively) so we would expect similar yields for products A, C and D. This is what the experiments found. Product B gave a lower yield in our experiments despite its lower activation energy barrier (Figure V-2b), presumably because the overall reaction energy is significantly less favorable (3.21 kcal/mol). This result is of practical importance since product B is the direct precursor of 2,3,7,8-TCDD.

The ring closure of predioxins to form dioxins occurs via intramolecular condensation. We computed activation barriers of ~55 kcal/mol for the neutral predioxins

(Table V-1), prohibiting condensation under ambient conditions. However, the activation significantly reduced for intramolecular condensations barriers are chlorophenoxyphenol predioxin anions (Table V-1); The condensation energies are -16.98 and -10.48 kcal/mol and the activation barriers are reduced to 13.19 and 16.10 kcal/mol for 2,3,7,8-TCDD and 1,2,4,7,8-PeCDD, respectively, similar to that of OCDD  $(E_A = 14.35 \text{ kcal/mol})$ ,  $E_R = -10.35 \text{ kcal/mol})$ . The OCDD condensation reaction is apparently most favorable since it occurs at room temperature (Gu et al., 2008). For OCDD there are two equivalent chlorinated positions for ring closure. Importantly, the  $pK_a$  of the OCDD predioxin (4.91) is substantially lower than those of the less chlorinated analogs (7.10 and 6.87 for predioxins of 2,3,7,8-TCDD and 1,2,4,7,8-PeCDD, respectively), as calculated by Advanced Chemistry Development (ACD/Labs) Software Solaris V8.14 (data from SciFinder), manifesting a comparatively higher population of OCDD chlorophenoxyphenol anions at typical soil pH, thereby favoring OCDD formation. Apparently, these factors together manifest a higher tendency for OCDD formation in the soil environment, in agreement with our experimental observations (Gu et al., 2008), and with the predominance of OCDD observed in field samples (Gaus et al., 2002; Green et al., 2004; Prange et al., 2002).

The quantum mechanical results demonstrate the formation of the immediate precursors of 2,3,7,8-TCDD and 1,2,4,7,8-PeCDD from the reactions of 2,4,5-TCP with a smectite clay under environmentally relevant conditions. 2,4,5-Trichlorophenol is a commonly used chlorophenol and a major product in the microbial decomposition of the herbicide 2,4,5-T which was widely applied to agricultural fields, home lawns, and as the

defoliant "Agent Orange" during the Vietnam war. Significant levels of 2,4,5-TCP have been found in surface water (Czaplicka, 2004), air and rain samples (Leuenberger et al., 1985), and soil microbes synthesize chlorophenols (Hoekstra et al., 1999). The predioxins themselves, once formed, are bioaccumulative and persistent in the environment (Domingo, 2006). Importantly, these predioxins are readily converted to highly toxic PCDDs, most notably 2,3,7,8-TCDD, under mild conditions, e.g. UV light (Freeman and Srinivasa, 1983), moderate heat or biotransformation (Huwe et al., 2000). This study implies that 2,4,5-TCP contaminated soils may be at risk for PCDD contamination. Furthermore, the more favorable formation of OCDD vs. TCDD demonstrated by our experimental results, and predicted by our quantum calculations and key physicochemical properties, provides a rationale for the elevated levels of OCDDs in soils, and helps resolve the existing imbalance (Baker and Hites, 2000) in PCDD global budgets.

 $\label{thm:cal_mol} Table~V-1.~Reaction~(E_R)~and~activation~energies~(E_A)~(in~kcal/mol)~of~the~predioxin~formations~calculated~at~B3LYP/6-31G*/LANL2DZ~level~of~theory^a$ 

Reaction	on Pathway		Activation Energy E <sub>A</sub>
w/o iron		kcal/mol	kcal/mol
0	2.4.5-TCP> $2.4.5$ -TCP radical cation + e	186.21	n/a
1	2,4,5-TCP> 2,4,5-TCP phenoxy· + H·	87.57	n/a
A	2,4,5-TCP phenoxy· + $2,4,5$ -TCP> product A + H· (overall)	43.54	52.90
	complex A> intermediate	29.42	32.23
	intermediate> intermediate'	-12.41	19.48
	Intermediate'> product A	26.53	35.89
В	2,4,5-TCP phenoxy· + $2,4,5$ -TCP> product B + Cl· (overall)	16.33	24.74
	complex B> intermediate	24.67	33.90
	intermediate> product B	-8.34	0.07
C	2,4,5-TCP phenoxy· + $2,4,5$ -TCP> product C + H· (overall)	50.29	55.90
	complex C> intermediate	18.30	22.35
	intermediate> product C	31.98	37.60
D	2,4,5-TCP phenoxy· + $2,4,5$ -TCP> product D + H· (overall)	53.05	60.09
	complex D> intermediate	19.45	22.85
	intermediate> product D	33.60	40.65
w iron			
0'	$FeO^{+}$ + 2.4.5-TCP> 2.4.5-TCP radical cation + FeO	-69.55	n/a
1'	$\text{FeO}^{+} + 2.4.5 - \text{TCP} > 2.4.5 - \text{TCP phenoxy} + \text{FeOH}^{+}$	-113.47	n/a
A'	$\text{FeO}^+ + 2,4,5\text{-TCP phenoxy} + 2,4,5\text{-TCP} \longrightarrow \text{product A} + \text{FeOH}^+ \text{(overall)}$	-35.13	40.96
	complex A> intermediate	37.29	$40.96^{b}$
	intermediate> product A	-72.42	-10.09
B'	$FeOH^+ + 2.4.5$ -TCP phenoxy· + 2.4.5-TCP> product B + $FeOHCl^+$	3.21	9.06
C'	+2.4.5-TCP phenoxy· + 2.4.5-TCP> product C + FeOH (overall)	-46.09	31.20
D'	$FeO^+ + 2.4.5$ -TCP phenoxy· + 2.4.5-TCP> product D + FeOH (overall)	-32.43	38.76

**Table V-1. (Continued)** 

Reaction	Pathway	Reaction	Activation
	T dan way	energy $E_{\mathbf{R}}$	Energy E <sub>A</sub>
		kcal/mol	kcal/mol
Ring closure <sup>c</sup>	product B> 2,3,7,8-TCDD + HCl	-3.75	52.05
img viesure	product B anion $> 2,3,7,8-TCDD + Cl$	-16.98	13.19
	product C> 1,2,4,7,8-PeCDD + HCl	-1.39	55.63
	product C anion $> 1,2,4,7,8$ -PeCDD $+ Cl^{-}$	-10.48	16.10
	3,4,5,6-tetrachloro-2-(pentachlorophenoxy)phenol> OCDD + HCl	-2.16	54.33
	3,4,5,6-tetrachloro-2-(pentachlorophenoxy)phenolic anion> OCDD + Cl	-10.35	14.35

<sup>&</sup>lt;sup>a</sup>Predioxins have conformational isomers due to rotation around the bridge oxygen. Since the rotational barrier is relatively small, reaction energies for those isomers are not listed. <sup>b</sup>This transition state is apparently a bimodal saddle point that oscillates but never quite converges for all criteria, so the value shown here is an estimate by partial convergence. <sup>c</sup>The ring closure reactions are through intramolecular condensation pathways to form dioxins.

Note: in Table V-1 above, reactions 0' and 1' were modeled differently from reactions A', B', C' and D', so these two sets of reaction energy calculations cannot be compared directly and interchanged. In reactions 0' and 1', on the left side of the reaction equations are FeO<sup>+</sup> and TCP at "infinite distance"; on the right side of the equation is the complex/cluster of Fe and TCP radicals. In contrast, for reactions A', B', C' and D', we have "complexes/clusters" on both sides of the reaction equations. The reaction energies calculated for the latter (A', B', C' and D') are exact, but the energies for the former (especially since 0' and 1' are charged systems) also include the electrostatic work done as the two charged species approach each other from infinite distance. The reason that 0' and 1' were treated in this manner is that we cannot locate an exact initial reactant complex (a reactant cluster of FeO<sup>+</sup> and PCP, in which Fe holds 5 spin and PCP remains neutral), since such a complex has extremely high energy and is very unstable. Therefore, the calculations on reactions 0' and 1' can only suggest that TCP phenoxy radical is more stable and more likely to be the radical responsible for what we observed in the experiment. This is why we chose TCP phenoxy radicals as the starting point, to compare different pathways and bypass the energy calculation difficulties that result if dimerization begins from two TCP molecules.

Figure V-1. Proposed reaction pathways for 2,4,5-TCP with Fe(III)-montmorillonite, leading to the formation of dimerized products, including predioxins (B and C).

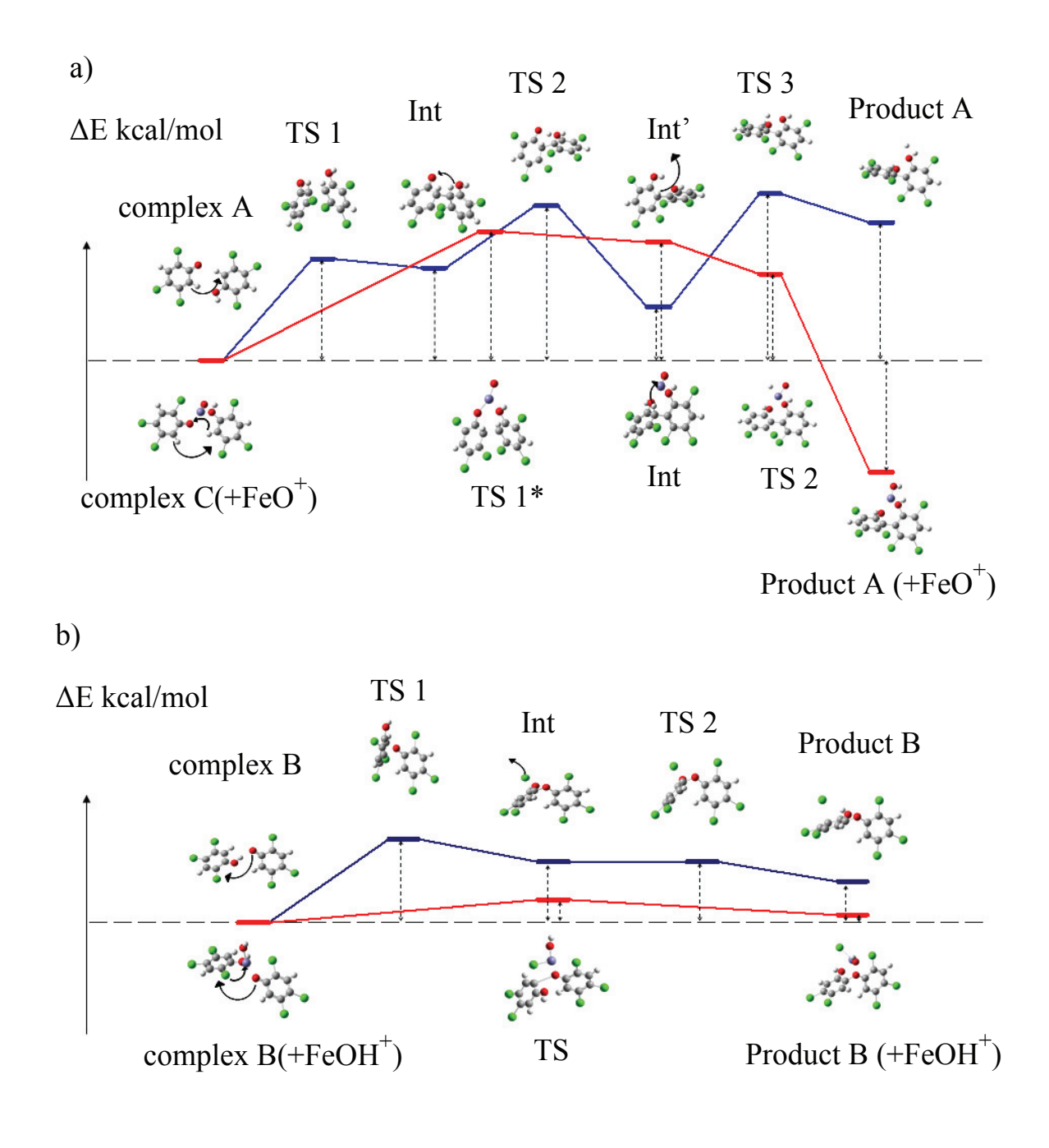


Figure V-2. Reaction profiles for the predioxin formation pathways from 2,4,5-TCP with or without  $Fe(III)O^+/Fe(II)(OH)^+$  (blue lines for systems w/o iron, and red lines for systems w iron). The energies of TCP phenoxy radical/2,4,5-TCP complexes with or without  $Fe(III)O^+/Fe(II)(OH)^+$  were set to zero. (See notes of Table V-1 for the description of TS1\* in pathway A)

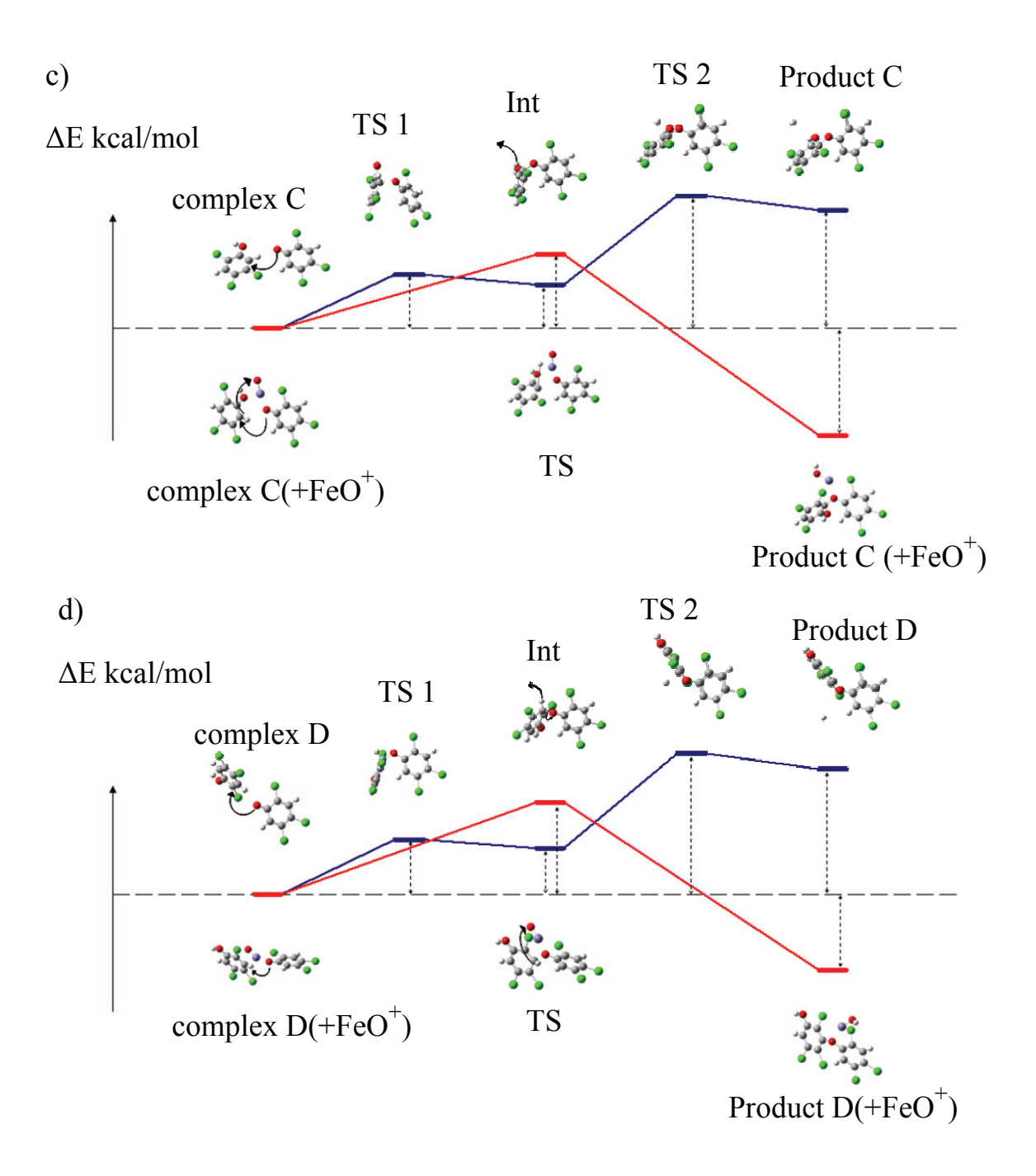


Figure V-2. (Continued)

LITERATURE CITED

#### LITERATURE CITED

- Baker, J.I., and R.A. Hites. 2000. Is combustion the major source of polychlorinated dibenzo-p-dioxins and dibenzofurans to the environment? A mass balance investigation. Environmental Science & Technology 34:2879-2886.
- Becke, A.D. 1993. Density-functional thermochemistry. III. The role of exact exchange. Journal of Chemical Physics 98:5648-5652.
- Boyd, S.A., and M.M. Mortland. 1985. Dioxin radical formation and polymerization on Cu(II)-smectite. Nature 316:532-535.
- Boyd, S.A., and M.M. Mortland. 1986. Radical formation and polymerization of chlorophenols and chloroanisole on copper(II)-smectite. Environmental Science & Technology 20:1056-1058.
- Czaplicka, M. 2004. Sources and transformations of chlorophenols in the natural environment. Science of the Total Environment 322:21-39.
- Domingo, J.L. 2006. Polychlorinated diphenyl ethers (PCDEs): environmental levels, toxicity and human exposure a review of the published literature. Environment International 32:121-127.
- EPA, U.S. 2007. Pilot survey of levels of polychlorinated dibenzo-p-dioxins, polychlorinated dibenzofurans, polychlorinated biphenyls and mercury in rural soils of the United States.
- EPA, U.S. 2010. Draft recommended interim preliminary remediation goals for dioxin in soil at CERCLA and RCRA sites.
- Franzblau, A., E. Hedgeman, Q. Chen, S.Y. Lee, P. Adriaens, and A. Demond. 2008. Case report: Human exposure to dioxins from clay. Environ Health Perspect 116:238-242.
- Freeman, P.K., and R. Srinivasa. 1983. Photochemistry of polychlorinated phenoxyphenols. Photochemistry of 3,4,5,6-tetrachloro-2-(pentachlorophenoxy)phenol. Journal of Agricultural and Food Chemistry 31:775-780.
- Gaussian, Inc. 2004. Gaussian 03 Revision E.01. Gaussian, Inc, Wallingford, CT.
- Gadomski, D., M. Tysklind, R.L. Irvine, P.C. Burns, and R. Andersson. 2004.

  Investigations into the vertical distribution of PCDDs and mineralogy in three ball clay cores from the United States exhibiting the natural formation pattern.

  Environmental Science & Technology 38:715-723.

- Gaus, C., G.J. Brunskill, D.W. Connell, J. Prange, J.F. Muller, and O. Papke. 2002. Transformation processes, pathways, and possible sources of distinctive polychlorinated dibenzo-p-dioxin signatures in sink environments. Environmental Science & Technology 36:3542-3549.
- Green, N.J.L., A. Hassanin, A.E. Jofinston, and K.C. Jones. 2004. Observations on historical contemporary, and natural PCDD/Fs. Environmental Science & Technology 38:715-723.
- Gu, C., H. Li, B.J. Teppen, and S.A. Boyd. 2008. Octachlorodibenzodioxin formation on Fe(III)-montmorillonite clay. Environmental Science & Technology 42:4758-4763.
- Hayward, D.G., and P.M. Bolger. 2005. Tetrachlorodibenzo-p-dioxin in baby food made from chicken produced before and after the termination of ball clay use in chicken feed in the United States. Environmental Research 99:307-313.
- Hoekstra, E.J., H. De Weerd, E.W.B. De Leer, and U.A.T. Brinkman. 1999. Natural formation of chlorinated phenols, dibenzo-p-dioxins, and dibenzofurans in soil of a Douglas fir forest. Environmental Science & Technology 33:2543-2549.
- Holmstrand, H., D. Gadomski, M. Mandalakis, M. Tysklind, R. Irvine, and P. Andersson. 2006. Origin of PCDDs in ball clay assessed with compound-specific chlorine isotope analysis and radiocarbon dating. Environmental Science & Technology 40:3730-3735.
- Horii, Y., B. van Bavel, K. Kannan, G. Petrick, K. Nachtigall, and N. Yamashita. 2008. Novel evidence for natural formation of dioxins in ball clay. Chemosphere 70:1280-1289.
- Huwe, J.K., V.J. Feil, R.G. Zaylskie, and T.O. Tiernan. 2000. An investigation of the in vivo formation of octachlorodibenzo-p-dioxin. Chemosphere 40:957-962.
- Lee, C., W. Yang, and R.G. Parr. 1988. Development of the Colle-Salvetti correlationenergy formula into a functional of the electron density. Physical Review B 37:785-789.
- Leuenberger, C., M.P. Ligocki, and J.F. Pankow. 1985. Trace organic compounds in rain. 4. Identities, concentrations, and scavenging mechanisms for phenols in urban air and rain. Environmental Science & Technology 19:1053-1058.
- Okamoto, Y., and M. Tomonari. 1999. Formation pathways from 2,4,5-trichlorophenol (TCP) to polychlorinated dibenzo-p-dioxins (PCDDs): an ab initio study. Journal of Physical Chemistry A 103:7686-7691.
- Peng, C., and H.B. Schlegel. 1993. Combining synchronous transit and quasi-Newton methods to find transition state. Israel Journal of Chemistry 33.

- Prange, J.A., C. Gaus, O. Papke, and J.F. Muller. 2002. Investigations into the PCDD contamination of topsoil, river sediments and kaolinite clay in Queensland, Australia. Chemosphere 46:1335-1342.
- Qu, X.H., H. Wang, Q.Z. Zhang, X.Y. Shi, F. Xu, and W.X. Wang. 2009. Mechanistic and kinetic studies on the homogeneous gas-phase formation of PCDD/Fs from 2,4,5-trichlorophenol. Environmental Science & Technology 43:4068-4075.
- Samara, F., B.K. Gullett, R.O. Harrison, A. Chu, and G.C. Clark. 2009. Determination of relative assay response factors for toxic chlorinated and brominated dioxins/furans using an enzyme immunoassay (EIA) and a chemically-activated luciferase gene expression cell bioassay. Environment International 35:588-593.
- Shiota, Y., and K. Yoshizawa. 2000. Methane-to-methanol conversion by first-row transition-metal oxide ions: ScO<sup>+</sup>, TiO<sup>+</sup>, VO<sup>+</sup>, CrO<sup>+</sup>, MnO<sup>+</sup>, FeO<sup>+</sup>, CoO<sup>+</sup>, NiO<sup>+</sup>, and CuO<sup>+</sup>. Journal of the American Chemical Society 122:12317-12326.
- Sun, Q., M. Altarawneh, B.Z. Dlugogorski, E.M. Kennedy, and J.C. Mackie. 2007. Catalytic effect of CuO and other transition metal oxides in formation of dioxins: Theoretical investigation of reaction between 2,4,5-trichlorophenol and CuO. Environmental Science & Technology 41:5708-5715.
- Van den Berg, M., L.S. Birnbaum, M. Denison, M. De Vito, W. Farland, and M. Feeley. 2006. The 2005 World Health Organization reevaluation of human and mammalian toxic equivalency factors for dioxins and dioxin-like compounds. Toxicological Sciences 93:223-241.